The Pennsylvania State University

The Graduate School

H63D *HFE* AS A GENETIC MODIFIER OF PARKINSON'S DISEASE: CLINICAL IMPACTS AND MOLECULAR MECHANISMS

A Dissertation in

Biomedical Sciences

by

Yunsung Kim

© 2020 Yunsung Kim

Submitted in Partial Fulfillment

of the Requirements

for the Degree of

Doctor of Philosophy

May 2020

The dissertation of Yunsung Kim was reviewed and approved* by the following:

James R. Connor
University Distinguished Professor
Vice-Chair of the Department of Neurosurgery
Dissertation Advisor
Chair of Committee

Mark C. Stahl
Medical Director
Neurocrine Biosciences
Special Member

Xuemei Huang
University Distinguished Professor
Vice-Chair for Research, Department of Neurology

Robert Levenson
University Distinguished Professor
Department of Pharmacology
Department of Neural and Behavioral Sciences
Co-Director Medical Scientist Training Program

Salvatore L. Stella, Jr.
Assistant Professor
Department of Neural and Behavioral Sciences

Ralph L. Keil
Associate Professor
Department of Biochemistry and Molecular Biology
Chair, Biomedical Sciences Graduate Program

ABSTRACT

Parkinson's disease (PD) is a neurodegenerative disorder that presents clinically with bradykinesia, resting tremor, and/or rigidity. With disease progression, these motor symptoms worsen while non-motor symptoms such as mood disorders, cognitive decline, and hallucinations may appear, leading to significant decline in quality of life. Approximately 1 million people in the U.S. currently live with PD. Furthermore, dopamine replacement therapy with levodopa/carbidopa, the standard of care for PD, is only effective in alleviating the motor symptoms and fail to alter the progression of the disease. Much needed development of novel therapies for PD requires better understanding of the underlying mechanisms of neurodegeneration as well as genetic and environmental contributions to the disease.

Pathologically, PD is characterized by the loss of dopaminergic neurons in the substantia nigra (SN) along with intracellular Lewy bodies composed mainly of α-synuclein. Iron accumulation is also a consistent feature of PD pathology, which has led to multiple studies investigating the role of iron related gene variants on risk for PD. In particular, the homeostatic iron regulator (HFE) has been of interest due to its role as a genetic modifier for other neurological diseases and the high prevalence of its variant in the general population. HFE regulates iron uptake into cells through its interaction with the transferrin receptor. H63D variant of *HFE*, which is estimated to be present in 14-21% of the U.S. population, has lower affinity for binding to the transferrin receptor leading to increased iron uptake into the cell. Previous studies have shown no association between H63D *HFE* and PD risk; however, what has been lacking is an evaluation of the effects of this variant on disease progression. This gap in knowledge is addressed in this dissertation using clinical data as well as cell culture and animal model to determine the mechanism underlying the impact of H63D *HFE* on PD clinical profiles.

The first chapter focuses on the role of iron and *HFE* in health and diseases of the central nervous system. Iron accumulation is a recurring pathological phenomenon in many neurological diseases including Parkinson's disease, Alzheimer's disease, and amyotrophic lateral sclerosis. While iron is essential for development and normal functions of the brain, excess iron can lead to build up of oxidative damage and cell death. This dual role of iron in context of disease is further explored in this section. Additionally, the impact of H63D *HFE* variant on risk and progression of neurological diseases along with potential underlying mechanisms are discussed. Finally, an update on development of iron targeting therapies is given, establishing the importance of iron and *HFE* in understanding disease pathogenesis as well as therapy development.

The second chapter assesses the impact of H63D *HFE* as a modifier of Parkinson's disease clinical findings and α-synuclein levels in biofluids. Striatal binding ratio from DaTscan SPECT imaging data and United Parkinson's Disease Rating Scale part III from the Parkinson's Progressive Markers Initiative database were used to investigate PD disease profile in patients with WT *HFE* genotype compared to H63D *HFE*. H63D *HFE* carriers were found to have a different disease phenotype. Moreover, H63D *HFE* carriers had altered blood *SNCA* RNA transcript and CSF α-synuclein levels compared to patients with WT *HFE*, demonstrating the impact of H63D *HFE* variant as a significant clinical modifier of PD.

Next, the mechanism underlying the impact of H63D *HFE* on PD pathology was explored. α-Synuclein is the main component of Lewy bodies and its aggregation is thought to be an essential step in PD pathogenesis. Therefore, the effects of H63D *HFE* on α-synuclein expression, aggregation, and cytotoxicity was assessed using cell culture and animal model. H63D *HFE* expression lowered endogenous α-synuclein levels and pre-formed fibril induced α-synuclein

aggregation and cytotoxicity. Using an *in vivo* paraquat exposure model, H67D *Hfe* (mouse homolog to human H63D *HFE*) mice were shown to decreased α-synuclein aggregation compared to WT *Hfe* mice. Elevated baseline autophagic flux was identified to be the protective mechanism with REDD1 inhibition of the mTORC1 pathway. Furthermore, while iron chelator (deferiprone) treatment rescued WT *HFE* cells from pre-formed fibril induced α-synuclein aggregation and toxicity, it exacerbated or was unable to rescue H63D *HFE* cells. In all, the data demonstrate that H63D *HFE* variant reduces α-synuclein pathology through induction of autophagy and has the potential to impact the efficacy of iron chelation therapy for PD.

The last section discusses the involvement of H63D *HFE* genotype on Parkinson's disease pathology beyond the direct effects on α-synuclein and consequent impact on development of novel therapies. Previous studies on H63D *HFE* variant have demonstrated its roles in reactive oxygen species handling, inflammation, and the adaptive immune system. Reactive oxygen species mediated cytotoxicity and chronic inflammation are key pathways present in PD pathology along with α-synuclein aggregation, as demonstrated by studies on neuroprotective effects of anti-inflammatory drugs and antioxidative therapies. Therefore, H63D *HFE* not only directly alters α-synuclein pathology but also may modulate disease indirectly through the immune system. In addition, the finding that H63D *HFE* induces baseline autophagy naturally leads to speculations on the impact of this genotype on diseases beyond the nervous system, including diseases in the muscular tissue and cancer.

Collectively, this dissertation identifies H63D *HFE* variant as a novel genetic modifier of Parkinson's disease with clinical and molecular consequences. High prevalence of H63D *HFE* further highlight the significance of its impact and clearly indicates the need for *HFE* genotype-

based stratification for future clinical trials and potential insights into the pathogenesis of the disease.

TABLE OF CONTENTS

LIST OF FIGURES

LIST OF TABLES

ACKNOWLEDGEMENTS

I would like to dedicate this thesis to my family for their support of all my academic pursuits throughout the years. I am thankful to have my mom who is always there for me to talk to in times of hardship, my dad who has and will always be my role model, and my sister who makes me laugh during times of stress. I would also like to thank my extended family in South Korea especially my grandmother who I love dearly. To my grandmother, 할머니, 사랑해요. 한국에 자주 가지 못해서 죄송하고 항상 건강하세요. 할머니 집에 놀러 갈게요.

I would like to also express my gratitude for all the mentorship that I have received. To Mark, thank you for always being enthusiastic about science and being the mentor who I most want to be like when I grow up. To Dr. Connor, I can't thank you enough for taking me into your lab and providing me with scientific and academic guidance for the last year. Finally, to all the members of the Stahl lab and the Connor lab, I couldn't have gotten to where I am now without your help and your support. Thank you for all you have done for me.

Lastly, to my friends, thank you for laughing, crying, and venting with me throughout the years. Your friendship makes every day at Penn State enjoyable. Special thanks to Kristen and Alfred for keeping me sane outside of the laboratory. I am forever grateful.

Chapter 1

The roles of iron and *HFE* genotype in neurological diseases

1.1 Abstract

Iron accumulation is a recurring pathological phenomenon in many neurological diseases including Parkinson's disease, Alzheimer's disease, amyotrophic lateral sclerosis, and others. Iron is essential for normal development and functions of the brain; however, excess redox-active iron can also lead to oxidative damage and cell death. Especially for terminally differentiated cells like neurons, regulation of reactive oxygen species is critical for cell viability. As a result, cellular iron level is tightly regulated. Although iron accumulation related to neurological diseases has been well documented, the pathoetiological contributions of the homeostatic iron regulator (HFE), which controls cellular iron uptake, is less understood. Furthermore, a common HFE variant, H63D HFE, has been identified as a modifier of multiple neurological diseases. This chapter will discuss the roles of iron and HFE in the brain as well as their impact on various disease processes.

1.2 Introduction

In 1922, Hallervorden and Spatz were first to report abnormal iron accumulation in the globus pallidus and substantia nigra of five siblings who exhibited progressive dementia and dysarthria[1]. Hallervorden-Spatz disease, now called Pantothenate Kinase-Associated Neurodegeneration (PKAN), was the first neurological disease found to be associated with iron imbalance in the brain.

This discovery was followed by the works of L'hermitte et al. in 1924 describing iron deposits in the brains of Parkinson's disease patients and Goodman in 1953 showing colocalization of iron and amyloid plaques in Alzheimer's disease pathology[2,3]. The importance of iron in disease processes and normal function of the brain has since been highlighted by numerous studies demonstrating the roles of iron in neuronal and glial function, neurodevelopment, and aging[4–6].

Iron is one of the most abundant metals found on the Earth and an essential biometal for all cells of the human body[7]. The ability of iron to easily transfer a single electron allows it to participate in redox and acid-base reactions as a cofactor for various enzymes. Proteins containing iron are involved in oxygen transport, DNA synthesis and repair, and mitochondrial respiration. Iron is also found in catalases and peroxidases (decomposition of H_2O_2), lipoxygenases (synthesis of leukotrienes), and cytochrome P450 enzymes (drug metabolism)[8]. Additionally, small pools of the non-protein bound form of iron, called labile iron, are present in the cytosol. These redox-active pools are capable of producing free radicals through Fenton chemistry[9]. Build-up of free radicals ($HO^{\bullet}$ and $RO^{\bullet}$) and other reactive oxygen species (ROS) including superoxides ($O_2^{\bullet -}$) in the cell have been associated with growth inhibition, DNA damage, and eventually cell death[10]. For this reason, iron metabolism is tightly regulated.

Non-heme iron is taken up by the cell in two main forms: non-transferrin-bound and transferrin-bound[11]. Non-transferrin-bound ferric iron (Fe^{3+}) is reduced to ferrous iron (Fe^{2+}) by ferrireductases on the cell surface; then, it enters the cell using transporters such as divalent metal transporter 1 (DMT1) and ZRT/IRT-like proteins (ZIPs)[12,13]. Transferrin-bound iron, the most abundant form of iron in the blood, undergoes receptor mediated endocytosis by binding to transferrin receptor 1 (TfR1)[11,14]. Acidification of the endosomes causes the release of ferric iron from transferrin, which is reduced by endosomal ferrireductases to ferrous iron and transported out to the cytosol as free

iron[11,15]. This free labile iron within the cell only make up ~5% of the total cellular iron because iron is quickly used to synthesize heme, Fe-S clusters, and other iron-containing metalloproteins, exported out of the cell by ferroportin (FPN1), or incorporated into ferritin, an iron storage protein[8]. Iron stored in ferritin is protected from ROS generation through sequestration and ferrireductase activity[16]. To utilize the stored iron, ferritin is broken down by NCOA4-mediated ferritinophagy and free iron is released into the cytosol[17].

Cellular iron homeostasis is maintained at multiple levels. Hypoxia inducible factors (HIFs) control transcription of iron related genes such as *TFR1*, *DMT1*, and *FPN1*[18]. At low oxygen or low intracellular iron levels, HIF1α or HIF2α forms dimers with HIF1β and translocate to the nucleus. HIF heterodimers bind to hypoxia response elements and activates transcription of nearby genes[18]. In iron-replete conditions, HIF1α and HIF2α are hydroxylated by iron-dependent prolyl hydroxylases that target them for ubiquitination and subsequent degradation by the proteasome[19]. At the translational level, interaction of iron response proteins (IRP1 and IRP2) with iron responsive elements (IREs) located in 5'-UTR or 3'-UTR of mRNAs control the synthesis of iron related proteins[20,21]. In iron-depleted cells, IRPs bind to IREs with high affinity. IRP binding to IRE at the 5'-UTR reduces translation by preventing the recruitment of the small ribosomal subunit[22]. H- and L-ferritin, HIF2α, and FPN1 mRNAs have IREs in their 5'-UTR. In contrast, IRP binding to IRE at the 3'-UTR increases the stability of the mRNA by protecting the RNA from nuclease degradation[23,24]. TfR1 and DMT1 mRNAs have IREs in their 3'-UTR. In high intracellular iron levels, IRPs are released from IREs and function as cytosolic aconitases or degraded by the proteasome[25]. Cellular iron uptake is also functionally controlled by the homeostatic iron regulator protein (HFE). HFE and transferrin-bound iron compete for an overlapping binding region of the TfR1; therefore, HFE negatively regulates iron uptake into the cell[26]. In the presence of high diferric

transferrin concentration, HFE mRNA and protein levels have been shown to increase[27]. HFE is a major histocompatibility complex class-1 like protein that contains a transmembrane domain[28]. It assembles on the cell surface with beta2-microglobulin (β2M) chaperone protein. This interaction is required for cell surface presentation of HFE[29]. Polymorphisms in the HFE gene were first identified in association with hereditary hemochromatosis (HH)[30]. Most common HFE variant associated with HH is C282Y. C282Y disrupts the disulfide bond in the α3 extracellular domain of HFE. This prevents binding to β2M and subsequent cell surface presentation[31]. Lack of HFE on the cell surface leads to excess iron uptake into the cell. C282Y variant is found in approximately 6-7% of the non-Hispanic white population in the United States[32]. A more common variant, H63D, found in 14-15% of the same ethnic population decreases the affinity for binding to TfR1[32]. H63D HFE variant rarely causes HH; however, this variant has been shown in context of multiple neurological diseases to be a risk and progression modifier[33]. Numerous studies in Parkinson's disease, Alzheimer's disease, and amyotrophic lateral sclerosis (ALS) patient populations as well as in preclinical disease models have shown a complex relationship between H63D HFE and neurological diseases. How H63D HFE variant may impact the clinical manifestations and underlying the disease processes is discussed further in this chapter.

1.3 Iron and H63D HFE in the brain

Iron plays critical roles in development and aging of the brain. Ribonucleotide reductase, the enzyme responsible for the rate limiting step of DNA synthesis utilizes iron as a cofactor, making iron essential for cell division and neural tube formation[34]. Oligodendrocytes, which are responsible for the myelin sheath around axons in the central nervous system, are the cell type that most robustly stain for iron and have the highest iron stores in the brain[35–37]. Myelin synthesis is dependent on

iron due to the role of iron in cholesterol and lipid biosynthesis and the relatively high rate of metabolic activity in oligodendrocytes to maintain the myelin sheath[38,39]. Iron deficiency in rats have shown impaired myelination with corresponding behavioral disturbances that persist even with brain iron reversal[40]. Functions of other glia such as astrocytes and microglia are likewise altered with iron deficiency. For example, primary astrocyte culture from pregnant rats fed with iron deficient diet showed decreased GFAP and CX43 staining indicative of an immature phenotype. Iron deficient microglia fail to respond to LPS stimulus and have decreased IL-1β expression[41] and IL-1β has been previously shown to promote remyelination through the induction of IGF-1[42] further tying the link between iron and myelination.

Beyond cell division, neurons need adequate and timely iron supply for dendritic arborization, synapse formation, and neurotransmitter synthesis[43–45]. For example, tyrosine hydroxylase and tryptophan hydroxylase involved in synthesis of monoamines (dopamine and serotonin) use iron as a cofactor. However, too much iron has been shown to induce dopaminergic neurodegeneration in mice[46]. Notably, β-propeller Protein Associated Neurodegeneration (BPAN), a subtype of neurodegeneration with brain iron accumulation (NBIA), where iron accumulation is found in the basal ganglia is associated with cognitive impairment and developmental delay followed by rapid neurodegeneration of the substantia nigra; however, it has not been definitely shown whether iron overload in BPAN is the cause of developmental impairment and neurodegeneration or a concurrent pathology[47].

Iron increases regionally in the brain with aging. Substantia nigra, putamen, globus pallidus, caudate nucleus, and cortices accumulate most iron[48–50]. The regional susceptibility for iron accumulation is not completely understood; however, the basal ganglia is an iron-rich region from

development and perhaps more prone to overload with time[51]. The amount of redox active iron in the cell is especially important for terminally differentiated cells like neurons. Furthermore, neurons consume approximately ten times more oxygen compared to other cell types in the body making them more vulnerable to ROS mediated damage[52]. It is no surprise that the two most prevalent neurodegenerative diseases associated with aging, Alzheimer's disease and Parkinson's disease, present pathologically with abnormal iron accumulation.

Given the excessive accumulation of iron in age-related neurodegenerative diseases, we considered that the common genetic variant in the iron homeostatic regulatory gene (*HFE*) could contribute to pathogenesis of these diseases. *HFE* is expressed in neurons as well as in glia, including astrocytes, microglia, and oligodendrocytes[53]. H63D *HFE* variant has been associated with increased brain iron as evidenced by the elevated expression of iron storage proteins H- and L-ferritin in H67D *Hfe* expressing mice[54]. Increased metabolic and oxidative stress in the brain has also been identified along with upregulation of nuclear factor E2-related factor 2 (Nrf2), which controls the reactive oxygen species responses of the cell[55]. This is one piece of evidence to suggest that H63D *HFE* expression leads to upregulation of adaptive mechanisms to handle the increased iron uptake into the cell. Furthermore, SH-SY5Y cells expressing H63D *HFE* had elevated ER stress independent of cellular iron levels, indicating activation of the unfolded protein response (UPR) pathway[56]. Similar to the upregulation of ROS responses, baseline autophagic flux was found to be elevated with H63D *HFE* expression by REDD1 inhibition of mTORC1 (Chapter 3). This increase in autophagy enables the cells to more quickly recycle damaged proteins and organelles. In addition to altered ROS response and elevated autophagy, H63D *HFE* expression has been shown to modulate lipid metabolism and white matter integrity. H63D *HFE* SH-SY5Y cells had 50% reduction in cholesterol content which was further shown in human and animal models as reduced MRI R2 values[57–59]. Pathways altered by H63D *HFE* expression in the brain are also fundamental

to various diseases such as Alzheimer's and Parkinson's disease, perhaps leading to the disease modifying effects of this genetic variant.

1.4 Iron and H63D HFE in neurological diseases

1.4.1 Parkinson's disease

Parkinson's disease (PD) is the fastest growing neurodegenerative disease and is clinically characterized by the presence of resting tremor, bradykinesia, and rigidity[60]. Pathologically, loss of dopaminergic neurons in the substantia nigra (SN) is found along with intracellular inclusions called Lewy bodies (LBs)[61]. LBs are made mostly of a presynaptic protein called α-synuclein (αSyn), as well as neurofilaments, vesicular components, and mitochondrial fragments[62,63]. Iron accumulation in the substantia nigra is also present as evidenced by multiple post-mortem and MRI studies[2,64,65]. Furthermore, Chen et al. used quantitative susceptibility mapping (QSM) to show that patients with late stage disease (Hoehn-Yahr stage ≥ 3) had higher susceptibility values in the substantia nigra and the red nucleus compared to early stage disease[66]. QSM has been shown to correlate with brain iron content using mass spectrometry and Perl's stain[67,68]. On-going trials of deferiprone as a disease modifying therapy for PD additionally highlight the importance of iron in the disease process[69].

With PD, iron accumulates in the SN; more specifically, increased iron-containing neuromelanin granules are found inside and outside of the neurons, the number of microglia loaded with ferritin is elevated, and iron (III) deposits are found in astrocytes, oligodendrocytes, and around LBs in neurons[70–73]. Iron accumulation is thought to occur through multiple mechanisms. Altered vascularization with neurodegeneration contributes to the increased iron[74]. Furthermore, DMT1

expression is increased in the SN of PD patients and MPTP mouse model[75,76]. Inhibition of autophagy and the ubiquitin-proteasome system that occurs with PD pathology also leads to the dysregulation of IRP2 and ferritin resulting in overall iron mismanagement[77]. Increased iron contributes directly to the disease process of PD through its interactions with αSyn (**Figure 1-1**). The main protein component of LBs, αSyn, is a 14 kDa protein highly expressed in neurons and red blood cells[78,79]. In neurons, its expression is localized to the cytosol and the presynaptic terminal, where it aids synaptic vesicle trafficking by acting as a chaperone for SNARE (soluble N- ethylmaleimide-sensitive fusion protein-attachment protein receptor) complex formation[80]. A putative iron response element (IRE) has been identified at the 5'-untranslated region (UTR) of the α-synuclein mRNA with sequence homology to H- and L-ferritin[81,82]. The interaction between IRE binding protein (IRP) and IRE is dependent on the cellular iron status and regulates protein expression at the translational level[83]. However, direct binding of IRP1 or IRP2 to α-synuclein mRNA has not been conclusively demonstrated[84–86]. Therefore, the functionality of the putative IRE in regulation of α-synuclein expression is unclear.

Figure 1-1

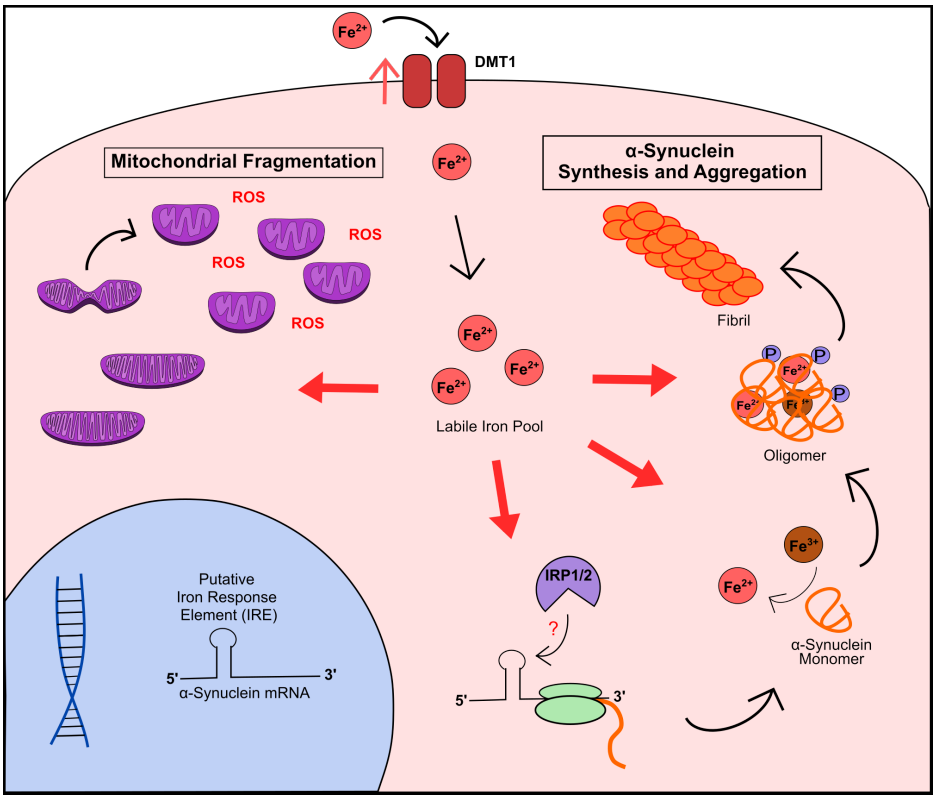

Figure 1-1: The role of iron in Parkinson's disease. Iron accumulation is found in the substantia nigra (SN) of Parkinson's disease patients. With PD, divalent metal transporter 1 (DMT1) expression is increased in the SN contributing to the increased iron uptake into the cell. Iron also directly interacts with α-synuclein, which acts as a ferrireductase converting Fe^{3+} to Fe^{2+}. A putative iron response element (IRE) located at the 5' untranslated region of α-synuclein mRNA is thought to be involved in translational regulation of the protein; however, IRP1/2 binding to the mRNA has not been clearly demonstrated. Furthermore, excess iron has been shown to promote aggregation of α-synuclein by promoting post-translational modifications. Mitochondrial dysfunction is another key feature of PD pathology. Iron overload promotes mitochondrial fragmentation and disrupt mitochondrial fission.

αSyn is intrinsically unfolded protein with three domains: a lipid-binding amino-terminal domain, a central NAC (non-amyloid-β component) domain, and a disordered carboxy-terminal domain[87]. The hydrophobic NAC domain has a random coil structure that can become misfolded into β-sheets and contribute to oligomerization of αSyn[88]. Iron directly binds to αSyn at carboxy-terminal domain residues Asp-121, Asn-122, and Glu-123[89]. Binding of metals to αSyn has been shown to induce ROS mediated damage and accelerate protein aggregation[90]. In particular, addition of excess iron in into the cell culture media increased aggregation and transmission of misfolded α-synuclein[91,92]. αSyn also has a high affinity binding for copper in its amino-terminal domain[93]. Overexpression of αSyn along with copper binding and the presence of NADH has shown to enable αSyn to function as a ferrireductase[94]. Ferrireductase converts Fe (III) to Fe (II) and its activity is especially important for dopaminergic neurons where tyrosine hydroxylase uses Fe (II) for the synthesis of L-DOPA[95]. Additionally, increased αSyn expression, as seen in PD, can result in build-up of redox active Fe (II) due to the excess ferrireductase activity. In vitro, co-treatment of αSyn oligomers with iron chelator deferoxamine was able to reduce the production of ROS[96].

Along with αSyn aggregation, mitochondrial dysfunction is one of the key features of Parkinson's disease pathophysiology. Multiple mitochondrial toxins, including paraquat, rotenone, and 1-methyl-4-phenylpyridinium (MPP+), have been associated with sporadic PD[97]. Identification of mitochondria related genes like Parkin, PTEN-induced putative kinase 1 (PINK1), DJ-1, and leucine-rich repeat kinase 2 (LRRK2) in hereditary PD cases has further solidified the importance of mitochondria[97]. Mitochondria not only synthesizes ATP, but is also critical for cellular calcium homeostasis and regulation of cell death[98]. Mitochondria isolated from PD patients have reduced complex I activity, decreased ATP production, decreased glutathione levels, and increased ROS-mediated damage[99–102]. Mitochondria are iron-rich organelles. Extracellular iron taken up by the

cell is preferentially transported to the mitochondria where heme and iron-sulfur clusters are synthesized[103]. Moreover, mitochondria are in constant exposure to ROS as electron leaking at complex I and complex III of the electron transport chain leads to the production of superoxide anions ($O_2^{\bullet -}$)[103]. Iron and mitochondria are tightly related; therefore, excess iron has been shown to induce mitochondrial dysfunction and vice versa. Iron overload by ferric ammonium acid treatment promoted mitochondrial fragmentation and increased Drp1 Ser637 dephosphorylation[104]. Drp1 activity in the mitochondria regulates mitochondrial fission[105]. On the other hand, mitochondrial dysfunction by MPTP inhibition of complex 1 induced iron accumulation by increased IRP1 activity and subsequent elevation of DMT1 and TfR1 expression[106].

H63D *HFE* is a common variant potentially carried by 15-25% of the Parkinson's disease population[32]. Although the H63D *HFE* polymorphism is expected to result in an increased amount of intracellular iron that could theoretically exacerbate Parkinson's-related pathology such as oxidative stress or α-synuclein aggregation, no association between this allele frequency and Parkinson's disease risk has been clearly identified (**Table 1-1**). However, molecular studies have shown significant effects of the H63D *HFE* genotype on cellular pathways associated Parkinson's disease pathology. H63D *HFE* expression in SH-SY5Y cells were protected from α-synuclein pre-formed fibril toxicity through the induction of autophagy (Chapter 3). Previous studies have also reported that the TH+ neurons in H67D *Hfe* mice are less vulnerable to paraquat induced toxicity as well as nasal manganese exposure[107,108]. Both of paraquat and manganese exposure cause neurodegeneration and parkinsonian symptoms in humans and mouse models. H63D *HFE* expression seems to trigger multiple response mechanisms that protects the cells from ROS- and aggregated protein-mediated toxicity. Although no clinical association between *HFE* genotype and Parkinson's disease *risk* has been identified to date, *HFE* genotype could help explain the disease

Table 1-1: Summary of studies investigating *HFE* genotype and risk for PD

	Study type	Patient population	Results
Borie, C., et al. (2002)[109]	genotype association	216 patients and 193 age-, sex-, and ethnically-matched controls	No difference in genotype or allele frequency between cases and controls
Buchanan, D.D., et al. (2002)[110]	genotype association	Australian cohort: 438 patients and 485 controls	No association found for H63D *HFE* C282Y *HFE* variant is protective (OR = 0.59, p = 0.014)
Dekker, M.C., et al. (2003)[111]	genotype association	Rotterdam study: 137 PD patients, 47 non-PD parkinsonism, 2914 controls Southwestern Netherlands: 60 PD patients, 25 non-PD parkinsonism	No association found for H63D *HFE* C282Y *HFE* increases risk for PD (OR = 5.4, p = 0.03) C282Y *HFE* increases risk for non-PD parkinsonism (p = 0.009, p = 0.006)
Guerreiro, R.J., et al. (2006)[112]	genotype association	Portuguese cohort: 132 patients and 115 healthy, age-matched controls	No association found for H63D *HFE* C282Y *HFE* increases risk for PD (p = 0.01)
Akbas, N.,et al. (2006)[113]	genotype association	278 patients and 280 ethnically matched controls PD patients were screened for hyperechogenicity of substantia nigra with transcranial ultrasound	No difference in genotype or allele frequency between cases and controls
Aamodt, A.H., et al. (2007)[114]	genotype association	Norway cohort: 388 patients, controls from comparable studies	No difference in genotype or allele frequency between cases and controls
Halling, J., et al. (2008)[115]	genotype association	Faroe Islands cohort:79 patients 154 controls	No difference in genotype or allele frequency between cases and controls
Biasiotto, G., et al. (2008)[116]	genotype association	Italian cohort: 475 patients, controls from comparable studies	No difference in genotype or allele frequency between cases and controls
Greco, V., et al. (2011)[117]	genotype association	Italian cohort: 181 patients and 180 controls	No difference in genotype or allele frequency between cases and controls

Mariani, S., et al. (2013)[118]	genotype association	Italian cohort: 78 patients and 139 healthy controls	No difference in genotype or allele frequency between cases and controls
Pichler, I., et al. (2013)[119]	Mendelian randomization modeling with *HFE* and *TMPRSS6* to estimate serum iron	20,809 PD cases and 88,892 controls	Increased iron levels associated with decreased risk for PD (relative risk reduction of 3% per 10 ug/dl increase in serum iron, p = 0.001)
Rhodes, S.L., et al. (2014)[120]	genotype association	Pooled data from 5 independent case-control studies	No difference in genotype or allele frequency between cases and controls
Xia, J., et al. (2015)[121]	meta-analysis	15 studies (1631 cases and 4548 controls for C282Y; 1192 cases and 4065 controls for H63D)	No association found for H63D *HFE* C282Y HFE is protective (OR = 0.22, p = 0.002)
Duan, C., et al. (2016)[122]	meta-analysis	9 studies (pooled OR used for analysis)	No difference in genotype or allele frequency between cases and controls
Mariani, S., et al. (2016)[123]	genotype association	95 patients and 112 healthy controls	No difference in genotype or allele frequency between cases and controls

heterogeneity seen in the patient population. Currently, there is a lack of mechanistic understanding behind the various manifestations of Parkinson's disease which include a spectrum of motor as well as non-motor symptoms[124]. In the publicly available Parkinson's Progression Marker Initiative (PPMI) Database, H63D *HFE* carriers were found to have lower striatal binding ratio in the caudate compared to WT *HFE* carriers at the baseline visit (0-3 years from diagnosis) (Chapter 2). DAT scan striatal binding ratio represents the presence of dopamine transporters in the brain and therefore is a marker for dopaminergic homeostasis. This is consistent with findings in the H67D *HFE* mouse model which showed decrease in tyrosine hydroxylase expression compared to WT *HFE* mice[107]. Decrease in the striatal binding ratio could represent a deviation from the Parkinson's pathophysiology that is unique in the H63D *HFE* carriers, consequently altering clinical presentation. These observations clearly indicate that evaluation of *HFE* genotype in the

heterogeneity of PD pathology is warranted; particularly given the potential for therapeutic approaches involving iron modification.

1.4.2 Alzheimer's disease

It is estimated that 5.8 million Americans age 65 and older are currently living with Alzheimer's Disease (AD), making it the most common neurodegenerative disorder[125]. As the aging population continues to grow, about 2.3-fold increase in disease prevalence is expected by 2050[126]. AD patients usually present with memory loss, language disorder, and anxiety. With disease progression, cognitive abilities continue to decline leading to loss of independence[127]. AD is characterized pathologically by the presence of plaques formed by deposition of extracellular β-amyloid (Aβ) proteins and neurofibrillary tangles formed by tau proteins[127]. Aβ is generated by an abnormal lysis of the amyloid precursor protein (APP), resulting in secretion and aggregation of the Aβ peptide[128]. Tau, which is hyperphosphorylated under pathological conditions, forms the intracellular neurofibrillary tangles[129].

Similar to Parkinson's disease, there is no effective disease-modifying treatment currently available for AD. The standard of care includes cholinesterase inhibitors (ChEI) which increases the availability of acetylcholine by blocking its degradation. Treatment with ChEIs has been shown to cause modest improvement in cognitive function (about -2.7 points in 70 point ADAS-Cog Scale)[130]. Much of the research into novel therapies for AD has focused on the β-amyloid pathway, targeting the synthesis and aggregation of Aβ; however, none of the phase III clinical trials were able to demonstrate significant effect in patients[131]. This has led to development of investigations for therapies outside of the β-amyloid pathway including antioxidants, glucagon-like peptide-1, rapamycin, cannabinoids, and iron chelators[132].

Abnormal iron distribution in the frontal cortex is seen in AD patients along with Aβ plaques and tau pathology[133]. Using Quantitative Susceptibility Mapping (QSM) MRI and 11-Carbon Pittsburgh-Compound-B PET, cerebral iron was found to colocalize with β-amyloid plaques in subjects with mild cognitive impairment (MCI) and Apolipoprotein E ε4 (APOE-e4) allele who are at increased risk for developing AD. Higher cortical iron also correlated with APOE-e4 allele and MCI status[134]. Increase in magnetic susceptibilities of the caudate nucleus was also associated with decreases in cognitive scores, demonstrating the efficacy of iron as a marker of disease progression[135]. Furthermore, strong correlation in brain iron content and the rate of cognitive decline in AD patients indicate a pathological role of iron[136].

At the cellular level, iron involved in Aβ synthesis as well as plaque and neurofibrillary tangle formation. 5'-untranslated region of amyloid precursor protein (APP) mRNA contain an iron-response element. IRP1 has been shown to bind to APP mRNA and control translation of the protein[137] (**Figure 1-2**). APP has also been proposed to stabilize ferroportin at the cellular membrane allowing for increased export of Fe^{2+} [138]. A recent study has further shown that secreted E2 domain of APP rather than the full-length APP increases ferroportin membrane occupancy[139]. Increased L-ferritin expression can also enhance the γ-secretase activity, leading to increase in Aβ synthesis through APP proteolysis [140]. Increased iron been shown to inhibit β-secretase activity while augmenting α-secretase activity, promoting non-amyloidogenic processing of APP[141,142]. Iron also directly binds to Aβ and tau. Fe (II) and Fe (III) binding promotes aggregation of the amyloid peptide by increasing the beta-sheet structure and activates kinases leading to hyperphosphorylated tau[143–145]. Beyond its interactions with the main pathological proteins of AD, iron is thought to play a role in neurodegeneration through ferroptosis. Ferroptosis is an iron-

dependent cell death pathway that involves ROS-mediated lipid peroxidation[146]. Using a mouse model of tauopathy, α-lipoic acid which has been previously shown to stabilize cognitive function of AD patients was shown to reduce iron accumulation and lipid peroxidation, effectively blocking ferroptosis[147,148].

Figure 1-2

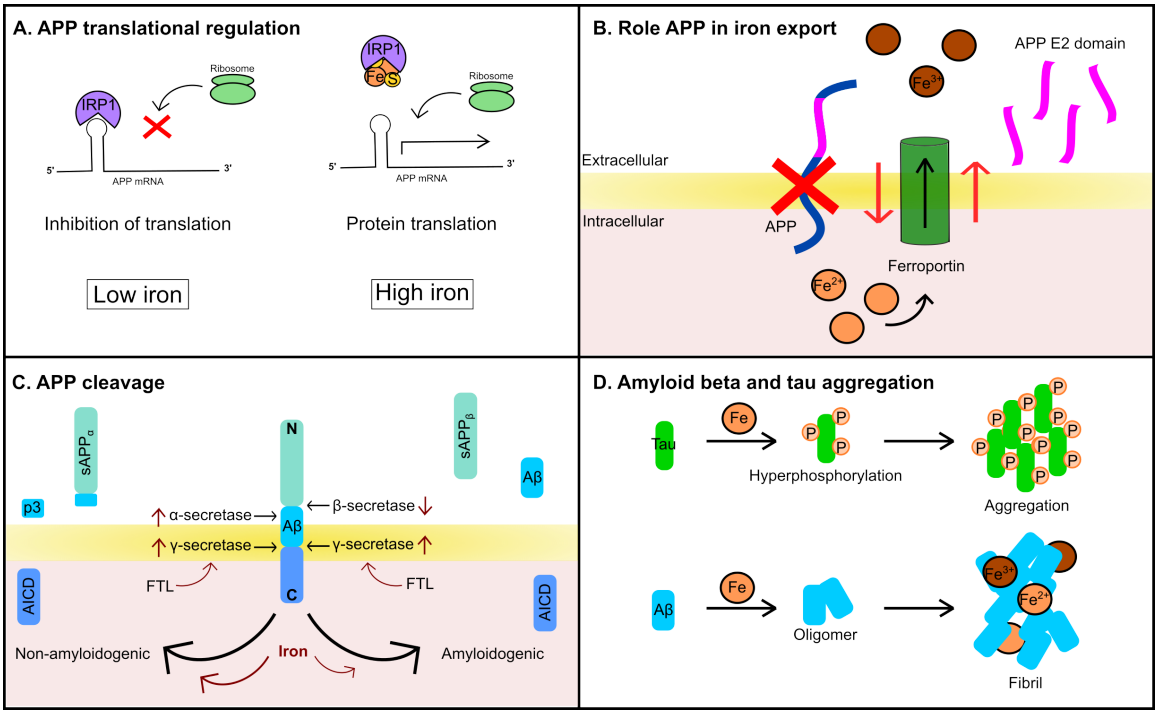

Figure 1-2: Effects of iron on Alzheimer's disease related pathology at the molecular level. (A) Amyloid precursor protein (APP) mRNA contains an iron response element (IRE) that regulates protein translation. With low cellular iron, iron response protein 1 (IRP1) binds to the IRE preventing initiation of translation. With abundant cellular iron, IRP1 binds to iron-sulfur clusters preventing its interaction with the mRNA and APP translation occurs. (B) APP knockout has been shown to decrease ferroportin levels at the cell surface leading to cellular iron accumulation. Specifically, soluble APP E2 domain increases ferroportin membrane occupancy facilitating cellular iron efflux. (C) Cleavage of full-length APP by secretases is a crucial step in

β-amyloid formation and subsequent β-amyloid aggregation. α-Secretase cleavage leads to non-amyloidogenic products while β-secretase activity produces β-amyloid. Iron has been shown to increase α-secretase activity and inhibit β-secretase, collectively promoting non-amyloidogenic cleavage of APP. Ferritin light chain (FTL) involved in cellular iron storage has also been shown to induce γ-secretase activity. (D) Through modulation of multiple kinases including CDK5 and GSK3β, iron has been shown to induce tau hyperphosphorylation leading to increase aggregation. Iron also directly interacts with β-amyloid to promote oligomerization and plaque formation.

The clinical and pathological impact of *HFE* variants on Alzheimer's disease have been studied extensively; however, conflicting data have been published in regards to the genotype effects on disease risk. Multiple studies have shown decreased risk for AD with H63D *HFE* or C282Y *HFE* variants compared to WT *HFE*. As much as 3-fold risk reduction has been reported along with slower rate of temporal lobe atrophy measured by MRI from the Alzheimer's disease neuroimaging initiative (ADNI) dataset[149–154]. On the other hand, some studies have shown that C282Y and H63D *HFE* variants increases the risk for and severity of AD, especially in synergy with polymorphisms in the *Tf* gene[155–157]. The conflicting clinical findings may indicate the presence of other genetic or environmental factors that impact AD risk along with *HFE* genotype. One consistent finding that has been replicated in multiple studies is the effect of H63D *HFE* variant on age of onset. Four studies have reported earlier age of AD onset for H63D *HFE* carriers compared to WT *HFE* patients[158–161].

Preclinical data also have shown complicated relationships between *HFE* variants and various disease processes associated with AD. Altered cholesterol metabolism and increased vulnerability to Aβ toxicity with H63D *HFE* expression in cell culture and impaired spatial memory in H67D

Hfe mouse model have been reported[59,162]. Furthermore, H67D *Hfe* mice had reduced white matter integrity, which was confirmed in cognitive normal human H63D *HFE* cohort[57,58,163]. UK MRC cognitive function and ageing study also showed that for non-APOE-e4 carriers, H63D HFE correlates with severity of white matter lesions associated with aging[164]. In contrast with the white matter changes, transcriptome of the Hfe-/- mouse brain has been reported to show up to 9-fold decrease in the transcript levels of amyloid-β protein precursor, tau, apolipoprotein E, presenilin 1, and γ-secretase components[165]. H63D *HFE* expression is also associated with increased autophagic flux (Chapter 3), which should promote cell viability and decrease protein aggregation.

Although it is not clear whether *HFE* variants are protective or contributory to AD, what is evident is the impact of this genotype on various underlying cellular processes involved in AD pathogenesis. Therefore, *HFE* genotype should be taken into consideration for future studies on novel therapies for AD.

1.4.3 Neurodegeneration with Brain Iron Accumulation

Neurodegeneration with brain iron accumulation (NIBA) is a group of hereditary diseases defined by the presence of elevated iron in the brain, particularly in the basal ganglia[166]. NIBA is genetically and clinically heterogeneous with ten identified subtypes each associated with different genes[167]. Only two genes (*CP* and *FTL*) are directly involved with iron metabolism. Remaining genes (*PANK2*, *PLA2G6*, *C19orf12*, *WDR45*, *FA2H*, *ATP13A2*, *DCAF17*, and *COASY*) encode proteins that have roles in coenzyme A biosynthesis, lipid metabolism, autophagy, and mitochondrial function[167]. Four subtypes of NBIA, which include Pantothenate Kinase-Associated Neurodegeneration (PKAN), Mitochondrial-membrane Associated Neurodegeneration (MPAN), PLA2G6-Associated Neurodegeneration (PLAN), and β-Propeller Protein-Associated

Neurodegeneration (BPAN) (**Table 1-2**), account for > 80% of all NBIA cases and therefore only these subtypes will be discussed in further detail [166]

Table 1-2: NBIA subtypes - associated mutation, pathologies, and iron chelator trials

NBIA Subtypes	Genetic Mutation	Location of Iron Accumulation	Protein Aggregation Pathology	Iron Chelator Treatment
Pantothenate-Kinase Associated Neurodegeneration (PKAN)	Pantothenate kinase 2 (*PANK2*)	Globus pallidus	Tau tangles in the cortex	TIRCON2012V1[168]: Deferiprone was well tolerated; At 18 months, drug treated group had slower disease progression but results were not statistically significant (p = 0.076)
Mitochondrial-membrane Associated Neurodegeneration (MPAN)	*C19orf12*	Globus pallidus	Extensive Lewy body pathology in the basal ganglia and the cortex	Case report[169]: Deferiprone was well tolerated; R2* and QSM measures significantly decreased in the substantia nigra while no changes seen in the globus pallidus
PLA2G6-Associated Neurodegeneration (PLAN)	*PLA2G6*	Variable degrees iron accumulation; most evident in globus pallidus	Lewy bodies in the basal ganglia and the cortex; hyperphosphorylated tau neurofibrillary tangles	None reported
β-Propeller Protein-Associated Neurodegeneration (BPAN)	*WDR45*	Globus pallidus and substantia nigra	Tau neurofibrillary tangles in the cortex, putamen, hippocampus and hypothalamus	Two case reports: Fonderico, et al. 2017[170] reported worsening of parkinsonian symptoms with deferiprone treatment; Lim, et al. 2018[171] showed tolerability of deferiprone with long-term treatment (1 year) but no clinical improvement

Mutations in the pantothenate kinase 2 gene (*PANK2*) are responsible for PKAN, the most common subtype of NBIA[166,172]. PANK2 protein is the only pantothenate kinase to localize to the mitochondria and phosphorylates pantothenate for synthesis of coenzyme A (CoA)[173]. CoA is

essential for the critic acid cycle, amino acid metabolism, and fatty acid synthesis[174]. Iron accumulation in PKAN is limited to the globus pallidus; however, axonal swelling and spheroid bodies along with degenerating neurons are also found in the cortices, typically presenting as progressive motor and cognitive regression in early childhood[175]. Interestingly, tau pathology has also been noted with PKAN represented by threads and tangles to varying degrees in the cortex[176,177]. Similar to PKAN, Mitochondrial-membrane Associated Neurodegeneration (MPAN) also involves mutations in a mitochondrial protein, C19orf12, and iron accumulation is limited to the globus pallidus[178]. MPAN accounts for 30% of all NBIA cases[166]. Unique to MPAN is the presence of extensive Lewy body pathology in the globus pallidus which can spread into the substantia nigra along with near complete neurodegeneration[178]. Normal function of C19orf12 is unknown and mutations in C19orf12 has been associated with multiple neurological diseases including pallido-pyramidal syndrome and hereditary spastic paraplegia type 43[179,180]. MPAN patients have also been reported to mimic signs of juvenile amyotrophic lateral sclerosis, showing predominant upper and lower motor neuron dysfunction without pyramidal involvement[181].

PLA2G6-Associated Neurodegeneration (PLAN) is associated with mutations in the gene that encodes for A_2 phospholipase (*PLA2G6*)[182]. PLA2G6 is expressed at the nuclear envelop, axon terminals, and the inner mitochondrial membrane. It hydrolyses glycolipids to produce lysophospholipids and free fatty acids that are used to maintain membranes, regulate apoptosis, and contribute to various signaling pathways[183]. Disruptions in lipid metabolism from PLA2G6 mutations are thought to lead to dysregulation of mitochondria, apoptosis, autophagy, and vesicular transport[184]. Patients with PLA2G6 mutation present in four clinical subtypes: infantile neuroaxonal dystrophy, atypical neuroaxonal dystrophy, adult-onset dystonia-parkinsonism, and autosomal recessive early-onset parkinsonism[185,186]. Neuroaxonal dystrophies share features with other NBIA subtypes such as childhood-onset progressive psychomotor deterioration and ataxia. On the other

hand, the two other subtypes are adult-onset and present as parkinsonian with bradykinesia, tremors, cognitive decline, and gait disturbances[185,186]. Pathological hallmark of PLAN is the presence of axonal swelling throughout the central nervous system including the cortices, globus pallidus, striatum, cerebellum, brain stem, and the spinal cord. Peripheral axonal swellings are also found in some patients[187]. Iron accumulation is variable depending on the clinical subtype, but it is most clearly notable in the globus pallidus with MRI imaging. Advanced tau and α-synuclein pathologies can also be seen in the degenerating brain areas along with tubulovesicular structures which are membrane-rich inclusions[188,189].

Beta-propeller protein-associated neurodegeneration (BPAN) is caused by a pathogenic mutation in WD repeat domain 45 (*WDR45*) gene located on the X chromosome[190]. Clinically, BPAN manifests in two phases. Patients first present with seizures, infantile-onset developmental delay, and abnormal behavior. During adolescence and early adulthood, some of these initial symptoms resolve while progressive parkinsonism and cognitive decline develop. The onset of neurologic deterioration ranges widely from ages 15-37 years[47]. WDR45 encodes a protein called WD repeat domain phosphoinositide-interacting protein 4 (WIPI4), which has been discovered to play a role in autophagy. A recent study has shown that WIPI4 interacts with ATG2, AMPK, and ULK1 to regulate the size of nascent autophagosomes[191]. Knockdown of WIPI4 with shRNA in a melanoma cell line resulted in about 4-fold decrease in autophagosome formation and accumulation cup-shaped elongated phagophore formation sites[191]. WIPI4 CNS-specific knockout mice recapitulate many BPAN disease phenotypes including memory/ learning defects and motor coordination problems with age[192]. In contrast with other NBIA subtypes, BPAN iron accumulation more prominent in the substantia nigra compared to the globus pallidus. Cerebellar and cerebral atrophy is also present along with tau pathology in the cortices, putamen, and the hippocampus[193].

Although iron accumulation is the defining feature of NBIA, the exact role of iron in the disease process of each subtype is unknown. Whether iron accumulation is the driving pathology behind the neurodegeneration or a byproduct remains to be determined. Mutations in genes such as *PANK2, C19orf12, PLA2G6,* and *WDR45* that are not directly related to the iron metabolism pathway all cause iron accumulation in the same area of the brain – globus pallidus and the substantia nigra. Interestingly, the intensity of iron accumulation for PKAN, MPAN, and PLAN is strongest at the globus pallidus; however, for BPAN, iron accumulation is strongest at the substantia nigra perhaps linking this subtype to Parkinson's disease where iron accumulation is seen in the substantia nigra.

Each subtype of NBIA share features with other more common neurodegenerative diseases. Tau pathology and lipid metabolism defects are found in Alzheimer's disease. Lewy bodies, iron accumulation in the substantia nigra, autophagy inhibition, and mitochondrial dysfunction are hallmarks of Parkinson's disease. Previous studies have shown that H63D *HFE* reduces cerebral white matter integrity in cognitively normal carriers and reduces spatial memory in the H67D *HFE* mouse model[58,59]. Combined with clinical studies that show earlier age of AD onset in H63D *HFE* carriers[158–161], the effects of *HFE* variant as a modifier of cognitive decline in NBIA patients can be speculated. Furthermore, SH-SY5Y cells expressing H63D *HFE* had increased basal autophagic flux, protecting them from α-synuclein induced toxicity (Chapter 3). NBIA subtypes that present with Lewy bodies (PLAN and MPAN) as well as BPAN which has direct autophagic impairment could also be modified by the H63D *HFE* variant.

1.4.4 Amyotrophic lateral sclerosis

Amyotrophic lateral sclerosis (ALS) is a neurodegenerative disease that is characterized the loss of both upper and lower motor neurons. Patients can present with spinal-onset, which involves

muscles of the limbs, or bulbar-onset, characterized by dysarthria and dysphagia. Muscle weakness and motor deficits continue to progress over weeks to months along with cognitive or behavioral changes[194]. Mean survival with disease ranges from 24 – 48 months[195]. Only two FDA approved drugs are available for treatment: riluzole and edaravone. In the original clinical trial, riluzole reported increased survival by 3 months[196,197]. Edaravone has been shown to slow disease progression in a small subset of patients with rapid progressing disease[198]. The underlying pathophysiology of ALS is poorly understood and multiple pathways have been identified to be associated with the disease including dysfunctions in mitochondria, axonal transport, protein degradation pathways, and reactive oxygen species handling[199]. The recurring pathological hallmark of ALS is the presence of ubiquitinated protein inclusions in motor neurons. Generally, these inclusions are composed of TAR DNA binding protein 43 (TDP-43)[200]. About 97% of patients have TDP-43 proteinopathy[194]. Loss of normal TDP-43 function as a transcription factor as well as gain of toxic function as aggregated protein are thought to be involved in the neurodegeneration. Similar to α-synuclein, TDP-43 may act like a prion to initiate cascades of protein misfolding[201].

Iron accumulation is also a commonly found pathology that has been identified in sporadic and familiar ALS as well as in mouse models. Mutation in C9orf72 is the most common genetic cause of ALS[202]. The 5'-untranslated region of C9orf72 mRNA has been identified to contain a putative iron responsive element that has secondary structure alignment with IREs found in mitochondrial cis-aconitase, L-ferritin, and H-ferritin, making C9orf72 expression potentially responsive to cellular iron levels[203]. Clinically, increased iron levels in the cerebral cortex of ALS patients have been detected using MRI scans[204]. Quantitative susceptibility mapping was used to map areas of iron accumulation in the brain of ALS patients. The motor cortex and the basal ganglia were found to have elevated iron levels[205]. Imaging studies were confirmed with postmortem histology showing iron accumulation with Perl's stain[204]. Transferrin saturation and serum ferritin are also increased

in ALS patients compared to healthy controls[206,207]. With the involvement of iron dysregulation in ALS pathology, recent studies have focused on markers of ferroptosis in animal models and in patients. SOD1 (G93A) overexpressing rats were shown to have abnormal mitochondria and lipid droplet accumulation, which are both signs of ferroptosis[208]. Furthermore, lipid peroxidation product hydroxy-2,3-nonenal (HNE) was elevated in serum and CSF of ALS patients and correlated with disease severity[209,210].

Two studies have shown that ALS patients with H63D *HFE* variant have longer survival[211,212]. Additionally, four other studies have found overrepresentation of H63D *HFE* variant in the ALS patient population compared to healthy controls[213–216] (**Table 1-3**). This may be interpreted as increased risk for ALS with this *HFE* variant; however, because some studies show increase in survival with disease, the overrepresentation of H63D *HFE* could be due enrollment bias, further supporting the idea that H63D *HFE* slows progression of ALS. Intriguingly, the preclinical data using H67D *Hfe*/SOD1(G93A) double mutant mice show an opposite effect with accelerated disease progression, increased caspase-3 level, and decreased Nrf2 expression[217]. The discrepancy in clinical and preclinical results may point to the difference in the impact of H63D *HFE* variant on sporadic ALS compared to SOD1 mutation associated familial ALS.

Table 1-3: Studies investigating clinical impact of HFE genotype in ALS

Study	Study type	Patient population	Results
Yen, et al. (2004)[218]	genotype association	51 ALS patients 47 controls US cohort	No difference in genotype or allele frequency between patients and controls. % H63D HFE variant in ALS population: **25.5**
Wang, et al. (2004)[214]	genotype association	121 ALS patients 133 controls US cohort	Significantly higher frequency of HFE mutation in ALS patient population compared to control % H63D HFE variant in ALS population: **30**
Goodall, et al. (2005)[215]	genotype association	379 ALS patients 400 controls Italian and Sardinian cohorts	H63D polymorphism is overrepresented in patients with ALS (OR = 1.85) % H63D HFE variant in ALS population: **34.3**
Sutedja, et al. (2007)[213]	genotype association	289 ALS patients 5886 controls Dutch cohort	H63D variant is associated with increased risk for ALS (OR = 1.7) % H63D HFE variant in ALS population: **27.8**
He, et al. (2011)[216]	genotype association	195 ALS patients 405 controls Chinese cohort	Increased risk for ALS in H63D HFE heterozygous carriers (OR = 3.10) % H63D HFE variant in ALS population: **10.26**
Praline, et al. (2012)[219]	genotype association	824 ALS patients 583 controls French cohort	H63D HFE polymorphism is not associated with ALS % H63D HFE variant in ALS population: **27**
Van Rheenen, et al. (2013)[220]	genotype association	3962 ALS patients 5072 controls European cohort	No association between H63D HFE polymorphism and ALS risk, age of onset, or survival % H63D HFE variant in ALS population: **26**
Su, et al. (2013)[212]	genotype and disease duration	38 ALS patients US cohort	Increased disease duration with H63D HFE carriers compared to WT HFE ALS patients ($p = 0.017$)
Li, et al. (2014)[221]	meta-analysis	14 studies: 5849 ALS patients 13,710 controls	C282Y HFE variant is protective against ALS ($p = 0.005$) but no association found between H63D HFE variant and ALS
Chio, et al. (2015)[211]	genotype and ALS phenotype	1351 ALS patients 1423 controls Italian and Sardinian cohorts	In subset of ALS patients with SOD1 mutation, H63D HFE variant carriers had longer survival compared to WT HFE carriers. % H63D HFE variant in ALS population: **31.4**

1.4.5 Other

Friedreich's ataxia (FRDA) is an autosomal recessive disease caused the GAA triplet repeat expansion in the frataxin (*FXN*) gene[222]. Function of the frataxin protein is not completely characterized; however, studies have shown that it is involved in iron-sulphur cluster formation in the mitochondria[223]. Yeast studies have also shown a strong association between frataxin and mitochondrial iron[224]. GAA triplet expansion results in loss of frataxin function leading to reduced activity of iron-sulphur cluster containing enzymes and aberrant mitochondria iron homeostasis[225]. Although iron accumulation has been shown in cardiomyocytes and glial cells, whether neuronal iron accumulation occurs in FRDA is unclear[225–227]. Neurodegeneration associated with FRDA which involves the peripheral sensory nerves as well as the spinal cord is thought to occur through mitochondrial dysfunction[228]. One study has been conducted investigating the relationship between FRDA and *HFE* variants. Adjusting for *FXN* GAA repeat size, C282Y *HFE* carriers were found to have earlier age of onset by 3.72 years. Neither H63D nor C282Y *HFE* variants affected clinical disease severity[229].

Multiple sclerosis (MS) is a chronic inflammatory disease of the central nervous system that is characterized by white matter lesions disseminated in time and space. Patients commonly present with relapsing-remitting disease and typical symptoms include fatigue, vision problems, dizziness, numbness, and gait difficulties[230]. On imaging, MS patients have iron depositions in deep gray matter structures such as the red nucleus as well as around white matter lesions[231,232]. Gray matter iron content has been shown to be correlated with atrophy and cognitive impairment[233,234]. Although imaging correlation with neurodegeneration has been identified, it is unclear how iron deposition is involved in the inflammatory processes of MS. As previously mentioned, H63D *HFE* carriers have reduced white matter integrity[57]. Because MS is a disease predominantly affecting the white matter, the impact of *HFE* variants on MS severity can be hypothesized. Few studies on *HFE*

variants have been conducted with the MS patient population. Two studies show no association in disease susceptibility with *HFE* variants; however, higher MS disability score and worse prognosis has been shown to correlate with H63D *HFE* and C282Y *HFE* carriers, respectively[235–238].

1.5 Iron targeting therapies

1.5.1 PD: FAIRPARK trial

Deferiprone is an iron chelator that is FDA approved for treatment of chronic refractory anemias as a result of frequent blood transfusions. Patients with acute leukemia or thalassemia major were first to be enrolled into clinical trials of deferiprone[239]. With the emerging themes of iron accumulation in association with neurodegeneration, deferiprone has been under investigations as a disease-modifying therapy for multiple conditions including Parkinson's disease. The safety and efficacy of deferiprone in reducing brain iron was first shown by trials in Friedreich's Ataxia[240]. Extensive preclinical trials have shown neuroprotective effects of deferiprone in multiple cell culture and animal models of Parkinson's disease. Mesencephalic cells and SH-SY5Y neuroblastoma cells treated co-treated with MPP+ and deferiprone showed decreased lipoperoxidation and cytotoxicity[241,242]. In 6-OHDA rat model, systemic deferiprone treatment prevented loss of dopaminergic neurons and striatal dopamine content was maintained[243]. A53T α-synuclein transgenic mice that have increased α-synuclein aggregation also showed improvements in rotarod and novel object recognition after deferiprone treatment[244]. Additionally, deferiprone was able to rescue SH-SY5Y cells from pre-formed fibril mediated cytotoxicity.

Phase I deferiprone trial (FAIRPARK-I)[69] used a delayed start/ delayed cessation paradigm to assess the safety and efficacy of deferiprone in reducing brain iron content. Dose established by the Fredrich's Ataxia trail (30mg/kg/day) was administered for 18 months. Brain iron content was

measured every 6 months by MRI R2* and clinical progression was monitored by United Parkinson's Disease Rating Scale (UPDRS) part III motor score. Significant decline of iron in the substantia nigra was found. Clinically, while the early start group showed improvement of ~2 points in UPDRS III, delayed start group failed to show significant improvement even after starting the deferiprone treatment[69]. Of significant note is that the FAIRPARK trial did not consider the *HFE* genotype of the enrolled patients. Pre-formed fibril model with SH-SY5Y cells showed that for H63D *HFE* variant expressing cells, deferiprone treatment was unable to protect the cells against PFF-mediated apoptosis (Chapter 3). *HFE* genotype of the enrolled patients in the ongoing FAIRPARK-II trial should be used to stratify the patients for improved interpretation of the results.

1.5.2 AD: Iron chelators - desferrioxamine, clioquinol, PBT2, deferoxamine, deferiprone

First iron chelator trial for Alzheimer's disease demonstrated the efficacy of longitudinal desferrioxamine treatment in slowing disease progression assessed by activities of daily living[245]. This study was followed by a pilot phase 2 trial of metal chelator clioquinol, which has moderate affinities for iron, copper, and zinc, further demonstrating the efficacy of iron chelation therapy in reducing amyloid plaques and delaying cognitive decline[246]. Two other chelators, PBT2 and deferoxamine, have also shown efficacy in preclinical models[247–250]. Iron chelator therapy development for AD is an active area of research with current phase 2 trial of deferiprone in patient recruitment. In the Deferiprone to Delay Dementia (The 3D Study) trial (NCT03234686), patients with prodromal and mild Alzheimer's disease will receive 30mg/kg/day of deferiprone or placebo. The primary outcome of the study is to determine whether deferiprone is able to delay cognitive decline measured by a neuropsychological test battery (NTB).

1.5.3 NBIA: PKAN and BPAN deferiprone trials

Because Neurodegeneration with Brain Iron Accumulation is characterized by elevated brain iron, logically, iron chelator deferiprone has been under investigation as a potential therapy. PKAN is the most common subtype of NBIA therefore most of the deferiprone trials have been focused on this subpopulation. Small pilot trials with around 5-6 patients confirmed the safety in longterm use of deferiprone and the efficacy of the drug in reducing iron content in the globus pallidus of PKAN patients measured by MRI R2*[251–254]. As a follow-up to the pilot trials, an international multicenter trial was conducted with 88 patients randomly enrolled into the drug or placebo groups. Again, imaging showed decreased iron in the basal ganglia with mild decrease in disease progression at 18 months into treatment. However, extension of 18 more months showed no additional benefits[168]. Two case reports of deferiprone treatment in BPAN patients have also been published. One patient showed exacerbation of UPDRS III score after 5 months of treatment and withdrew while the second patient saw no effects[170,171]. The failure of iron chelator therapy to dramatically improve PKAN and BPAN even with reduction in brain iron content demonstrates the complexity of the underlying pathophysiology while raising the question on the role of iron in the neurodegenerative processes of NBIA.

1.5.4 ALS: FAIR-ALS trial

Based on previous studies that demonstrated efficacy of iron chelators in decreasing neuronal death, preventing TDP-43 protein aggregation, and improving motor functions in SOD1(G93A) mouse model of ALS[255–257], a pilot phase I trial was conducted to test the safety of 30 mg/kg/day deferiprone treatment[258]. A total of 23 early sporadic ALS patients were enrolled and treated for up to 12 months. Decrease ALS Functional Rating Scale (ALSFRS-R), which is indicative of disease progression, was significantly smaller for the deferiprone treatment group at the 3-month time point[258]. The body mass index of treated patients decreased slightly during the first 3 months but

remained unchanged for the next 9 months[258]. Although this pilot study was conducted with a small patient cohort, the disease modifying effect of deferiprone seems promising. Phase 2 trial (FAIR-ALS II) is currently in recruitment (NCT03293069).

1.6 Conclusion

Maintaining iron homeostasis is essential for all cells in the body. In particular, the importance of iron in normal functions of the brain as well as in disease development has been well established. Although iron accumulation is a common pathological finding in the brain, the role of iron in each disease slightly differs. Furthermore, iron is only available through interaction with the environment (i.e. dietary, inhalation) making iron and iron regulating genes strong contributors to the gene-environment interaction that is central to many neurological disease processes. Polymorphisms in iron regulating genes like *HFE* have been demonstrated to have significant clinical and pathophysiological impact in the nervous system. Of special importance is the role of the H63D *HFE* variant. H63D *HFE*, present in up to 15-20% of the general population, is a significant modifier of multiple neurological diseases with subsequent implications in therapy development. Patient stratification by *HFE* genotype is strongly encouraged for better interpretation of future clinical trials and potential insights into pathogenic processes that could be targeted for modification.

Chapter 2

H63D variant of the homeostatic iron regulator gene (*HFE*) is a genetic modifier of Parkinson's disease

2.1 Abstract

Background: Iron accumulation in the substantia nigra is a consistent pathological finding in Parkinson's disease, leading to multiple studies investigating the impact of polymorphisms in iron related genes on disease risk. However, effects of these polymorphisms on disease progression or biomarkers have not been explored.

Objective: We interrogated the effects of commonly occurring H63D variant of the homeostatic iron regulatory (*HFE*) gene on DaTscan SPECT imaging, United Parkinson's Disease Rating Scale part III, and α-synuclein RNA and protein levels.

Methods: Using data from the Parkinson's Progressive Markers Initiative, clinical disease profile in WT *HFE* and H63D *HFE* carriers were analyzed. Blood *SNCA* RNA count and CSF α-synuclein levels at baseline were also compared between the two genotypes.

Results: H63D *HFE* carriers were found to have lower contralateral caudate striatal binding ratio at baseline along with slower reduction in the striatal binding ratio with increasing disease duration. Furthermore, the estimated rate of change in the Unified Parkinson's Disease Rating Scale part III for H63D *HFE* carriers (1.63 points per year; 95% CI, 1.21 – 2.05) was less than patients with WT *HFE* (2.16 points per year; 95% CI, 1.89 – 2.43) with rate difference of 0.53 points (95% CI, -1.03

to -0.03, p = 0.039). Lastly, H63D *HFE* carriers had altered the blood *SNCA* RNA transcript and CSF α-synuclein levels compared to patients with WT *HFE*.

Conclusion: These findings support that H63D *HFE* is a genetic modifier of Parkinson's disease and has the potential to impact interpretation of clinical trials.

2.2 Introduction

Parkinson's disease (PD) is a progressive movement disorder characterized clinically by the presence of resting tremor, bradykinesia, and rigidity. It is the fastest growing neurodegenerative disorder with rising global disease burden[259]. The current standard of care for PD which consist mainly of dopaminergic replacement therapies fail to alter the progression of the disease[260]; therefore, there is an imminent need for identification and development of novel therapeutics.

The Parkinson's Progression Markers Initiative (PPMI) was developed to address one of the major obstacles in therapy development for PD, which is the lack of biomarkers for tracking disease progression. The PPMI is an international multicenter study that collects imaging, clinical, and biological information from de novo PD patients over time[261]. Using this PPMI database, we investigated the effects of the H63D *HFE* variant on the progression of Parkinson's disease measured by the United Parkinson's Rating Scale (UPDRS) and the DaTscan striatal binding ratio. UPDRS is widely used for tracking PD progression and is divided into 4 parts, which include Part I: Non-Motor Aspects of Experiences of Daily Living, Part II: Motor Aspects of Experiences of Daily Living, Part III: Motor Examination, and Part IV: Motor Complications[262]. Multiple studies have shown the efficacy of the UPDRS in tracking disease progression[263–265]. DaTscan SPECT imaging uses I-123 Ioflupane, which has a high affinity for presynaptic dopamine transporters. Striatal binding ratio calculated by using the intensity of the Ioflupane signal from the SPECT

images is used as a marker for dopaminergic neurons. DaTscan SBR has been shown to be correlated with disease severity and duration[266,267].

α-Synuclein is the main protein component of Lewy bodies and toxicity of its aggregated form is thought to be one of the main causes for neurodegeneration in Parkinson's disease[268]. Due to its critical role in disease pathogenesis, α-synuclein has been under investigation as a potential biomarker. Studies have shown increased phosphorylated form of α-synuclein in skin and gut mucosal biopsies of Parkinson's disease patients[269,270]. On the other hand, α-synuclein in body fluids like CSF, plasma, and serum was lower in patients compared to healthy controls[271–274]. Furthermore, conflicting studies have been published on whether α-synuclein correlate with disease severity[275]. Better understanding of factors affecting α-synuclein level is needed to determine the efficacy of this protein as a marker for disease progression.

Homeostatic iron regulator (HFE) regulates iron uptake into cells through its interaction with the transferrin receptor[276]. Polymorphisms in the *HFE* gene have been identified to be a disease modifier of multiple neurodegenerative diseases including amyotrophic lateral sclerosis and Alzheimer's disease[214,217,277,278]. Because iron accumulation is an important component of Parkinson's disease pathophysiology, *HFE* variants, especially the highly prevalent H63D *HFE*, have the potential to affect α-synuclein pathology as well as the disease progression. H63D *HFE* is estimated to be present in 13.5% of the US population and previously been shown to increase brain iron content as well as to protect dopaminergic neurons from paraquat toxicity in an animal model[55,107,279].

Although the common H63D *HFE* polymorphism is expected to result in an increased amount of intracellular iron that could theoretically exacerbate Parkinson's-related pathology, no association between this allele frequency and Parkinson's disease risk has been clearly identified[111,113,114,120,280]. However, what has been lacking in these studies is an evaluation of the progression of Parkinson's disease. Using existing human dataset, this current study examines the effects of H63D *HFE* genotype on Unified Parkinson's Disease Rating Scale (UPDRS) part III motor score and DaTscan striatal binding ratio, a marker for dopaminergic neurons. Lastly, we examined the effects of the H63D *HFE* genotype on blood *SNCA* transcript and CSF α-synuclein protein levels.

2.3 Materials and Methods

2.3.1 Human dataset

All human data sets were downloaded from Parkinson's Progression Marker Initiative (PPMI) website (http://www.ppmi-info.org/data). PPMI is an international multicenter study that include institutions in United States, Europe, and Australia. All data sets were sex- and age-matched (**Table 2-1, Table 2-3, Table 2-5, Table 2-7).** *HFE* genotype was identified for each patient using NeuroX SNP data. Patients with other *HFE* polymorphisms including C282Y *HFE* were excluded from analysis. Patients homozygous for H63D *HFE* were included in the H63D *HFE* carrier group to represent a dominant allele model. With the CSF α-synuclein protein level data[281], samples with no RBC count information or > 50 cells/ mm^3 were excluded, consistent with previously published guidelines for α-synuclein biomarker studies [282]

2.3.2 DaTscan

DaTscan SPECT data was acquired at PPMI imaging centers and all raw SPECT images were analyzed at the Institute for Neurodegenerative Disorders, New Haven, CT. Briefly, images were normalized to the standard Montreal Neurologic Institute space and the slice with highest striatal uptake was identified. 8 slices around the hottest slice were averaged to generate a single slice. Regions of interest (ROIs) including right and left caudate, right and left putamen, and the occipital cortex (reference) were identified. Count densities for each ROI was extract and the striatal binding ratio (SBR) was calculated as (target region/reference region) -1. Ipsilateral and contralateral sides were determined using the patient's dominant side information from PPMI. If no dominant side is present, an average of the right and left sides was used. Mean striatum SBR was calculated by (sum of all 4 ROIs)/4.

2.3.3 Statistical analysis

Patients with DaTscan imaging diagnosis of Scans Without Evidence of Dopaminergic Deficit (SWEDD) were excluded from all analyses. DaTscan baseline striatal binding ratio (SBR) was analyzed using generalized linear model controlling for age at scan and sex. Linear mixed effect model was used to model the progression of contralateral caudate SBR with increasing disease duration. Disease duration was calculated using the date of scan acquisition and disease diagnosis date. Participant- and study site-specific random effect was used to account for any correlation among repeated measurements. Potential confounders such as age, disease duration at baseline, and sex were adjusted. 5-year progression of UPDRS part III score[263] was evaluated using a linear mixed effect model fit by maximum likelihood. UPDRS III score data from baseline visit to 5-year visit were used for the analysis. UPDRS III subscores were calculated as follows: Tremor (items 3.15-3.17), Bradykinesia (items 3.4-3.7, 3.14), Rigidity (items 3.3), Postural/ Gait Instability (items 3.10-3.13). Participant- and study site-specific random effect was used to account for any

correlation among repeated measurements. Known and potential confounders, including age at diagnosis, sex, baseline Montreal Cognitive Assessment (MoCA) score, and DaTscan contralateral caudate striatal binding ratio, were adjusted [283,284]. Statistical analyses for α-synuclein NanoString transcript count data[273] and CSF α-synuclein protein level data[285] were performed with log-transformed due to positive skewing. Two-way ANOVA with multiple comparisons test were used to compared unadjusted means (**Table 2-6**). Least-squares means and 95% confidence intervals were calculated after general linear model (GLM) controlling for age, sex, and RBC count (blood RNA only). lsmeans R package was used to calculate and contrast least-square means. Residuals from the models were checked for normality and homoscedascity. Analyses were performed using R version 3.5.3 and GraphPad Prism version 8.2.1. Unless otherwise noted, values in figures are presented as mean with standard error of the mean. Generally, Student's t-test or one-way ANOVA with *post hoc* multiple comparisons test were used. Statistics used for each figure is noted in the legend.

2.4 Results

2.4.1 DaTscan striatal binding ratio at baseline and with progression

Using the de novo Parkinson's disease cohort within the PPMI database, the effect of *HFE* genotype on the DaTscan striatal binding ratio at baseline and with progression with increasing disease duration was investigated. Total of 339 Parkinson's disease (PD) patients and 156 healthy controls (HC) were present in PPMI with baseline with *HFE* genotype information from the NeuroX chip data. The PD cohort included 90 patients who were H63D *HFE* carriers and the HC cohort had 55 H63D HFE carriers. The cohorts were age- and sex-matched (**Table 2-1**). For further

analysis, patients with normal DaTscan results labeled as Scans Without Evidence of Dopaminergic Deficit (SWEDD) were excluded.

Table 2-1: *HFE* Genotype Frequencies and Demographics

	PD (N = 339)	Healthy Control (N = 156)	p-value*		
***HFE* (N, %)**			**OR**	**95% CI**	**p-value**
WT	248 (73.45%)	101 (64.74%)	0.663	0.442 – 0.999	**0.0486**
H63D	90 (26.54%)	55 (35.36%)			
Baseline Age (mean, SD)	61.34 (9.89)	60.43 (11.75)	0.3715		
Sex (N, %)					
Male	225 (66.37%)	101 (64.74%)	0.7598		
Female	114 (33.63%)	55 (35.36%)			

* Odds ratio, 95% confidence interval, and p-value for *HFE* frequency were calculated using logistic regression with diagnosis as dependent variable and *HFE*, baseline age, and sex as independent variables. Student's t-test (baseline age) and Fisher's exact test (sex) were used to compare PD and control groups.

The striatal binding ratios (SBR) for caudate and putamen were calculated from raw SEPCT images at the Institute for Neurodegenerative Disorders, New Haven, CT and provided by the PPMI. Ipsilateral and contralateral sides were determined using the dominant side information. Left and right-side values were averaged if no dominant side was present. Generalized linear mixed effect model was used to adjust for age, sex, and disease duration at scan acquisition.

At baseline, the mean striatum SBR was calculated by taking the average of SBR values from left and right caudate and putamen. The mean striatum SBR was not significantly different between WT and H63D *HFE* carriers within the PD and the HC cohorts. However, H63D *HFE* PD patients were trending towards lower mean striatum SBR (p-value = 0.0665) (**Fig. 2-1A**). Ipsilateral caudate, ipsilateral putamen, and contralateral putamen SBR were also found to be similar between

WT and H63D *HFE* carriers (**Fig. 2-1B, D, E**). On the other hand, contralateral caudate SBR was significantly lower in the H63D *HFE* PD patients compared to WT *HFE* patients (**Fig. 2-1C**).

Figure 2-1

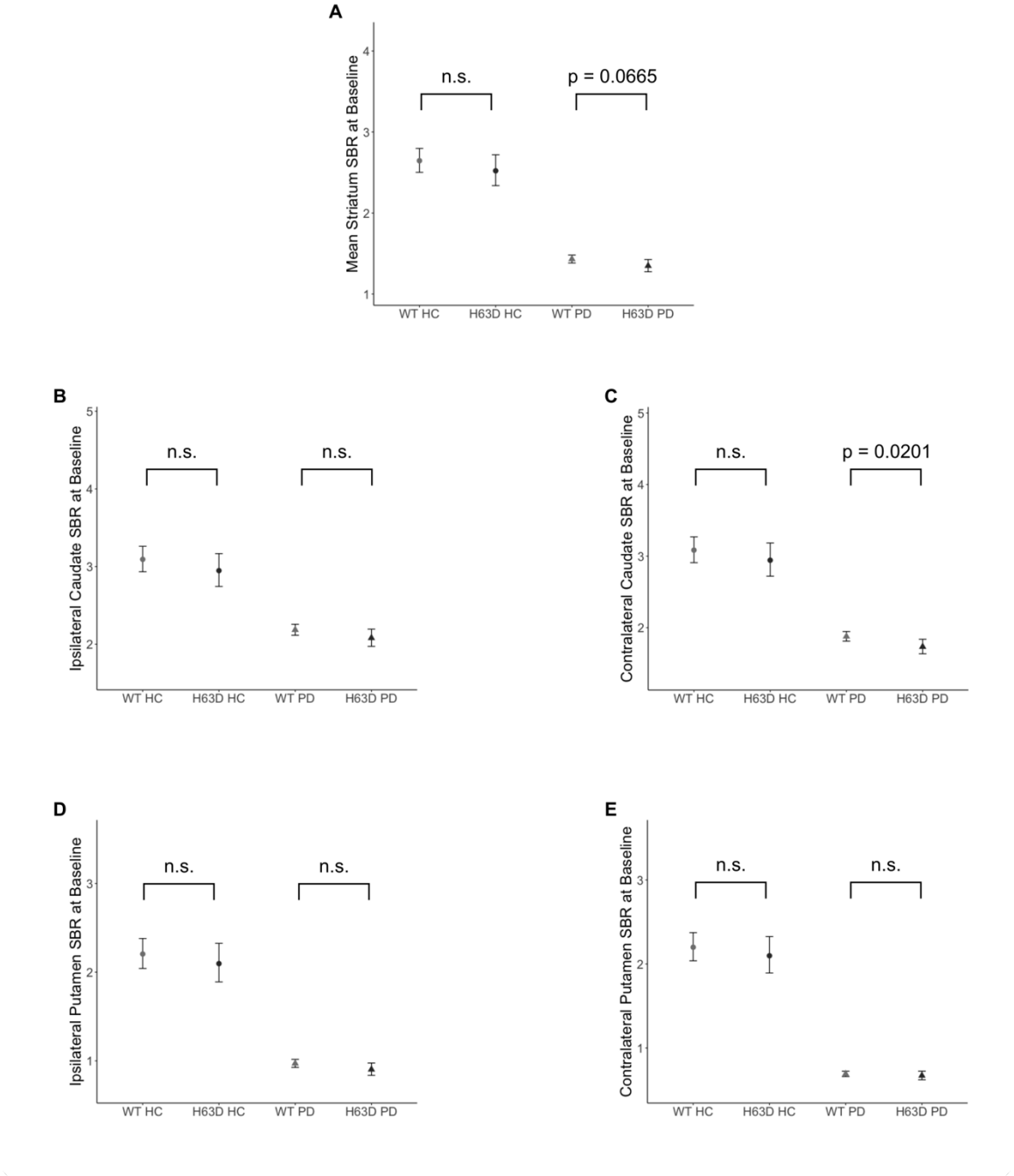

Figure 2-1: Baseline DaTscan Striatal Binding Ratios (SBR). DaTscan SPECT was acquired at PPMI imaging centers. Total of 137 healthy controls (HC) and 334 Parkinson's disease (PD) patients had DaTscan data available from the baseline visit. Within the healthy control group were 48 H63D *HFE* carriers and within the Parkinson's disease group there were 244 H63D *HFE* carriers. (A) Mean striatum SBR was calculated by taking the average of the 4 regional SBRs (left and right caudate, left and right putamen). In the healthy control population, there was no difference between WT and H63D *HFE* carriers while H63D *HFE* carriers in the PD group were trending lower. (B-C) Ipsilateral and contralateral caudate SBR were analyzed using generalized linear model. H63D *HFE* carriers with Parkinson's disease were found to have significantly lower contralateral caudate SBR at baseline. (D-E) Similar to the caudate SBR values, ipsilateral and contralateral putamen SBR was analyzed with generalized linear model. No significant differences were found between WT and H63D *HFE* carriers. Least-squares means ± 95% confidence intervals are shown.

The contralateral caudate SBR data was further investigated by analyzing the progression of the SBR values with increasing disease duration. In the WT *HFE* PD group, SBR decreased with longer disease duration by 0.124 points per year (95% CI: 0.264 to 0.026). H63D *HFE* PD patients had a significantly lower reduction in SBR (0.110 point per year, 95% CI: 0.120 to 0.010) (**Fig. 2-2**). The rate difference between the groups was -0.0139 (95% CI: -0.026 to -0.018, p-value = 0.024) (**Table 2-2**).

Figure 2-2

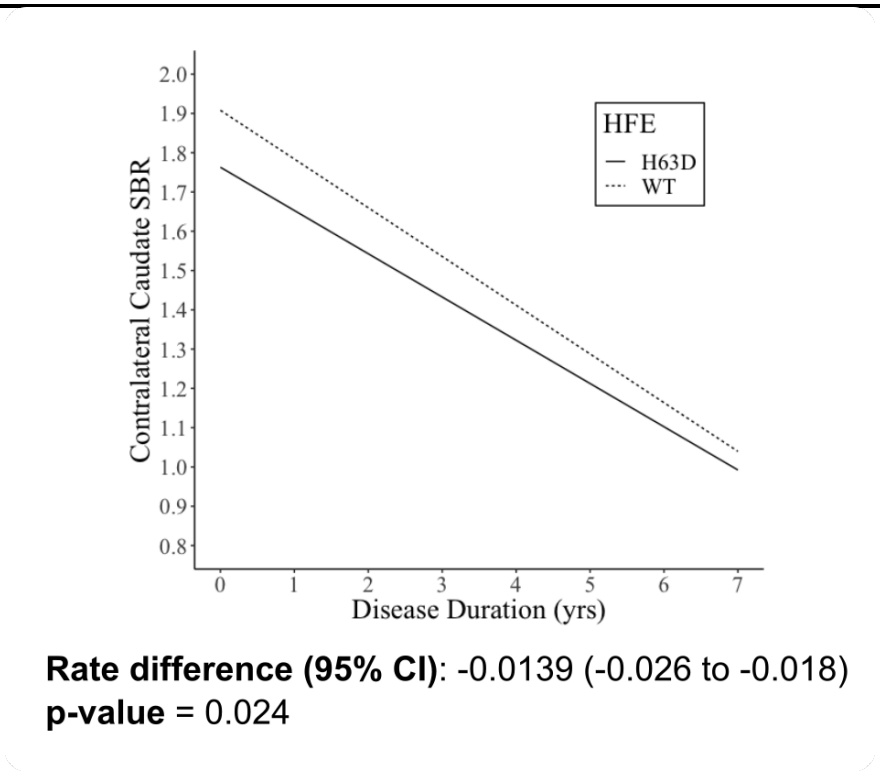

Figure 2-2: **Contralateral Caudate SBR Progression.** Contralateral caudate SBRs, which showed baseline difference between WT and H63D *HFE* carriers were further analyzed for effects of *HFE* genotype on SBR progression with increasing disease duration. Covariates were fixed at the following values: Baseline disease duration (yrs) = 0.57497, Age at diagnosis = 60.866, Sex = average between male and female. Contralateral caudate SBR was found to decrease with disease duration at 0.124 points (95% CI: 0.264 to 0.026) per year for WT *HFE* PD patients. Rate of decrease in SBR was significantly lower in H63D *HFE* PD patients with 0.110 points (95% CI: 0.120 to 0.010) with rate difference of 0.0139 (p-value = 0.024).

Table 2-2: Contralateral Caudate SBR Progression Model

Independent variables	**β (95% CI)**	**p - value**
Disease duration at baseline (yrs)	0.123 (0.046 to 0.199)	**0.002**
HFE genotype (reference: WT)	-0.124 (-0.130 to -0.118)	**0.044**
Age at diagnosis	-0.0021 (-0.0058 to 0.0016)	0.254
Sex (reference: female)	-0.044 (-0.154 to 0.066)	0.431
Rate difference	-0.0139 (-0.026 to -0.0018)	**0.024**

2.4.2 Total UPDRS part III and subscores progression

Baseline demographic and clinical features between Parkinson's disease patients with WT and H63D *HFE* genotype were generally similar as shown in **Table 2-3**. In **Fig. 2-1**, we showed that Parkinson's disease patients with H63D *HFE* genotype were found to have significantly lower contralateral caudate DaTscan SBR compared to WT *HFE* patient population. DaTscan SBR is a marker for dopaminergic dysfunction and previous studies have found that it correlates with disease severity and duration[266,267]; therefore, contralateral caudate SBR was used as an independent variable in analysis of UPDRS part III progression.

Table 2-3: UPDRS Part III Progression Baseline Characteristics

Characteristics	PD patients		p -value*
	WT HFE (n = 248)	H63D HFE (n = 90)	
Demographics			
Age at diagnosis (mean, SD)	60.74 (9.96)	60.79 (9.95)	0.966
Age (mean, SD)	61.35 (10.05)	61.23 (9.53)	0.926
Sex (N, %)			
Male	159 (64.11%)	65 (72.22%)	0.193
Female	89 (35.89%)	25 (27.78%)	
Disease Severity (mean, SD)			
Disease duration (yrs)	0.61 (0.72)	0.44 (0.62)	0.056
Hoehn & Yahr scale	1.52 (0.50)	1.52 (0.50)	0.9214
UPDRS I	5.92 (4.07)	5.45 (4.23)	0.3776
UPDRS II	5.81 (4.29)	5.86 (4.07)	0.9339
UPDRS III	20.20 (8.54)	21.70 (10.10)	0.176
Total MoCA	27.03 (2.32)	27.14 (2.13)	0.688
Imaging (mean, SD)			
DaTscan contralateral caudate striatal binding ratio	1.87 (0.59)	1.73 (0.45)	**0.020**

*p-values calculated with Student's t-test or Fisher's exact test (sex).

Linear mixed-effects models were used to examine the association of H63D *HFE* variant and the rate of change in UPDRS part III score, adjusting for age at diagnosis, sex, baseline total MoCA score, and DaTscan contralateral caudate SBR (**Table 2-4**). The progression of UPDRS part III subscores were also similarly analyzed. The estimated rate of change in the Unified Parkinson's Disease Rating Scale III motor score for H63D *HFE* carriers (1.63 points per year; 95% CI, 1.21 – 2.05) was less than patients with WT *HFE* (2.16 points per year; 95% CI, 1.89 – 2.43) with rate difference of 0.53 points (95% CI, -1.03 to -0.03, p = 0.039) (**Fig. 2-3A**). The Tremor subscore of UPDRS part III showed significant difference between WT and H63D *HFE* carriers. Increase in Tremor subscore was 0.223 points per year (95% CI: 0.151 to 0.297) for WT *HFE* PD patients

Table 2-4: Total UPDRS Part III Progression Model

Independent variables	**β (95% CI)**	**p - value**
Disease duration at visit (yrs)	2.15 (1.88 to 2.43)	**< 0.001**
HFE genotype (reference: WT)	1.90 (-0.31 to 4.12)	0.50
Age at diagnosis	0.16 (0.07 to 0.24)	**< 0.001**
Total Montreal Cognitive Assessment score at baseline	-0.15 (-0.55 to 0.25)	0.45
DaTscan contralateral caudate striatal binding ratio at baseline	-2.03 (-3.60 to -0.46)	**0.01**
Sex (reference: female)	2.52 (0.74 to 4.30)	**0.005**
Rate difference	-0.53 (-1.03 to -0.03)	**0.039**

while for H63D *HFE* PD patients, the subscore increased by 0.029 points per year (95% CI: -0.085 to 0.143) (**Fig. 2-3B**). The rate of change in Bradykinesia subscore was also trending lower in the H63D HFE PD patients compared to WT HFE with rate difference of -0.19 (95% CI: -0.41 to 0.03, p-value = 0.095) (**Fig. 2-3C**). There was no difference in progression of the Rigidity and the Posture/Gait Instability subscores between WT and H63D *HFE* carriers (**Fig. 2-3D, E**).

Figure 2-3

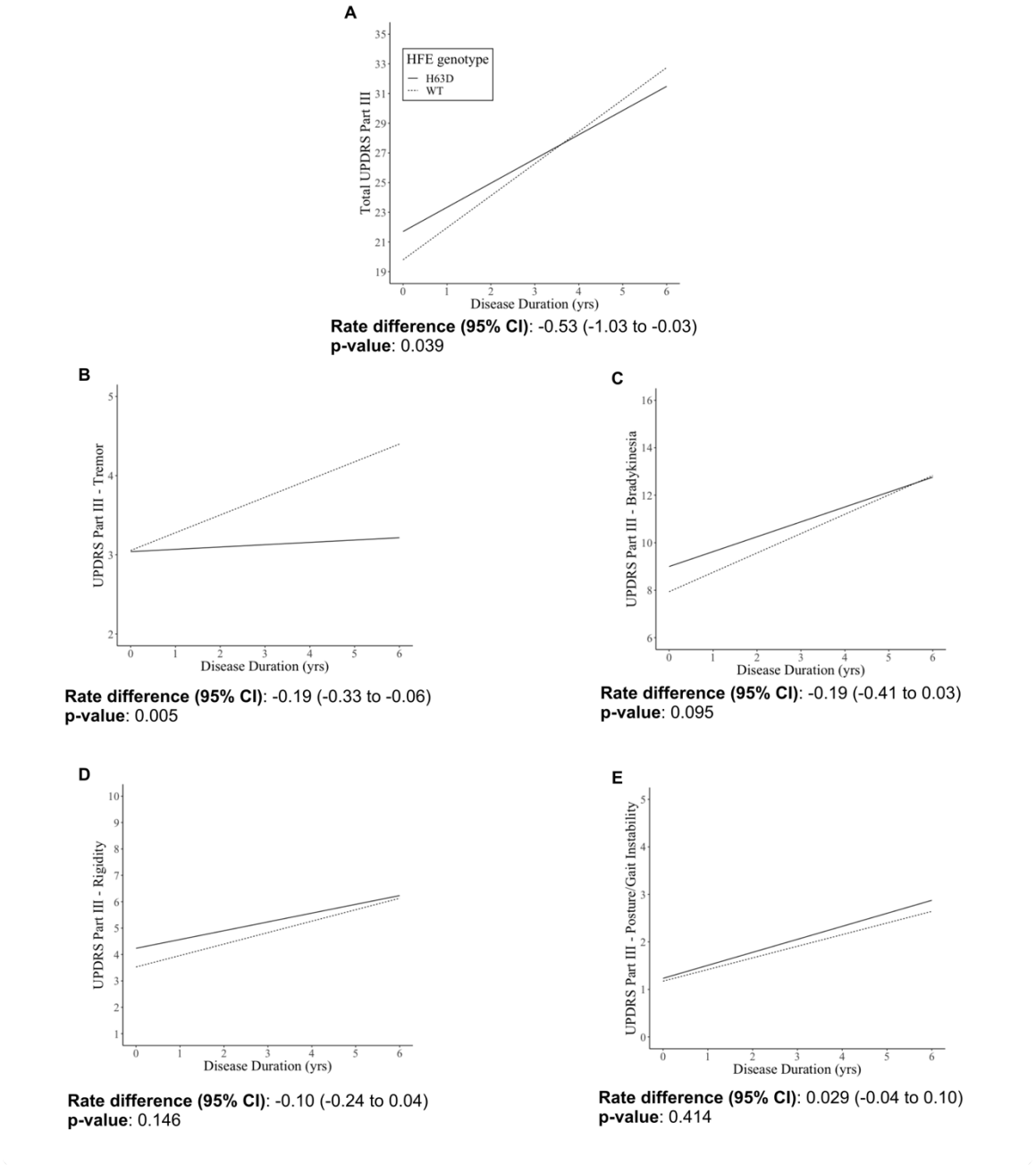

Figure 2-3: UPDRS III progression. (A) Mean UPDRS part III longitudinal progression trajectory of Parkinson's disease patients with WT *HFE* or H63D *HFE* was determined using linear mixed-effects models. Covariates were fixed at the following values: Age at diagnosis = 60.582, MoCA

score = 27.1, Contralateral caudate striatal binding ratio at baseline = 1.82, Sex = average between male and female. The effect of *HFE* genotype on the rate of change in mean UPDRS part III was found to be statistically significant (p = 0.039) with H63D *HFE* carriers having slower progression by 0.53 points per year. (B-E) UPDRS III subscores were calculated for Tremor, Bradykinesia, Rigidity, and Posture/Gait Instability. H63D HFE carriers had slower Tremor subscore progression by 0.19 points per year (p = 0.005). There was also a trend for a slower progression of the Bradykinesia subscore (p = 0.095). There was no difference in the progression of the Rigidity subscore or the Posture/ Gait Instability subscore between WT and H63D *HFE* carriers.

2.4.3 Blood *SNCA* transcript isoforms and CSF α-synuclein protein level

We investigated the effect of *HFE* genotype on *SNCA* transcript level in blood and α-synuclein protein level in CSF. *SNCA* transcript isoform levels were first reported by Locascio, et al., 2015. Alternative SNCA isoforms are through to be involved in the Parkinson's disease pathology through mislocalization (long 3'-UTR isoform) or increased aggregation (truncated isoforms) of α-synuclein[286,287]. Data for 173 Parkinson's disease patients and 120 controls were included in the analysis (**Table 2-5**). Carriers of C282Y *HFE*, another *HFE* variant, or those without *HFE* genotype information were excluded. Data was adjusted for covariates of age, gender, RBC count, and WBC count [273]. Unadjusted values control RNA counts are available in **Table 2-6**.

Table 2-5: SNCA blood RNA patient characteristics

	WT		H63D		p-value*		
	PD (N = 126)	**Control (N = 80)**	**PD (N = 47)**	**Control (N = 40)**			
Age (mean, SD)	58.82 (7.65)	59.54 (11.62)	60.83 (7.36)	58.60 (13.45)	**p_d**	**p_g**	**p_i**
					0.55	0.67	0.24
Sex (N, %)							
Male	77 (61.1%)	51 (63.8%)	33 (70.2%)	21 (52.5%)	0.3876		
Female	49 (39.0%)	29 (36.3%)	14 (29.9%)	19 (47.5%)			
Clinical Features (N, %)							
Resting tremor	100 (76.4%)	-	36 (76.6%)	-	0.6828		
Bradykinesia	101 (80.2%)	-	41 (87.2%)	-	0.3740		
Rigidity	96 (76.2%)	-	36 (76.6%)	-	> 0.9999		
Postural imbalance	6 (4.8%)	-	2 (4.3%)	-	> 0.9999		
Disease Severity (mean, SD)							
Disease duration (yrs)	0.61 (0.77)	-	0.38 (0.61)	-	0.0672		
Hoehn & Yahr scale	1.52 (0.50)	-	1.47 (0.50)	-	0.5593		
UPDRS I	6.29 (4.48)	-	4.98 (3.62)	-	0.0741		
UPDRS II	5.76 (4.22)	-	5.02 (3.51)	-	0.2855		
UPDRS III	21.10 (8.59)	-	22.06 (8.88)	-	0.5179		
Total MoCA	27.44 (2.00)	-	27.11 (2.08)	-	0.3410		
DatSCAN Striatal Binding Ratio (mean, SD)							
Right caudate	2.07 (0.57)	3.06 (0.67)	1.92 (0.56)	2.94 (0.66)	**p_d**	**p_g**	**p_i**
					<0.0001	0.09	0.84
Left caudate	2.06 (0.58)	3.15 (0.73)	1.92 (0.49)	2.98 (0.60)	**<0.0001**	0.05	0.85
Right putamen	0.83 (0.34)	2.19 (0.61)	0.82 (0.42)	2.11 (0.56)	**<0.0001**	0.46	0.57
Left putamen	0.79 (0.34)	2.20 (0.61)	0.79 (0.31)	2.09 (0.56)	**<0.0001**	0.32	0.41
Lab values (mean, SD)							
WBC, G/L	6.18 (1.45)	6.21 (1.74)	6.35 (1.81)	6.25 (1.45)	**p_d**	**p_g**	**p_i**
					0.87	0.61	0.75
RBC, T/L	4.66 (0.43)	4.71 (0.47)	4.79 (0.38)	4.69 (0.32)	0.65	0.31	0.17
Platelet, G/L	248.66 (57.11)	243.95 (58.32)	235.70 (48.56)	256.15 (67.50)	0.29	0.96	0.09

*p-values were calculated with two-way ANOVA (Age, WBC, RBC, Platelet, DatSCAN SBR; p_d: disease status, p_g: genotype, p_i: interaction), chi-square (Sex), Fisher's exact test (Clinical Features), and Student's T-test (Disease Severity)

Table 2-6. Unadjusted means, standard deviations, and p-values

	WT			H63D			ANOVA p-values*		
	PD	**Control**	**p#**	**PD**	**Control**	**p#**			
SNCA isoform RNA counts (mean, SD)									
SNCA-007	18.88 (12.38)	21.73 (13.93)	0.30	23.62 (14.94)	21.38 (12.11)	0.95	**p_d** 0.58	**p_g** 0.17	**p_i** 0.32
SNCA-3'UTR-1	1708.34 (981.80)	2058.21 (1329.22)	0.57	1674.21 (1118.8)	2147.90 (916.54)	**0.05**	**0.02**	0.53	0.17
SNCA-3'UTR-2	511.37 (306.21)	627.51 (399.10)	**0.04**	501.94 (382.55)	630.10 (292.26)	0.16	**0.007**	0.94	0.89
SNCA-E3E4	11791.39 (5823.08)	14045.68 (7247.01)	0.31	12914.4 (6341.5)	12689.48 (5108.12)	0.96	0.33	0.71	0.59
SNCA-E4E6	2425.13 (1315.66)	3045.01 (1662.16)	0.16	2781.55 (1500.8)	2728.68 (1232.73)	0.97	0.25	0.67	0.44
Control RNA counts (mean, SD)									
GLT25D1	296.90 (116.15)	294.19 (129.34)	0.50	290.00 (126.66)	324.93 (164.23)	0.60	0.86	0.56	0.18
GUSB	110.60 (44.95)	112.14 (48.33)	0.87	108.68 (47.42)	122.40 (61.74)	0.61	0.63	0.63	0.32
MON1B	154.02 (65.11)	147.04 (61.55)	0.36	150.32 (63.62)	163.25 (74.61)	0.75	0.88	0.45	0.21
SRCAP	270.94 (114.12)	274.20 (124.72)	0.64	282.36 (132.90)	279.43 (136.26)	0.99	0.63	0.63	0.65
UBC	24510.37 (9164.66)	23679.89 (8598.85)	0.50	23440.0 (8877.9)	26416.88 (11073.1)	0.51	0.78	0.58	0.15
CSF α-synuclein (mean, SD)									
Baseline	1455.33 (641.36)	1617.44 (736.58)	0.16	1447.93 (586.76)	1730.14 (655.79)	**0.05**	**0.004**	0.42	0.39
2-year	1382.80 (604.19)	1735.40 (730.35)	**0.001**	1428.45 (616.45)	1731.72 (752.33)	0.18	**0.001**	0.84	0.57

*p-values calculated for log-transformed data using two-way ANOVA (p_d: disease status, p_g: genotype, p_i: interaction); #Sidak's multiple comparison for PD vs. Control within genotype

Truncated (SNCA-007) transcript levels were not significantly different between Parkinson's disease and control within both *HFE* genotypes (**Fig. 2-4A**). For long 3'-UTR (SNCA-3UTR) transcript, two different probes were used to measure the transcript count: SNCA-3'-UTR-1 and SNCA-3'-UTR-2. For both probes, there was a significant effect of disease status with adjusted p = 0.0038 and p = 0.0043, respectively. Multiple comparisons show significantly lower count of long 3'-UTR isoform in Parkinson's disease with WT *HFE* genotype and trends in H63D *HFE* carriers (**Fig. 2-4B, Fig. 2-4C**). Probes targeting exon 3/4 boundary (SNCA-E3E4) and skipped exon 5 (SNCA-E4E6) show similar patterns where within WT *HFE* genotype, Parkinson's disease group has decreased transcript level compared to control while this is absent in H63D *HFE* carriers (**Fig. 2-4D, Fig. 2-4E**).

Figure 2-4

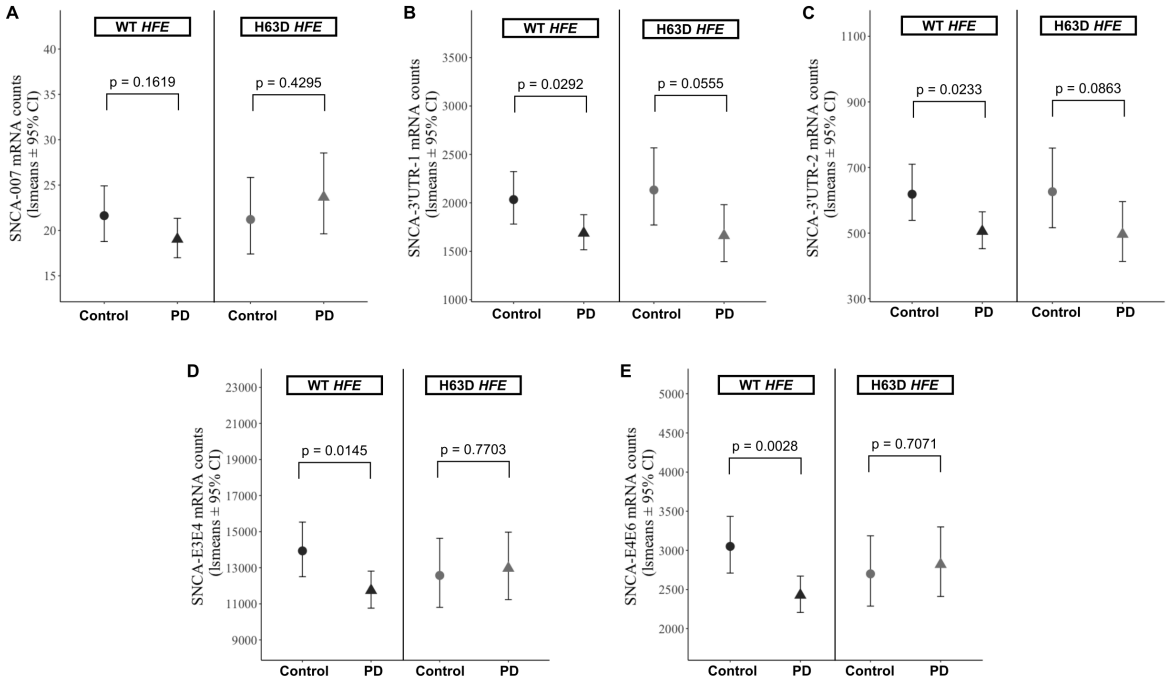

Figure 2-4: Blood *SNCA* transcript isoforms at baseline (A-E) *SNCA* RNA isoforms measured using digital NanoString nCounter Gene Expression Assay were divided into WT *HFE* and H63D *HFE* carrier groups. Data was adjusted for age, gender, RBC count, and WBC count. Short SNCA transcript (SNCA-007) and long 3'-UTR (SNCA-3UTR-1, SNCA-3UTR-2) did not show significant differences between control and disease groups within each genotype. Probes targeting exon 3/4 (SNCA-E3E4) and skipped exon 5 (SNCA-E4E6) show decreased transcripts in Parkinson's disease group ($p = 0.0145$ and $p = 0.0028$) for WT *HFE* while this is absent in H63D *HFE* carriers. Least-squares means ± 95% confidence interval; log-transformed data was used for statistical analysis.

CSF α-synuclein levels were measured using ELISA[281,285]. 241 Parkinson's disease patients and 111 controls were included in the analysis (**Table 2-7**). Similar to *SNCA* transcript data, CSF α-synuclein data was adjusted for covariates of age, gender, and total protein. Significant disease effect on CSF α-synuclein level was found at baseline ($p_{adj} = 0.0051$). α-Synuclein protein levels from Parkinson's disease CSF samples generally trended below control CSF with statistically significant difference for the WT *HFE* group (**Fig. 2-5A**). Longitudinal change in CSF α-synuclein was significant ($p = 0.025$) with negative slope. However, no difference between genotypes was detected (**Fig. 2-5B**).

Table 2-7: CSF α-synuclein baseline patient characteristics

	WT		H63D		p-value*		
	PD (N =177)	**Control (N =71)**	**PD (N =64)**	**Control (N =40)**			
Age (mean, SD)	61.48 (10.33)	59.52 (11.22)	61.13 (9.68)	59.83 (13.33)	**p_d**	**p_g**	**p_i**
					0.22	0.98	0.80
Sex (N, %)							
Male	118 (66.7%)	50 (70.4%)	48 (75.0%)	22 (55.0%)	0.1847		
Female	59 (33.3%)	21 (29.6%)	16 (25.0%)	18 (45.0%)			
Clinical Features (N, %)							
Resting tremor	137 (77.4%)	-	49 (76.5%)	-	0.8640		
Bradykinesia	144 (81.4%)	-	56 (87.5%)	-	0.3330		
Rigidity	138 (78.0%)	-	51 (79.7%)	-	0.8603		
Postural imbalance	10 (5.6%)	-	6 (9.4%)	-	0.3784		
Disease Severity (mean, SD)							
Disease duration (yrs)	0.54 (0.69)	-	0.36 (0.57)	-	0.0675		
Hoehn & Yahr scale	1.54 (0.52)	-	1.55 (0.50)	-	0.8930		
UPDRS I	5.40 (3.95)	-	5.55 (3.55)	-	0.7875		
UPDRSII	5.77 (4.28)	-	5.98 (4.31)	-	0.7371		
UPDRSIII	19.99 (8.42)	-	21.16 (8.94)	-	0.3528		
Total MoCA	27.00 (2.28)	-	27.14 (1.99)	-	0.6623		
CSF lab values (mean, SD)							
RBC count (cells/uL)	5.54 (10.63)	3.81 (8.55)	5.71 (10.74)	6.28 (8.95)	**p_d**	**p_g**	**p_i**
					0.64	0.29	0.36
WBC count (cells/uL)	1.35 (1.75)	1.69 (3.59)	1.08 (1.30)	1.38 (1.84)	0.23	0.28	0.93
Total protein (mg/dL)	46.62 (23.91)	43.17 (16.11)	45.11 (16.54)	39.50 (11.19)	0.07	0.30	0.66
Total glucose (mg/dL)	63.03 (9.88)	61.89 (11.09)	59.55 (10.36)	61.12 (7.60)	0.86	0.08	0.27

*p-values were calculated with two-way ANOVA (Age, WBC, RBC, Total protein, Total glucose; p_d: disease status, p_g: genotype, p_i: interaction), chi-square (Sex), Fisher's exact test (Clinical Features), and Student's T-test (Disease Severity)

Figure 2-5

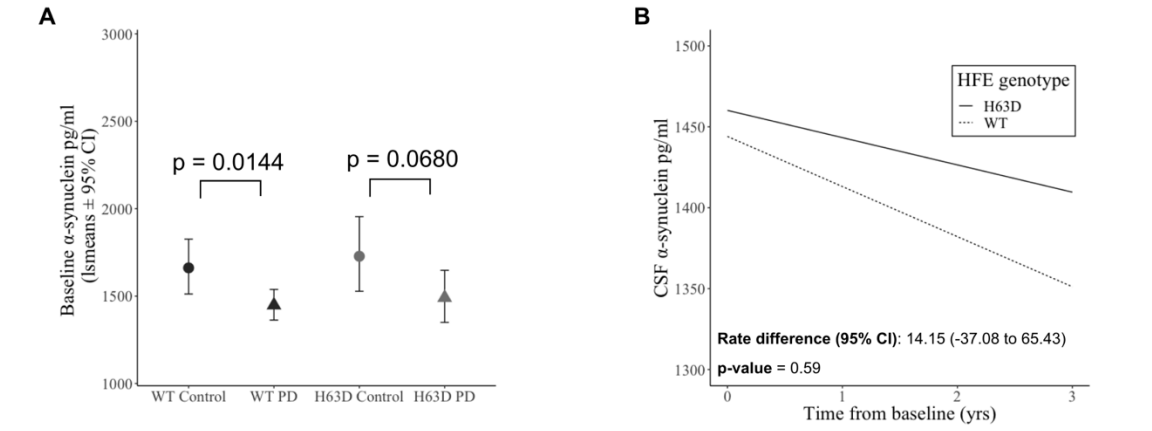

Figure 2-5: CSF α-synuclein levels at baseline and longitudinal progression. (A) Baseline CSF α-synuclein levels measured by ELISA were adjusted for age and sex. Regardless of genotype, Parkinson's disease group had lower α-synuclein protein levels in CSF compared to healthy controls with statistically significant difference between WT *HFE* carriers. Log-transformed data was used for statistical analysis. (B) Longitudinal change in CSF α-synuclein protein levels was modeled with linear mixed effect model. Change in CSF α-synuclein with time was significant (p = 0.025); however, no difference between genotypes was found. Covariates were fixed at the following values: Age at baseline = 61.22, Sex = average between male and female, disease duration at baseline = 0.51 years.

2.5 Discussion

In contrast to the previous reports of a lack of impact of H63D *HFE* variant on Parkinson's disease risk, the current study focuses on the effect of the genotype on patient clinical profiles. Parkinson's disease is heterogeneous with patients presenting with a spectrum of motor and non-motor symptoms[124]. Using the PPMI database, we found that the Parkinson's disease patient with H63D *HFE* had lower DaTscan contralateral caudate striatal binding ratio (SBR) at baseline along with a slower decline in the SBR with increasing disease duration. This seemingly contradictory finding is consistent with a previous study in the H67D *HFE* animal model (homologous to the human H63D HFE) which showed that compared to WT *HFE* mice, H67D *HFE* mice had lower tyrosine hydroxylase (TH) staining in the substantia nigra. TH+ dopaminergic neurons in H67D *HFE* were also less vulnerable to paraquat induced neurodegeneration[107]. Interestingly, this difference in DaTscan SBR was not reflected in the baseline UPDRS III score, which was similar between WT and H63D *HFE* groups. DaTscan SBR is an imaging marker for dopaminergic neurons and therefore suggests that although H63D *HFE* carriers have fewer dopaminergic neurons at the beginning of the disease, the remaining neurons are more resistant to degeneration.

H63D *HFE* carriers also had slower change in UPDRS part III with increasing disease duration compared to WT *HFE* patients. UPDRS part III score is reflective of a patient's motor examination result and therefore has been found to correlate with DaTscan SBR values[266,267]. Because baseline DaTscan contralateral caudate SBR was lower in H63D *HFE* patients compared to WT *HFE* patients, SBR was included as an independent variable in the longitudinal progression analysis of UPDRS part III. The linear mixed effect model showed that H63D *HFE* carriers had slower change in UPDRS part III. Subscore analysis revealed that the Tremor component of the UPDRS part III was significantly affected by the *HFE* genotype.

The presence of α-synuclein protein and RNA in biologic fluids was investigated to determine the effects of *HFE* genotype on potential biomarkers of PD. *SNCA* gene encodes for α-synuclein and different isoforms of *SNCA* RNA has been linked to Parkinson's disease process. *SNCA* RNA isoform with long 3'-UTR has been shown to lead to mislocalization and mitochondrial toxicity [286]. This isoform showed similar trends between Parkinson's disease and controls for both WT and H63D *HFE* carriers. Truncated *SNCA* isoforms have been shown to increase α-synuclein aggregation [287]. Interestingly, SNCA isoform with skipped exon 5 (SNCA-E4E6) was decreased in Parkinson's disease only with WT *HFE*. Exon 5 skipping has been shown to be induced by oxidants like MPTP [288]. The altered levels of *SNCA* isoform with skipped exon 5 could indicate modulation in handling of oxidants in H63D *HFE* carriers, leading to altered α-synuclein aggregation in this subset of Parkinson's disease patients.

CSF α-synuclein protein levels are decreased in Parkinson's disease patients compared to control for both WT and H63D *HFE* genotype groups. This disease effect was stronger in the WT *HFE* group. H63D *HFE* carriers showed no statistical difference in α-synuclein level between Parkinson's disease and control. Using data from baseline, 1-year, 2-year, and 3-year visit, the longitudinal change in CSF α-synuclein levels was investigated. There was a significant decrease in α-synuclein protein levels with time; however, no difference between genotypes were detected. This is consistent with previous longitudinal studies that have showed that CSF α-synuclein level does not correlate with Parkinson's disease motor progression [281,289].

Collectively, the data presented in this study show that H63D *HFE* genotype is a genetic modifier of Parkinson's disease and is clinically meaningful in understanding patient heterogeneity.

Furthermore, blood from H63D *HFE* carrying Parkinson's disease patients showed different α-synuclein transcript profiles compared to WT *HFE* carriers. Because H63D *HFE* is a common variant potentially carried by 15-25% of the patient population, *HFE* genotype should be taken into consideration for future studies investigating clinical features of Parkinson's disease.

2.6 Acknowledgements

Data used in this article were obtained from the Parkinson's Progression Markers Initiative (PPMI) database (www.ppmi-info.org/data). For up-to-date information on the study, visit www.ppmi-info.org. PPMI - a public-private partnership – is funded by the Michael J. Fox Foundation for Parkinson's Research and funding partners, including Abbvie, Allergan, Avid radiopharmaceuticals, Biogen, BioLegend, Bristol-Myers Squibb, Celgene, Denali, GE Healthcare, Genentech, GlaxoSmithKline, Eli Lilly and Company, Lundbeck, Merck, Meso Scale Discovery, Pfizer, Piramal, Prevail therapeutics, Roche, Sanofi Genzyme, Servier, Takeda, Teva Pharmaceuticals, UCB, Verily, Voyager Therapeutics, and Golub Capital (http://www.ppmi-info.org/about-ppmi/who-we-are/study-sponsors/).

Chapter 3

H63D *HFE* alters α-synuclein expression, aggregation, and cytotoxicity

3.1 Abstract

Background: Previous studies have suggested that iron accumulation in the substantia nigra contributes to the Parkinson's disease pathology through reactive oxygen species production and accelerated α-synuclein aggregation. However, effects of polymorphisms in iron regulating genes on α-synuclein have not been investigated.

Objective: The current study examines the effects of commonly occurring H63D variant of the homeostatic iron regulatory *(HFE*) gene on α-synuclein pathology in cell culture and animal model.

Methods: H63D *HFE* expressing SH-SY5Y neuroblastoma cells and H67D *Hfe* (mouse homolog of the human H63D *HFE* variant) C57BL/6J × 129 mice were exposed to α-synuclein pre-formed fibrils or paraquat to induce α-synuclein aggregation. α-Synuclein expression, aggregation, and cytotoxicity were assessed.

Results: H63D *HFE* expressing cells had lower endogenous α-synuclein levels and significantly decreased pre-formed fibril induced α-synuclein aggregation compared to wildtype. With the paraquat exposure model, H67D *Hfe* mice showed decreased α-synuclein aggregation. H63D *HFE* cells were also protected from pre-formed fibril induced apoptosis. Autophagic flux, a major pathway for α-synuclein clearance, was increased in H63D *HFE* cells. mTORC1 inhibition by increased REDD1 expression was identified as the mechanism of autophagy induction.

Furthermore, while iron chelator (deferiprone) treatment rescued WT *HFE* cells from pre-formed fibril induced α-synuclein aggregation and toxicity, it exacerbated or was unable to rescue H63D *HFE* cells.

Conclusions: Collectively, the data indicate that H63D *HFE* variant may modify α-synuclein pathology through induction of autophagy and has the potential to impact the efficacy of iron chelation therapy for Parkinson's disease.

3.2 Introduction

Iron accumulation is a consistent feature of Parkinson's disease pathology. Multiple post-mortem and MRI based studies have shown that compared to healthy controls, patients with Parkinson's disease have higher iron in the basal ganglia[64,290–292]. Iron is an important cofactor for many cellular processes and its intracellular concentration is tightly regulated due to potential production of reactive oxygen species (ROS) through the Fenton reaction[293,294]. In Parkinson's disease, excess iron is thought to contribute to increased expression and aggregation of α-synuclein, the main protein component of Lewy bodies[295–297]. The role of iron in Parkinson's disease progression is under active clinical investigation in ongoing studies of an iron chelator, deferiprone, as a potential therapeutic option for Parkinson's disease[69,298].

α-Synuclein oligomers and fibrils are widely considered to be the main toxic components of Parkinson's disease pathology[299,300]. Neurons containing aggregated α-synuclein demonstrate loss of normal neurotransmission and disruption of multiple cellular processes including protein degradation pathways and mitochondrial function[301]. Various models of α-synuclein aggregation have been developed to study its toxicity. Exposure to paraquat, a mitochondrial toxin, has been

shown to not only cause dopaminergic neuron damage but also α-synuclein aggregation *in vivo*[302,303]. More recently, α-synuclein pre-formed fibrils (PFFs) have been observed to induce prion-like spread of α-synuclein aggregates. Exogenous treatments with α-synuclein PFFs have been shown to induce aggregate formation by 'seeding' recruitment of endogenous soluble α-synuclein[304–306]

Autophagy is one of the main pathways for clearance of aggregated α-synuclein and has been shown to be a vital homeostatic pathway in terminally differentiated cells such as neurons[307–309]. Macroautophagy is the 'classical' autophagy pathway involving autophagosome formation followed by fusion with the lysosome. This study focuses on macroautophagy as the pathway of α-synuclein degradation. Nutrient-sensitive mTORC1 is the main negative regulator of autophagy through its interaction with autophagy initiating ULK1 complex[310,311]. REDD1 inhibits mTORC1 and induction of REDD1 expression has been associated with hypoxia, ER stress, and iron chelation[312–314]. Autophagy has been a focal point of investigations in the context of Parkinson's disease pathogenesis in part due to the high prevalence of glucocerebrosidase (*GBA*) mutations in the Parkinson's disease population. *GBA* mutation is the most common genetic risk factor for Parkinson's disease[315,316]. Dysfunction of glucocerebrosidase causes lysosomal storage disease (Gaucher's) and has been shown to promote α-synuclein accumulation through autophagic inhibition[317].

The direct effects of iron on α-synuclein homeostasis has been postulated through the identification of a putative iron response element at the 5'-UTR of α-synuclein mRNA along with metal binding sites located on the protein[81,318]. However, the impact of genes involved in iron regulation on Parkinson's disease risk and molecular pathology is poorly understood. Polymorphisms in the *HFE*

gene which encodes for the homeostatic iron regulator protein, HFE, have been identified to be a disease modifier in multiple neurodegenerative diseases including amyotrophic lateral sclerosis and Alzheimer's disease[214,217,277,278]. HFE limits iron uptake into cells through its interaction with the transferrin receptor[276]. The highly prevalent H63D *HFE* variant, which is estimated to be present in 13.5% of the US population, has been shown to increase brain iron content and therefore has the potential to affect α-synuclein pathology and Parkinson's disease progression[55,319]. Furthermore, H67D *Hfe* expression in mice (homologous to human H63D *HFE*) reportedly protects dopaminergic neurons from paraquat toxicity[107].

In this study, we investigated the effects of the H63D *HFE* variant on α-synuclein metabolism *in vitro* using pre-formed fibrils and *in vivo* using paraquat exposure model of Parkinson's disease. We also tested the effects of an iron chelator, deferiprone, on the toxicity of α-synuclein PFFs in cells expressing WT and H63D *HFE*.

3.3 Materials and Methods

3.3.1 Cell culture

SH-SY5Y neuroblastoma cells transfected to stably express WT or H63D *HFE* were used for all experiments [320]. Cells were cultured in accordance with guidelines from American Type Culture Collection (ATCC). Briefly, cells were cultured in DMEM/F12 medium (Invitrogen) containing 10% fetal bovine serum (HyClone), 100 U/mL penicillin-streptomycin (Gibco), MEM non-essential amino acids (Gibco), and 250ug/mL Geneticin (Gibco). Cells were incubated in 5% CO_2 at 37^{o}C and media was changed every 3-5 days.

3.3.2 Calcein assay

Calcein-AM (Sigma) was used to measure the labile iron pool in SH-SY5Y cells. Cells were seeded in 6 well plates and treated with Ca-AM (0.15uM in assay buffer: PBS, 1mg/mL bovine serum albumin, 20mM HEPES, pH 7.3) for 10 min in 37ºC. Cells were trypsinized, washed, and resuspended with 1mL of assay buffer. 100uL of cell suspension was added per well to a 96 well plate and fluorescence was measured (SpectraMax Gemini EM; excitation 488nm, emission 518 nm). Remaining cell suspension was spun down at 8000 rcf for 3 min and cell pellet was lysed with RIPA lysis buffer (150mM NaCl, 1.0% NP-40, 0.5% sodium deoxycholate, 0.1% SDS, 50mM Tris, pH 7.4) plus Roche Complete Protease Inhibitor tablet. Total protein concentrations of the lysates were measured using the Qubit Protein Assay Kit (Invitrogen).

3.3.3 ELISA and Western blots

α-Synuclein ELISA was performed using Invitrogen Human α-synuclein ELISA kit (KHB0061). Cells were lysed in Cell Extraction Buffer (150mM NaCl, 1.0% Triton x-100, 50mM Tris, pH 7.4, 1mM PMSF, Roche Complete Protease Inhibitor tablet) by incubation on ice for 30 min with occasional vortexing. Lysates were centrifuged at 13,000xg, 4ºC, for 10 minutes. Total protein concentration was quantified using the Qubit Protein Assay Kit. Protocol from the ELISA kit was followed and 96 well plate was read with SpectraMax 340pc. For western blots, cells were washed twice with cold PBS and collected using cell scrapers. RIPA buffer with protease inhibitor (Roche) and phosphatase inhibitor (Roche) was used for lysis. Samples were incubated on ice for 30 min, sonicated, and centrifuged at 16,000 xg for 20 min. Total protein concentrations of the lysates were measured using the Qubit Protein Assay Kit. Loading dye and reducing agent from SDS-Sample Prep Kit (Thermo) were added and the lysates were boiled at 70ºC for 10 min. For PFF treated cell lysates, reducing agent was omitted in sample preparation. Samples were separated on 4-12% Bis-Tris gel (Life Technologies) in NuPAGE MES SDS Running Buffer (Invitrogen) and transferred

to PVDF membrane using the iBlot2 transfer system (Invitrogen) at P3 setting. PageRuler Plus Prestained Protein Ladder (ThermoFisher) was loaded along with the samples. For α-synuclein blots, membrane was then incubated in 0.4% paraformaldehyde for 30 min to increase the signal as previously published [321]. Membranes were block in 5% milk or 5% BSA in TBST (25mM Tris, 150mM NaCl, 0.1% Tween 20, pH 7.5) for 1 hour. Primary antibody (Novus α-Synuclein 2A7, BD Biosciences α-Synuclein Syn1, Cell Signaling H-ferritin, Cell Signaling LC3B D11, ProteinTech REDD1, ProteinTech β-actin) was then added for overnight incubation at 4^{o}C, followed by washes with TBST. Appropriate secondary antibody (Goat anti-mouse IgG HRP conjugated secondary, Goat anti-rabbit IgG HRP conjugated secondary) was added for 1.5 hour at room temperature. Detailed list of antibodies can be found in **Table 3-1**. Pierce ECL western blot substrate (Thermo) was used for detection. Images were acquired with GE Amersham Imager 600. Band densities were quantified using ImageJ version 1.52a.

Table 3-1: Antibodies

Name	Host	Type	Dilution	Citation
α-Synuclein [2A7]	Mouse	Monoclonal	WB – 1:1000 ICC – 1:1000	RRID: AB_1555287 Novus Cat# NBP1-05194
α-Synuclein [Syn1]	Mouse	Monoclonal	WB – 1:500	RRID: AB_398107 BD Biosciences Cat# 610786
α-Synuclein [EPR20535]	Rabbit	Monoclonal	IHC – 1:5000	Abcam Cat# ab212184
Phospho Ser129 α-Synuclein	Rabbit	Monoclonal	IHC – 1:500	RRID: AB_869973 Abcam Cat# ab51253
H-ferritin [D1D4]	Rabbit	Monoclonal	WB – 1:1000	RRID: AB_11217441 Cell Signaling Technology Cat# 4393
LC3B [D11]	Rabbit	Monoclonal	WB – 1:1000	RRID: AB_2137707 Cell Signaling Technology Cat# 3868
LC3B	Rabbit	Polyclonal	ICC – 1:1000	RRID: AB_10003146 Novus Cat# NB100-2220
REDD1	Rabbit	Polyclonal	WB – 1:500	RRID: AB_2245711 Proteintech Cat# 10638-1-AP
ULK1 [D8H5]	Rabbit	Monoclonal	WB – 1:1000	RRID: AB_11178668 Cell Signaling Technology Cat# 8054
Phospho Ser757 ULK1	Rabbit	Polyclonal	WB – 1:500	RRID: AB_10829226 Cell Signaling Technology Cat# 6888
WDR45/WIPI4	Mouse	Polyclonal	WB – 1:1000	RRID: AB_1581911 Abnova Cat# H00011152-B01P
β-actin	Mouse	Monoclonal	WB - 1:10,000	RRID: AB_2289225 Proteintech Cat# 60008-1-Ig
Goat Ant-Mouse IgG - H&L (HRP)	Goat	Polyclonal	WB – 1:2500	RRID: AB_955439 Abcam Cat# ab6789
Goat Anti-Rabbit IgG-H&L (HRP)	Goat	Polyclonal	WB – 1:2500	RRID: AB_524669 Novus Cat# NB 7160
Goat Anti-Rabbit IgG H&L (Alexa Fluor® 488)	Goat	Polyclonal	ICC – 1:2000	RRID: AB_2630356 Abcam Cat# ab150077
Goat Anti-Mouse IgG H&L (Alexa Fluor® 568)	Goat	Polyclonal	ICC – 1:2000	Abcam Cat# ab175473
Biotinylated Anti-Rabbit IgG	Goat	Polyclonal	IHC – 1:200	RRID: AB_2336820 Vector Laboratories Cat# PK-6101

3.3.4 α-Synuclein pre-formed fibrils

Purified α-synuclein monomers for PFF fibrilization was purchased from Proteos, Inc. and PFFs were formed according to the provided protocol. Briefly, monomer was diluted to 5mg/ml with final buffer composition of 100mM NaCl, 10mM Phosphate, pH 7.2-7.6 and constantly agitated at 600rpm, 37^{o}C for 7 days. Fibril formation was confirmed using Thioflavin T fluorescence assay and sedimentation followed by gel electrophoresis. Thioflavin T (final concentration 0.25uM dissolved in PBS) was added to α-synuclein monomer, α-synuclein PFF, and PBS only and incubated at room temperature for 15 minutes in a 96 well plate. Fluorescence was measured using SpectraMax Gemini EM plate reader (excitation 440nm, emission 482nm). Sedimentation was performed by centrifugation at 100,000xg for 30 min. Samples were loaded on 4-12% Bis-Tris gel (Life Technologies) and ran at 200V for 25min. Gels were stained with coomassie blue. α-Synuclein PFFs were aliquoted and stored in -80^{o}C until use. For SH-SY5Y cell treatment with PFFs, cells were seeded in 6 well plates (~1x10^{6} cells/ well). Cells were seeded on coverslips for immunocytochemistry. α-Synuclein PFFs were thawed at room temperature, diluted to 0.1mg/mL with sterile DPBS, and sonicated (1s pulses at 10% power for 5 minutes). Sonicated PFFs were diluted with cell culture media then added to 6 well or 96 well plates.

3.3.5 Immunocytochemistry and image analysis

Cells were grown on coverslips and fixed with 4% paraformaldehyde (in PBS) for 10 min at room temperature. Fixed cells were washed 3 times with cold PBS then permeabilized with 0.1% Triton X-100 in PBS for 20 min. Coverslips were washed 3 times with PBST (PBS with 0.1% Tween 20) and blocked in 5% BSA in PBST for 1 hour at room temperature. Primary antibody (Novus α-Synuclein 2A7, Novus LC3B) incubation was overnight at 4^{o}C (**Table 3-1**). Thioflavin S was dissolved in 1:1 ethanol/PBS solution. Coverslips were incubated in 0.025% ThS for 8 min and washed 3 times with 80% ethanol/PBS solution. Appropriate secondary antibodies (Goat anti-rabbit

IgG Alexa Fluor 488 secondary, Goat anti-mouse IgG Alexa Fluor 568 secondary) were added for 1 hour at room temperature, then finally washed before being mounted on microscope slides with Vectashield antifade mounting medium with DAPI (H-1200). LC3 images were taken with confocal microscope (Nikon Eclipse FN-1/C2+). Slides were blinded for image acquisition. α-Synuclein and ThS fluorescence images were taken with Echo Revolve hybrid upright-inverted microscope. LC3-positive puncta/cell and fluorescence intensities were quantified using ImageJ version 1.52a [322]. Corrected total fluorescence (CTF) was calculated by using the formula: [integrated density – (selected area * mean fluorescence of background)]/ number of cells in selected area.

3.3.6 Cell viability and apoptosis assays

Cell viability was measured using ATP-based CellTiter-glo assay (Promega) and 96 well plate was read with SpectraMax Gemini EM plate reader. Caspase 3/7 activity was measured with Caspase-glo assay (Promega). For Annexin V-FITC/ 7-AAD flow cytometry experiments, cells were treated seeded in 6 well plates and treated with 1.5uM α-synuclein monomer or 1.5uM monomer + 5uM PFF for 7 days. Cells were trypsinized, washed with PBS, and resuspended with Annexin binding buffer (BioLegend). Samples were incubated with Annexin V-FITC antibody for 15 min at room temperature. 5ul of 7-AAD was added for each 500uL sample. 10-color BD FACSCanto (BD Biosciences) in Penn State College of Medicine's Flow Cytometry Core was used to detect Annexin V-positive cells.

3.3.7 Mouse paraquat injections

Paraquat intraperitoneal injections were given as described in Nixon, et al. 2018. Three month old C57Bl/6J x 129 male mice expressing wild-type of H67D *Hfe* (JAX stock #: 023025) were used

for the study [55]. The mice were individually housed in standard mouse cages at the in-house animal facility of Penn State College of Medicine. Mice had access to food and water *ad libitum*. Penn State College of Medicine Institutional Animal Care and Use Committee approved all procedures. Eight mice were randomly divided into two groups (saline or 10mg/kg paraquat) and injected once a week for 3 weeks. Baseline weight of the C57BL/6J x 129 was not available. Because animals were only subject to brief minor discomfort, no anesthetic was used for injections.

3.3.8 Immunohistochemistry

At endpoint (1 week after the last injection), mice were injected with ketamine/xylazine cocktail and perfused with Ringer's solution. Brains were removed and preserved with 4% paraformaldehyde in 0.1M PBS. Paraformaldehyde was replaced with 70% ethanol, then tissue was paraffin-embedded and sectioned into 5um slices. Slides were deparaffinized, rehydrated, and incubated in sodium citrate buffer for antigen retrieval. Sections were blocked with 2% milk in PBS for 1hr at room temperature. Primary antibody incubation was performed overnight at 4°C. Biotinylated anti-rabbit secondary antibody was added and immunoreactivity was detected with 3,3'-diaminobenzidine Peroxidase (HRP) substrate kit (Vector Laboratories). Slides were imaged with Echo Revolve hybrid upright-inverted microscope.

3.3.9 WDR45/WIPI4 siRNA knockdown

WDR45/WIPI4 siRNA (Sigma, EHU023161) and control EGFP siRNA (Sigma, EHUEGFP) were transfected with Lipofectamine RNAiMAX (ThermoFisher, 13778100). siRNAs and lipofectamine were diluted in Opti-MEM (ThermoFisher, 31985062). 250uL of 100nM siRNA in Opti-MEM + Lipofectamine solution was added to each 6 well. 48 hours after treatment, cells were trypsinized and seeded for Bafilomycin A1 treatment or harvested for lysis and further sample preparation for western blot.

3.3.10 Statistical analysis

Statistical analyses were performed using GraphPad Prism version 8.2.1. Unless otherwise noted, values in figures are presented as mean with standard error of the mean. Generally, Student's t-test or one-way ANOVA with *post hoc* multiple comparisons test were used. Statistics used for each figure is noted in the legend.

3.4 Results

3.4.1. H63D *HFE* cells have increased iron and decreased α-synuclein expression

The intracellular labile iron pool (LIP) was increased in SH-SY5Y neuroblastoma cells expressing H63D *HFE* compared to wildtype, as shown by the decrease in calcein fluorescence (**Fig. 3-1A**). Calcein fluorescence is quenched by iron and therefore is inversely related to LIP. H-ferritin expression, which is controlled by an iron response element and iron regulatory protein interaction at the 5'-UTR, was increased in H63D *HFE* cells (**Fig. 3-1B**). Collectively, these results confirm that intracellular iron is increased in the H63D *HFE* SH-SY5Y cells. The consequence of H63D *HFE* expression on α-synuclein expression was investigated by western blot (**Fig. 3-1C**) and ELISA (**Fig. 3-1D**), both of which demonstrated significantly lower α-synuclein level in H63D *HFE* cells compared to WT cells.

Figure 3-1

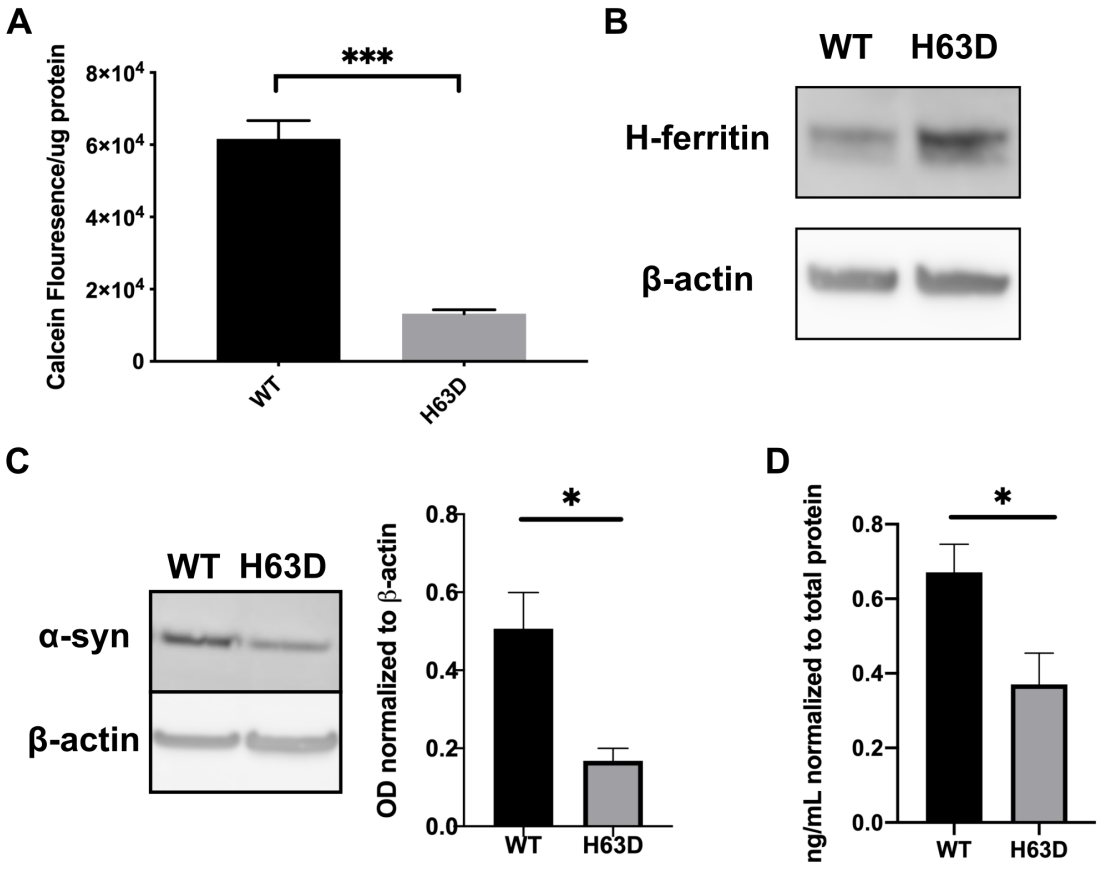

Figure 3-1: **H63D *HFE* expressing cells have decreased α-synuclein** (A) Calcein fluorescence was measured from WT and H63D *HFE* expressing cells as a marker of intracellular labile iron. Ca fluorescence is inversely related to LIP. n = 3, *** $p < 0.001$, Student's t-test (B) H-ferritin western blot shows increased expression in H63D *HFE* cells compared to wildtype. (C) Representative immunoblot showing decreased α-synuclein level in SH-SY5Y cells expressing H63D *HFE* compared to WT *HFE* expressing cells. Quantification is shown on the right. n = 3 (D) ELISA was performed to quantify α-synuclein content (ng/mL) normalized to total protein. n = 4, * $p < 0.05$, Student's t-test

3.4.2 H63D *HFE* decreases PFF induced α-synuclein aggregation and cell death

α-Synuclein preformed-fibrils were used to induce α-synuclein aggregation in WT and H63D *HFE* expressing SH-SY5Y cells. PFF formation was confirmed by sedimentation and Thioflavin T fluorescence (**Fig. 3-2**). Cells were treated with 1.5uM α-synuclein monomer or PFF for 7 days, then stained with Thioflavin S (ThS), anti-α-synuclein antibody, and 4′,6-diamidino-2-phenylindole (DAPI) stain as the nuclear stain (**Fig. 3-3A**). Fold change (PFF/monomer) in corrected total fluorescence (CTF) for ThS and α-synuclein was decreased for H63D *HFE* cells, indicating lower level of α-synuclein aggregation (**Fig. 3-3B**). CTF was calculated by subtracting background intensity from integrated fluorescence density. This was confirmed with time course experiments in which Thioflavin T fluorescence was measured from cell culture media collected 3, 5, and 7 days post-PFF treatment (**Fig. 3-3C**). By day 7 post-treatment, ThT fluorescence was significantly higher in media collected from WT *HFE* cells. Similarly, α-synuclein western blots were performed using whole-cell lysates prepared 3, 5, and 7 days post-PFF treatment (**Fig. 3-3D**). At all time-points, the total α-synuclein level was higher in WT *HFE* cells than in H63D *HFE* cells.

Figure 3-2

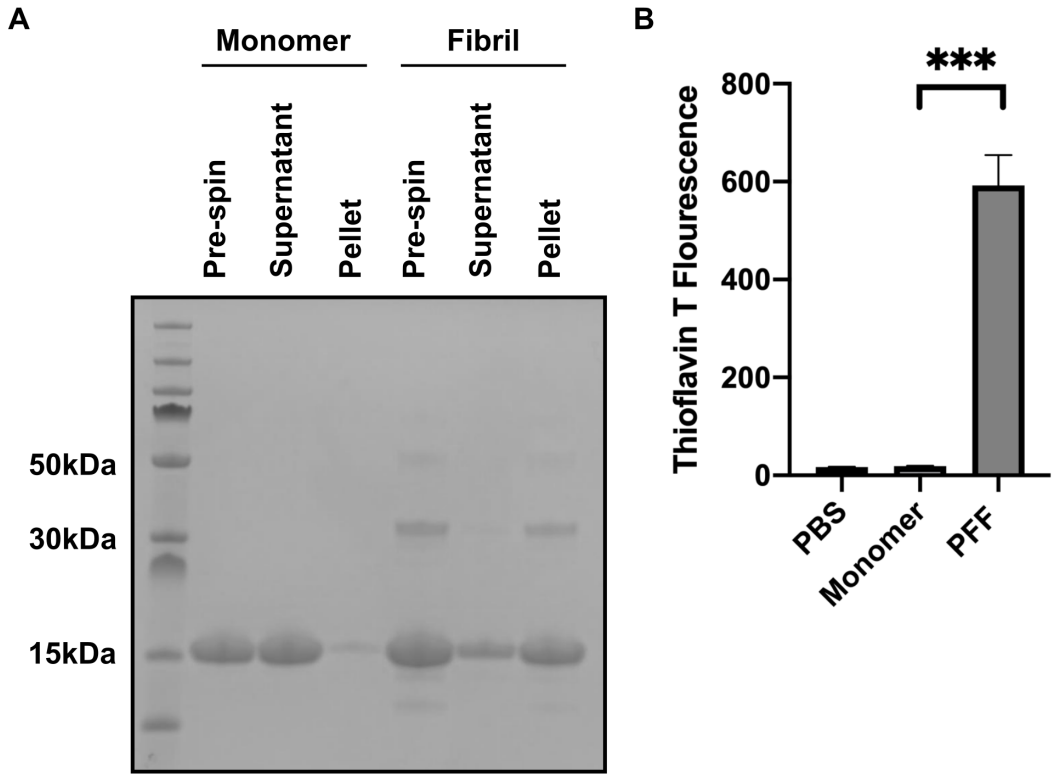

Figure 3-2: α-Synuclein pre-formed fibril confirmation (A) Ultracentrifugation was performed to separate supernatant and pellet from α-synuclein monomer and PFF samples. Pre-spin, supernatant, and pellet fractions were run on 4-12% Bis-Tris gel and stained with Coomassie blue. Most protein in α-synuclein monomer stays in the supernatant after centrifugation while with the PFF sample, more protein can be found in the pellet. (B) Thioflavin T fluorescence was measured with PBS control, α-synuclein monomer, and PFF. Increased fluorescence with PFF formation was detected. n = 3, *** $p < 0.001$, Student's t-test.

Figure 3-3

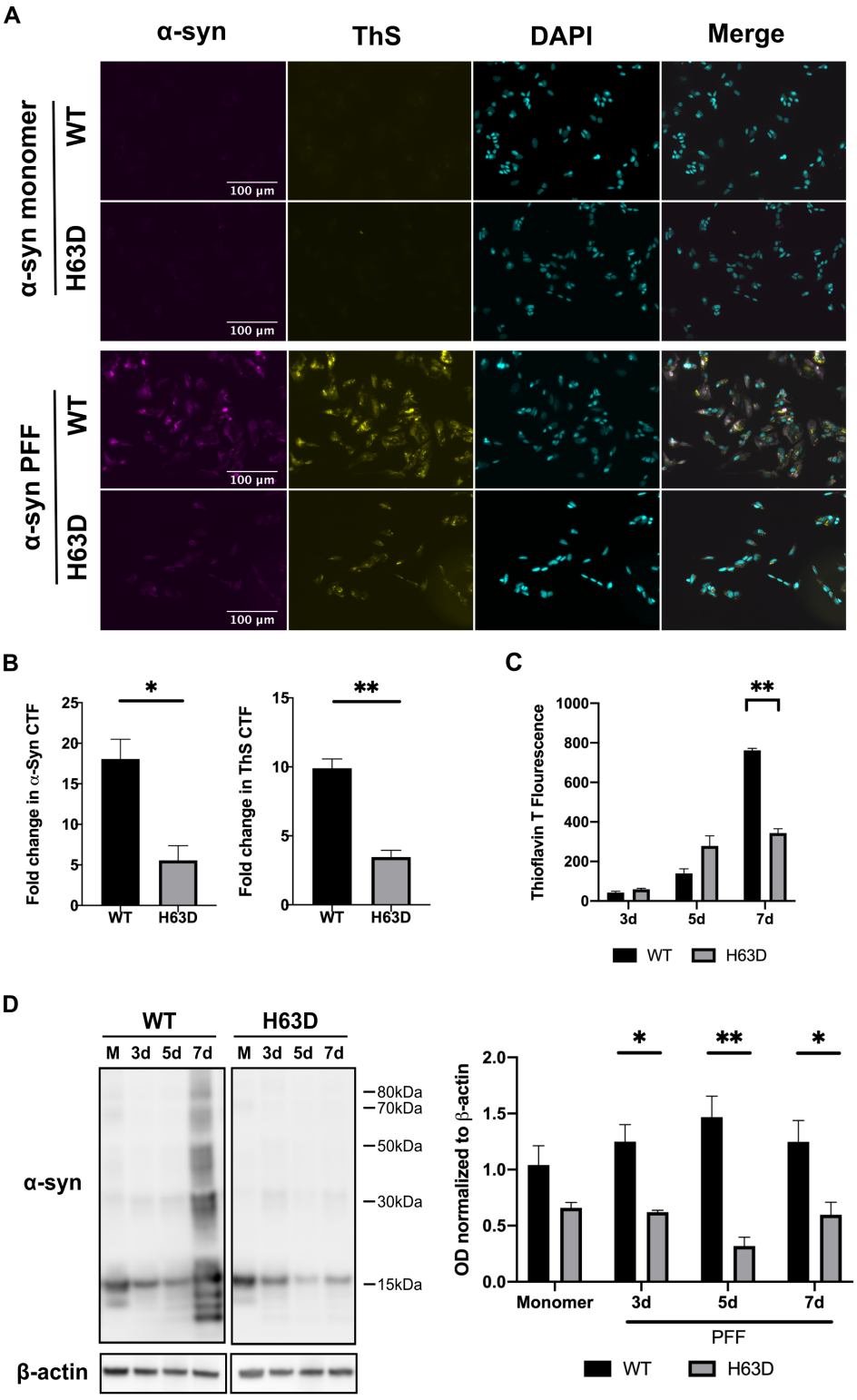
A
α-syn
ThS
DAPI
Merge
α-syn monomer
WT
H63D
α-syn PFF
WT
H63D
100 μm
B
Fold change in α-Syn CTF
Fold change in ThS CTF
WT
H63D
C
Thioflavin T Flourescence
3d
5d
7d
WT
H63D
D
WT
H63D
M 3d 5d 7d
M 3d 5d 7d
α-syn
β-actin
80kDa
70kDa
50kDa
30kDa
15kDa
OD normalized to β-actin
Monomer
3d
5d
7d
PFF
WT
H63D

Figure 3-3: α-Synuclein aggregation is decreased in H63D *HFE* cells after PFF treatment. (A) Representative images showing Thioflavin S, α-synuclein, and DAPI fluorescence staining on WT and H63D *HFE* cells after 7 days of 1.5uM α-synuclein monomer or PFF treatment. (B) Fold change in α-synuclein and ThS Corrected Total Fluorescence (CTF) with PFF treatment compared to control is shown. CTF was calculated from 3 independent experiments with at least 4 images taken per slide then normalized to number of cells in field of view. * $p < 0.05$, ** $p < 0.01$, Student's t-test (C) Thioflavin T fluorescence was measured from cell culture media collected at 3, 5, 7 days post 1.5uM PFF treatment. n = 3, ** $p < 0.01$, ANOVA with Sidak's test for multiple comparisons. (D) Representative western blots showing α-synuclein aggregation at 3, 5, and 7 days post 1.5uM PFF treatment. Quantification is shown at right. n = 3, * $p < 0.05$, ** $p < 0.01$, ANOVA with Sidak's test for multiple comparisons.

PFF-induced cell death was also measured. Previous work[323] demonstrated that treatment of SH-SY5Y cells with α-synuclein PFFs results in measurable toxicity only in the presence of additional α-synuclein monomers; therefore, cells were treated with combinations of 1.5uM monomer and increasing concentrations of PFFs (1.5 – 10uM) for 7 days. A PFF dose-dependent decrease in cell viability was seen with both WT and H63D *HFE* cells (**Fig. 3-4A**). Notably, H63D *HFE* cells showed greater cell viability compared to wildtype. The lower levels of apoptotic cell death in H63D *HFE* cells occurred after 1.5uM monomer + 5uM PFF treatment was confirmed with caspase 3/7 activity assay (**Fig. 3-4B**) and annexin V-FITC/ 7-AAD flow cytometry (**Fig. 3-4C**). Fold change in caspase 3/7 activity and percent annexin V-positive cells after PFF treatment were significantly lower for H63D *HFE* cells than WT *HFE*.

Figure 3-4

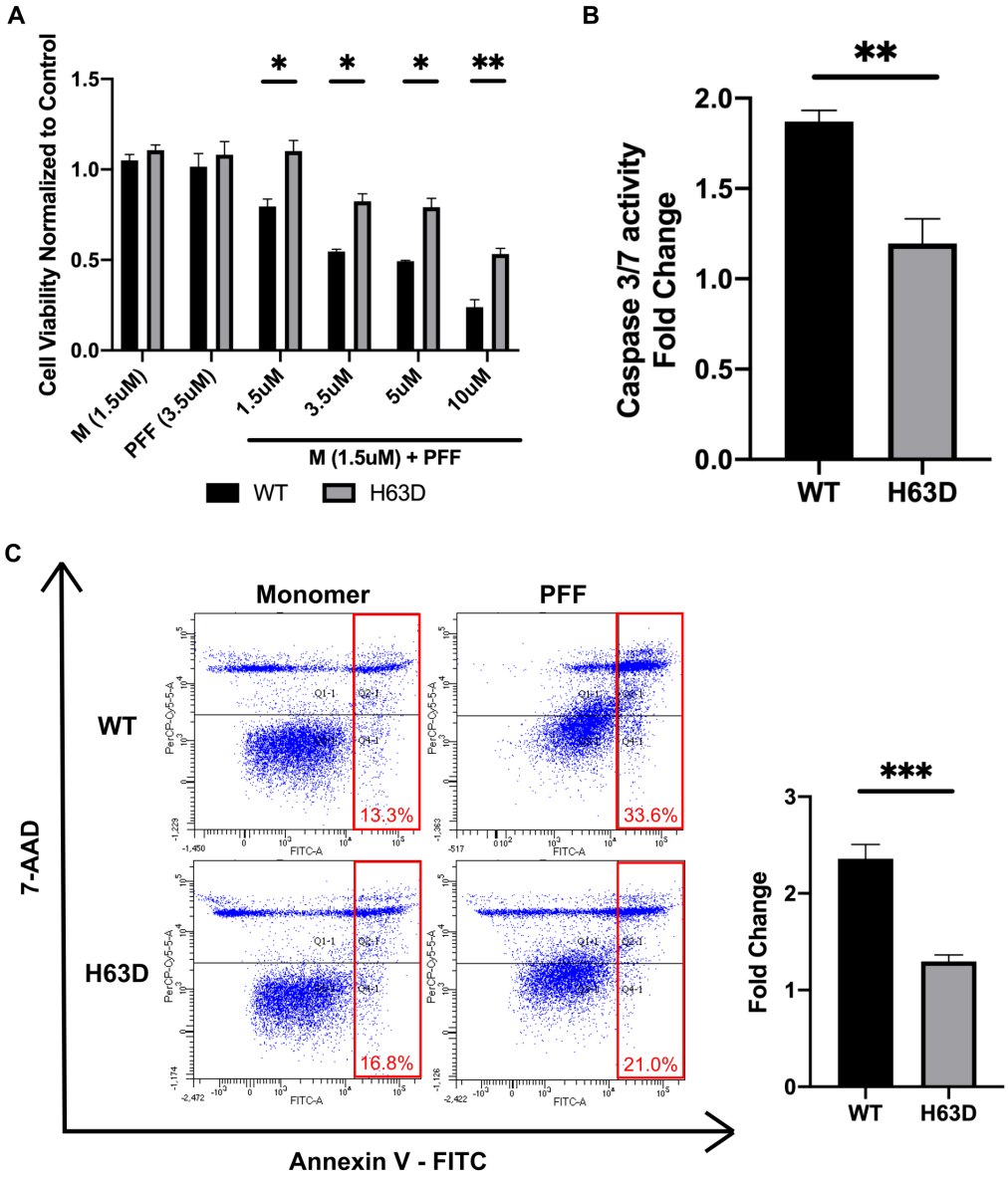

Figure 3-4: **H63D *HFE* cells are protected from PFF mediated toxicity.** (A) Cell viability was measured using CellTiter-glo and normalized to PBS treated control. Cells were treated with 1.5uM α-Syn monomer, 3.5uM PFF, or combination of 1.5uM monomer and increasing PFF concentrations for 7 days. n = 4, * $p < 0.05$, ** $p < 0.01$, ANOVA with Sidak's test for multiple

comparisons. (B) H63D *HFE* cells had decreased induction of caspase 3/7 activity after 7-day 5uM PFF + 1.5uM monomer co-treatment. Caspase activity was measured with Caspase-glo and PFF/monomer fold change was calculated. n = 3, ** $p < 0.01$, Student's t-test (C) Cells were treated with 5uM PFF + 1.5uM monomer for 7 days then stained with Annexin V-FITC and 7-AAD to assess for apoptosis. Representative flow cytometry output is shown. Fold change in % Annexin V positive cells with PFF treatment was quantified from 3 independent experiments. *** $p < 0.001$, Student's t-test.

3.4.3 Paraquat-induced α-synuclein aggregation is decreased in H67D *Hfe* mice

Previous studies with H67D *Hfe* (mouse homolog of the human H63D *HFE* variant) expressing mice have shown altered brain iron regulation[55] and protection from paraquat induced toxicity[107]. Paraquat exposure is known to induce α-synuclein aggregation. Using, the paraquat exposure model, effects of H67D *Hfe* on α-synuclein aggregation was investigated. Male C57BL/6J × 129 WT and H67D *Hfe* expressing mice were intraperitoneally injected with 10mg/kg paraquat or saline once a week for 3 weeks. Brain tissue was harvested and paraffin embedded for immunohistochemistry from three mice per genotype per injection condition. Staining with antibodies against total α-synuclein and phospho-Ser129 α-synuclein showed decreased staining intensity in the H67D *Hfe* midbrain slice compared to WT *Hfe* (**Fig. 3-5**), confirming our findings in the SH-SY5Y cell culture model.

Figure 3-5

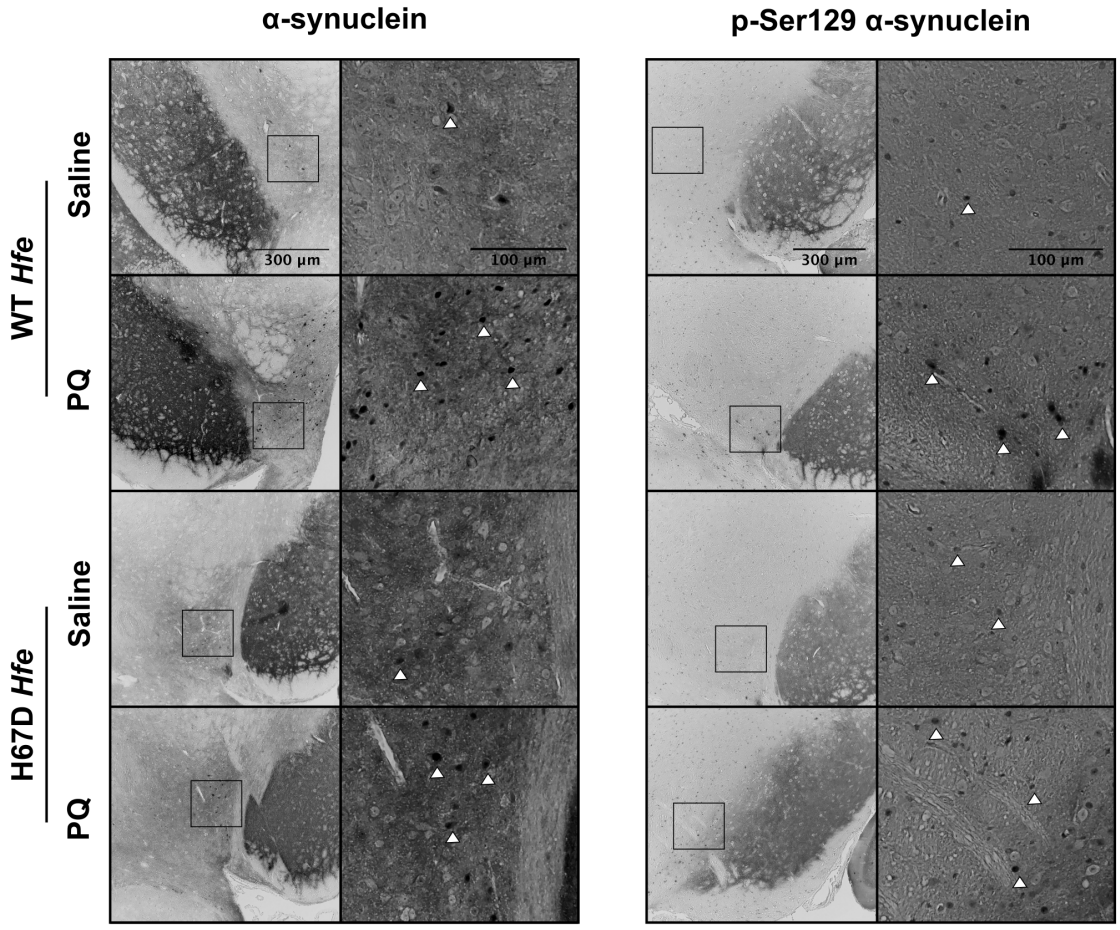

Figure 3-5: Paraquat-induced α-synuclein aggregation is decreased in H67D *Hfe* mice. 3-month-old H67D *Hfe* or WT *Hfe* expressing mice were injected with 10mg/kg paraquat or saline once a week for 3 weeks. Immunohistochemistry was performed on midbrain slices for total α-synuclein and α-synuclein phosphorylated at Ser129. Increased α-synuclein staining intensity in WT *Hfe* can be observed for both forms of α-synuclein (arrowheads) in these representative images.

3.4.4 H63D *HFE* increases autophagy through REDD1 inhibition of mTORC1

Autophagy is the main pathway for clearance of aggregated α-synuclein. Baseline autophagic flux in WT and H63D *HFE* SH-SY5Y cells was measured using autophagy inhibitors bafilomycin A1 (BafA1) and chloroquine (CQ). Cells were treated with 100nM BafA1 for 4hr or 50uM CQ for 2.5 hrs. Lysates were used for western blot against LC3B. LC3B-II band densities were quantified and autophagic flux was calculated by the difference in LC3B-II band density between control and autophagy inhibitor treated groups normalized to β-actin. Autophagic flux was significantly increased in H63D *HFE* cells (**Figs. 3-6A, 3-6B**). As expected, immunofluorescence revealed build-up of LC3-positive puncta with BafA1 treatment. Greater increase in LC3-positive puncta/cell was observed for H63D *HFE* cells compared to wildtype (**Fig. 3-6C**), confirming the LC3B-II western analysis.

Figure 3-6

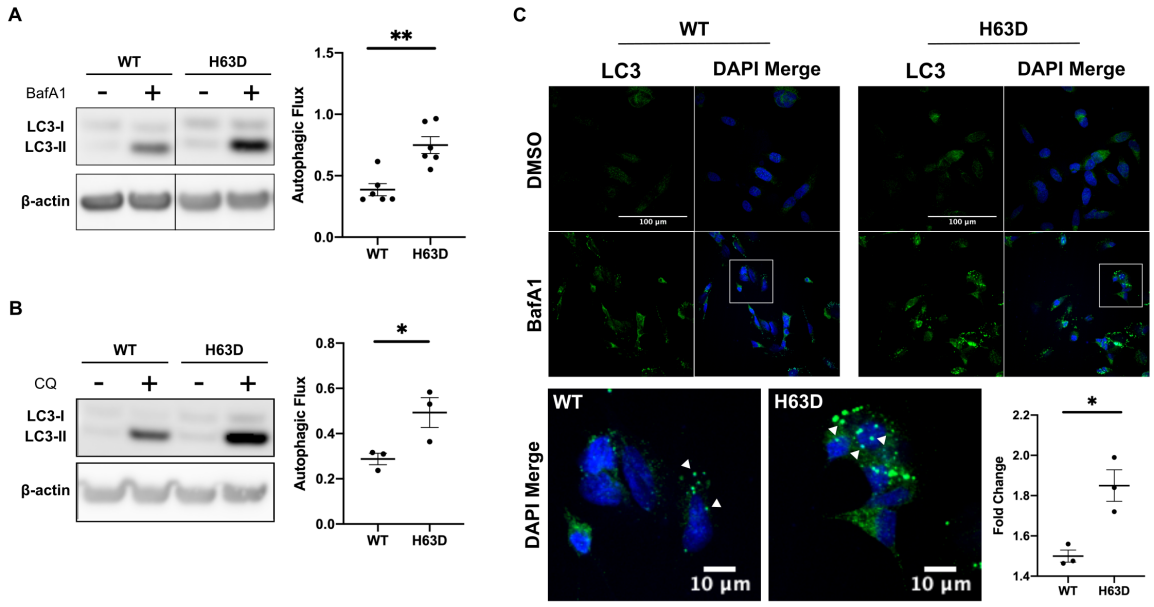

Figure 3-6: **Baseline autophagic flux is increased in H63D *HFE* cells.** (A) Representative LC3 western blot with 4hr 100nM bafilomycin A1 or DMSO treatment. Autophagic flux is calculated as the difference in LC3-II band intensity between DMSO and BafA1 treatment group normalized to β-actin. n = 6, ** $p < 0.01$, Student's t-test. (B) Cells were treated with 50uM chloroquine or PBS for 2.5 hrs and lysed for western blot. Representative blot shows larger increase in LC3-II band intensity with CQ treatment. n = 3, * $p < 0.05$, Student's t-test. (C) Top panels show increase in LC3 fluorescence signal with BafA1 treatment in WT and H63D *HFE* cells. Bottom panels show LC3 positive puncta formation (arrows) in WT and H63D *HFE* cells with BafA1 treatment. Fold change in number of LC3 positive puncta per cell after BafA1 treatment was calculated. 3 independent experiments were performed and at least 100 cells were quantified per slide. n=3, * $p < 0.05$, Student's t-test.

A potential mechanism for increased baseline autophagy is through the inhibition of mTORC1. mTORC1 is a negative regulator of autophagy and its activity can be inhibited by TSC1/TSC2 complex and drugs like rapamycin[311], resulting in a net increase in autophagic flux. When WT and H63D *HFE* cells were treated with rapamycin, autophagy induction was only detected in WT *HFE* cells (**Fig. 3-7A**). The lack of further autophagy induction by rapamycin in the H63D *HFE* cells suggested the possibility that mTORC1 pathway was maximally inhibited. To evaluate this, we compared the levels of phosphorylated ULK1 in WT and H63D *HFE* cells. ULK1 is phosphorylated by mTORC1 and is involved in autophagy initiation. ULK1 phosphorylation at Ser757 was decreased in H63D *HFE* cells (**Fig. 3-7B**). Furthermore, REDD1, which is known to inhibit mTORC1, was found be to elevated (**Fig. 3-7C**). Overall, these results indicated that H63D *HFE* cells have increased levels of autophagic flux via elevated REDD1 expression and subsequent mTORC1 inhibition.

WDR45/WIPI4 is another protein that is involved in initiation of autophagosome formation that works downstream from mTORC1 in the autophagy pathway. It is unknown whether WDR45/WIPI4 activity is affected by mTORC1. Mutations in WDR45/WIPI4 are found in a subtype of Neurodegeneration with Brain Iron Accumulation called Beta-Propeller Protein Associated Neurodegeneration[324]. Previous studies have shown that WDR45/WIPI4 knockout impairs autophagy[191]. WDR45/WIPI4 level was higher in H63D *HFE* cells compared to WT *HFE* cells (**Fig. 3-8A**). Additionally, when WDR45/WIPI4 was knocked down with siRNA, higher autophagic flux was maintained in H63D *HFE* cells, demonstrating that mTORC1-inhibition induced autophagic induction can overcome reduced WDR45/WIPI4 activity (**Fig. 3-8B**).

Figure 3-7

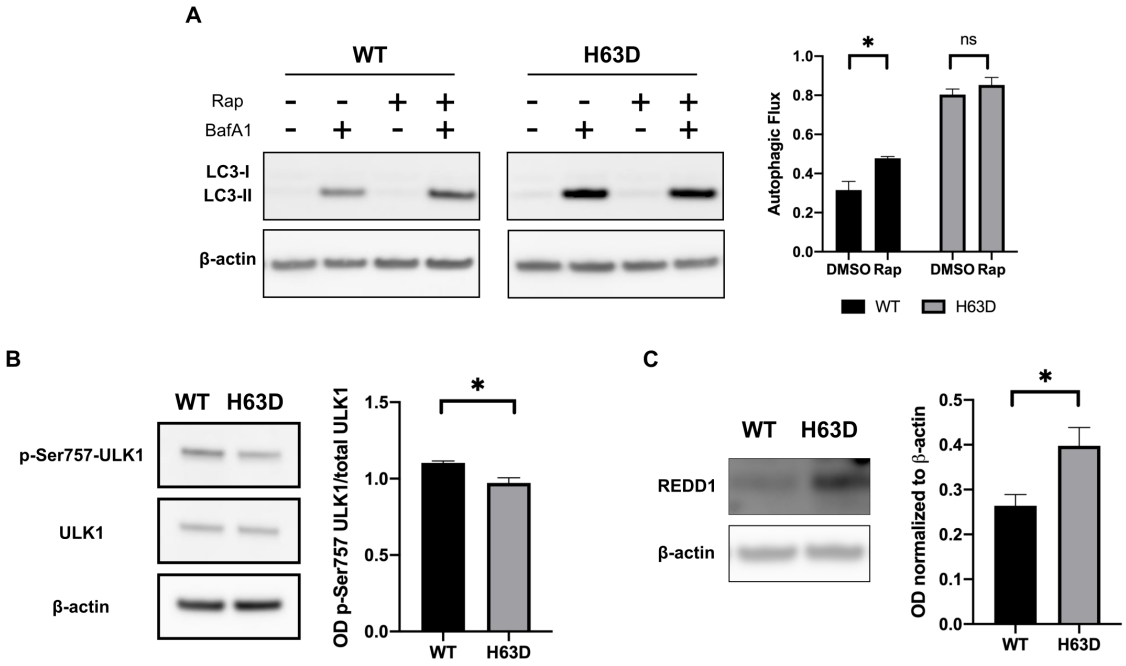

Figure 3-7: **H63D *HFE* cells are unresponsive to rapamycin treatment and have elevated REDD1 level.** (A) Cells were co-treated with 200nM Rap and 100nM BafA1 for 4hrs. Representative immunoblot for LC3 is shown. Autophagic flux was calculated from LC3-II and β-actin band intensities. n = 3, * $p < 0.05$, Student's t-test. (B) Western blots for ULK1 phosphorylated at Ser757, total ULK1, and β-actin loading control. Quantification was performed and ratio of p-Ser757-ULK1 to total ULK1 was calculated. n = 3, * $p < 0.05$, Student's t-test. (C) Representative blot of REDD1 from WT and H63D *HFE* cell lysates. Band density was quantified and normalized to β-actin. n = 3, * $p < 0.05$, Student's t-test.

Figure 3-8

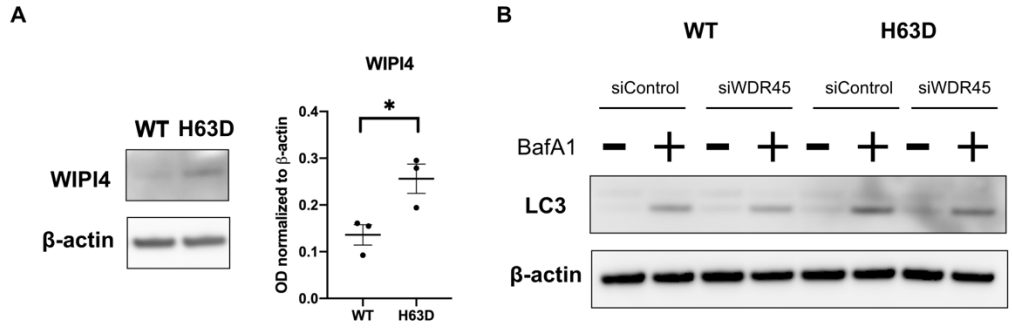

Figure 3-8: WDR45 expression is increased in H63D *HFE* cells. (A) WDR45/WIPI4 expression levels in WT and H63D *HFE* expressing SH-SY5Y cells were measured with western blot. WDR45/WIPI4 expression was higher in SH-SY5Y cells. n = 3, * $p < 0.05$, Student's t-test. (B) Furthermore, with siRNA knockdown of WDR45/WIPI4, higher autophagic flux was maintained in H63D *HFE* cells. Representative western blot shown.

3.4.5. H63D *HFE* alters response to DFP treatment

We investigated the effects of H63D *HFE* gene on the neuroprotective properties of the iron chelator deferiprone (DFP) in the pre-formed fibril model. Cells were treated with 1.5uM PFF for 5 days, then 1, 10, 30uM of deferiprone was added to the media for 2 additional days. Iron chelation has been previously reported to repress mTOR activity through the induction of REDD1 expression[312]. Changes in autophagic flux with DFP treatment was assessed using LC3 western blot (**Fig. 3-9A)**, which showed autophagy induction in WT *HFE* cells but decreased flux at lower DFP concentration or return to baseline at higher DFP concentration in H63D *HFE* cells. Consistent with this result, co-treatment with DFP and α-synuclein PFFs resulted in a decrease in total α-synuclein level in WT cells that was significant at the highest DFP dose. In contrast, H63D *HFE* cells had significantly elevated levels of α-synuclein at the low DFP concentration of 1uM while

at high concentrations, α-synuclein levels were essentially unaffected (**Fig. 3-9B)**. Similar response patterns were observed for cell viability after 1.5uM monomer + 5uM PFF treatment (**Fig. 3-9C**).

Figure 3-9

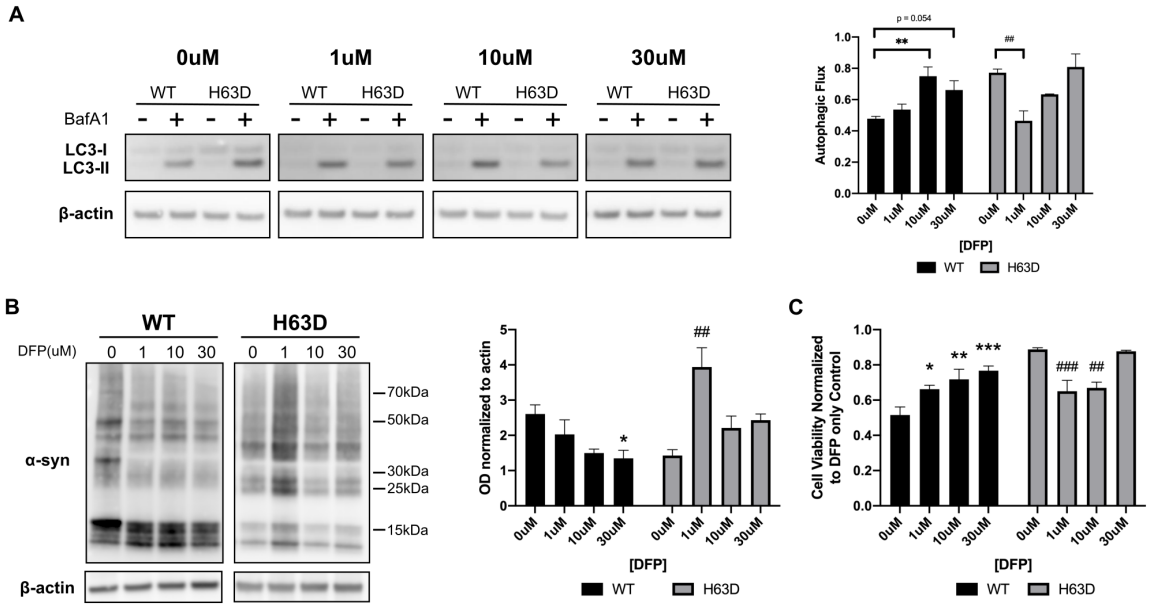

Figure 3-9: H63D *HFE* modulates response to DFP treatment. (A) After 2 days of DFP treatment, cells were treated with 100nM BafA1 or DMSO for 4hrs. Representative LC3 western blots are shown. Autophagic flux was calculated from LC3-II band intensity normalized to β-actin. n = 3, ** $p < 0.01$, ## $p < 0.01$, ANOVA with Dunnett's test for multiple comparisons (B) WT and H63D HFE cells were treated with 1.5uM PFF for 7 days. Deferiprone (0, 1, 10, 30uM) was added for the last two days. Representative western blot from cell lysates is shown. Total α-synuclein was quantified and normalized to β-actin. n = 3, * $p < 0.05$, ## $p < 0.01$, ANOVA with Dunnett's test for multiple comparisons. (C) Cell viability was measured using CellTiter-glo after 1.5uM monomer + 5uM PFF and DFP treatment. Values were normalized to DFP only control. n = 4, * $p < 0.05$, ** $p < 0.01$, *** $p < 0.001$, ## $p < 0.01$, ### $p < 0.001$, ANOVA with Dunnett's test for multiple comparisons.

3.5 Discussion

Although the common H63D *HFE* polymorphism is expected to result in an increased amount of intracellular iron that could theoretically exacerbate Parkinson's-related pathology such as oxidative stress or α-synuclein aggregation, no association between this allele frequency and Parkinson's disease risk has been clearly identified [111,113,114,120,280]. In this study, we found that the presence of this gene variant altered the metabolism of α-synuclein in cell culture and in an animal model, consistent with increased autophagic flux. We also showed that H63D *HFE* expressing neuroblastoma cells were resistant to the neuroprotective effects of an iron chelator (deferiprone). Overall, our data support the idea that H63D *HFE* gene variant modulates sensitivity to α-synuclein toxicity via its effects on protein degradation, which may lead to altered Parkinson's disease pathology.

The PFF model of Parkinson's disease is well established in cells and animals for inducing α-synuclein 'seeding' and spread, which are key components of Parkinson's disease α-synucleinopathy [304,305]. H63D *HFE* cells showed decreased α-synuclein aggregation and increased cell viability with PFF treatment. Mice that carry H67D *Hfe* (homologous to human H63D *HFE*) have also been reported to have decreased sensitivity to paraquat treatment, a mitochondrial neurotoxin model of Parkinson's disease [107]. Paraquat exposure is known to induce α-synuclein expression and aggregation [302]. We show that with paraquat exposure, H67D *Hfe* mice have decreased α-synuclein aggregation in the midbrain, supporting the concept that H63D *HFE* variant may be protective against Parkinson's disease.

The relationship of iron and α-synuclein expression has been postulated as a direct molecular effect through a putative iron responsive element (IRE) in the 5'-UTR of α-synuclein mRNA that has sequence homology to that found in the mRNA for H- and L-ferritin[81,318]. The release of IRE binding protein (IRP) from IRE in iron-replete conditions allows for increased ribosome binding of the mRNA and translation[83]. The putative IRE has been used to explain why multiple studies have observed increased α-synuclein levels with exogenous iron treatment[92,295], but studies using the yeast three hybrid system do not detect binding of IRPs to the IRE[85]. Herein we report that H63D *HFE* expressing cells in which the mutation is associated with increased labile iron and a functioning IRE-IRP system, as indicated by the induction of H-ferritin expression, α-synuclein expression level is decreased. A functional IRE/IRP in the 5' UTR would have been expected to be associated with an increase expression of α-synuclein. Thus, our study is consistent with the data that the IRE-like sequence of α-synuclein is nonfunctional, although we cannot rule out that the impact of the H63D *HFE* variant which significantly alters other aspects of cellular metabolism such as autophagy (shown herein) and cholesterol synthesis[325] that may indirectly alter the expression of α-synuclein.

We tested the hypothesis that the mechanism by which the H63D *HFE* variant altered α-synuclein level was through altered autophagy. Although autophagy was first discovered as a starvation response mechanism, many studies have now shown that constitutive autophagy is an essential homeostatic process, especially for neurons. Knockout mice lacking key proteins for autophagy (ATG8, ATG5) show signs of neurodegeneration, motor deficiencies, and accumulation of protein aggregates[309]. Hara, et al. 2006 further showed that baseline autophagy in neurons is responsible for turnover of diffuse cytosolic proteins. Dysregulation of autophagy has been shown in multiple models of Parkinson's disease; therefore, we investigated autophagy as a potential protective

mechanism in H63D *HFE* cells. Compared to wildtype, H63D *HFE* cells had increased baseline autophagic flux. H63D *HFE* cells and also failed to induce autophagy with mTORC1 inhibitor, rapamycin, treatment indicating that mTORC1 activity is already inhibited. This is consistent with the increased expression of REDD1, a known mTORC1 inhibitor. Phosphorylation of ULK1 at Ser757 was also decreased in H63D *HFE* cells. ULK1 complex initiates autophagy and Ser757 phosphorylation by mTORC1 has been shown to inhibit its activity[326]. REDD1 expression has been shown to be affected by various cellular stresses including hypoxia and ER stress[312–314]. The H63D HFE protein has been shown to induce prolonged ER stress independent of cellular iron status[56]. Additionally, expression of WDR45/WIPI4 which is involved in autophagosome formation was higher in H63D *HFE* expressing cells compared to WT *HFE* cells. With WDR45/WIPI4 siRNA knockdown, autophagic flux decreased in both WT *HFE* and H63D *HFE* cells; however, the higher flux in H63D HFE cells was maintained, demonstrating that mTORC1 inhibition upstream of WDR45/WIPI4 is likely to be the mechanism of autophagy induction. Taken together, our data show that elevated autophagy through REDD1 inhibition of mTORC1 in H63D *HFE* cells is responsible for the decreased α-synuclein level.

Because the H63D *HFE* variant alters iron status and α-synuclein metabolism, we hypothesized that iron chelation therapy would be impacted by the presence of this genotype. Deferiprone (DFP) is an iron chelator that is under active investigation as a disease modifying therapy for Parkinson's disease (Clinicaltrials.gov Identifier: NCT02655315). DFP treatment has been shown to reduce brain iron levels by MRI[69]. Preclinical models using 6-OHDA and MPTP have shown that DFP is neuroprotective[69,243]. While those neurotoxins cause dopaminergic neuronal cell death, they fail to model α-synuclein aggregation. Using PFFs, we showed that DFP is effective in reducing α-synuclein aggregation and protecting from cell death in WT *HFE* expressing cells but had mixed

effects in the H63D *HFE* cells which mirrored changes in autophagy. In H63D *HFE* cells, the decrease in autophagy with low dose of DFP treatment could be due to the loss of increase in intracellular iron from the *HFE* variant. With higher dose of DFP, cellular iron deficiency can be achieved leading to autophagy induction. The pilot clinical trials of DFP for Parkinson's disease have shown conflicting results. DFP treatment was shown to decrease brain iron content by MRI; however, one study failed to show clinical improvement after 6 months of treatment[69,298]. Our data suggest that stratifying the Parkinson's disease patients according to their *HFE* genotype could clarify some of the mixed clinical results.

In conclusion, the findings presented in this study demonstrate that H63D *HFE* variant has a significant impact on α-synuclein homeostasis of the cell through its modulation of autophagy, leading to protection in *in vitro* PFF model and *in vivo* paraquat exposure models of Parkinson's disease. Deferiprone treatment, as expected, was found to be effective in reducing α-synuclein aggregation and increasing cell viability but only with WT *HFE* expression. Given the high prevalence of H63D *HFE* variant in the general population, our study establishes *HFE* genotype as a potential disease modifier of Parkinson's disease pathology. Furthermore, our findings argue for the importance of stratification by *HFE* genotype for evaluation of therapeutic trials with iron chelator therapy.

3.6 Acknowledgements

We thank Penn State Flow Cytometry Core for their technical support, Sang Lee, Ph.D. for providing *HFE* transfected SH-SY5Y cells, Anne Nixon, Ph.D. for animal experiments, and Salvatore Stella, Jr., Ph.D. for confocal imaging support.

Chapter 4

H63D *HFE* variant in Parkinson's disease and beyond

4.1 Introduction and brief summary of main findings

The work presented in this dissertation demonstrates the clinical impact of H63D *HFE* in the Parkinson's disease population and provides a direct mechanistic link between the *HFE* variant and α-synuclein pathology. Previous studies have shown that the H63D *HFE* variant, which increases iron uptake into the cell through the transferrin receptor, decreases age of onset of Alzheimer's disease and slows progression of amyotrophic lateral sclerosis. In Parkinson's disease, investigations into the role of *HFE* variants on disease risk has been inconclusive. In chapter 2, DaTscan SPECT imaging data and United Parkinson's Disease Rating Scale part III from the Parkinson's Progressive Markers Initiative database were used to investigate the impact of *HFE* genotype on patient clinical profiles. H63D *HFE* carriers were found to have lower contralateral caudate striatal binding ratio at disease baseline and have slower UPDRS part III change with time. Moreover, H63D *HFE* carriers had altered blood *SNCA* RNA transcript and CSF α-synuclein levels compared to patients with WT *HFE*, demonstrating the impact of H63D *HFE* variant as a modifier of Parkinson's disease progression and biomarker. Next, the effects of H63D *HFE* on α-synuclein expression, aggregation, and cytotoxicity were assessed using cell culture and animal models. H63D *HFE* expression lowered endogenous α-synuclein levels and pre-formed fibril induced α-synuclein aggregation and cytotoxicity. Using an *in vivo* paraquat exposure model, H67D *Hfe* mice

were shown to decreased α-synuclein aggregation compared to WT *Hfe* mice. Elevated baseline autophagic flux was identified to be the protective mechanism with REDD1 inhibition of the mTORC1 pathway. Furthermore, while iron chelator (deferiprone) treatment rescued WT *HFE* cells from pre-formed fibril induced α-synuclein aggregation and toxicity, it exacerbated or was unable to rescue H63D *HFE* cells. In all, the preclinical and the clinical data stablish H63D *HFE* as a significant genetic modifier of Parkinson's disease.

4.2 H63D *HFE* in Parkinson's disease pathology

Beyond the direct effects on α-synuclein metabolism through modulation of autophagy, H63D *HFE* may impact Parkinson's disease pathology through other pathways. As previously reported, H67D *Hfe* mice have elevated Nrf2 expression[55]. Nrf2 is a transcription factor responsible for regulation of the glutathione and other reactive oxygen species response systems in the cell[327]. In postmortem brain tissue from Parkinson's disease patients, glutathione to glutathione disulfide (GSH:GSSG) ratio was found to be decreased indicating increased oxidative stress[328]. Response to oxidative stress is especially important in the context of the increased vulnerability of dopaminergic neurons for neurodegeneration in Parkinson's disease. Dopamine can interaction with ROS and undergo auto-oxidation to form dopamine quinones and free radicals, contributing to further to the neurodegeneration[329]. Beyond the antioxidant response, Nrf2 is also involved in modulating mitochondrial function. Nrf2 has been shown to regulate mitochondrial biogenesis and mitophagy[330,331]. The increased Nrf2 expression with H63D *HFE* expression may provide additional protection from oxidative agents used to model Parkinson's disease such as paraquat[107]. Furthermore, investigations into the mechanism underlying Nrf2 activation in H63D *HFE* can provide insights into novel targets for therapy development.

Another intriguing consideration into how *HFE* status impacts disease progression is the role of *HFE* in the immune system. HFE is non-classical MHC-1b molecule[332]MHC I molecules in the immune system plays a role in peptide presentation to T lymphocytes in response to intracellular pathogens[332]. Although HFE does not seem to have antigen binding capacity, it has been reported to interact with T cells and shape T cell function[333–335]. This is further supported by the altered CD4/CD8+ T cell ratios found in hemochromatosis patients[336]. Further immune disturbances have been noted in hereditary hemochromatosis patients such as reduced NKT cells, decreased CD8+ T cells, reduced overall MHC I expression at the cell surface, and increased Th2 polarization by elevated IL-10 and IL-4 levels[335,337–339].

Both innate and adaptive immunity have been shown to play a significant role in Parkinson's disease pathology. Although the central nervous system is thought to be generally immune privileged, recent studies have shown that T cells and B cells can be found in the dural lymphatic vessels[340]. Furthermore, compromised blood-brain barrier due to Parkinson's disease pathology can promote immune infiltration into the brain[341]. In particular importance is the role of T cells in immune mediated injuries associated with Parkinson's disease. Cytotoxic CD8+ T cells can induce apoptosis through calcium-dependent release of lytic granules. These granules contain cytotoxic effector proteins like perforins and granzymes that can form transmembrane pores and digest enzymes[342]. Increased recruitment of CD8+ and CD4+ T cells into substantia nigra of Parkinson's disease patients as well as in MPTP mouse models has been reported[343,344]. Peripheral T cell activation has also been reported in Parkinson's disease patients and T cell profile in the blood has been shown to correlate with UPDRS part III score, indicating an active role of the immune system in Parkinson's disease progression[345]. *HFE* variants have been shown to alter T cell population profile and phenotype. Decrease in CD8+ T cell population as well as increased anti-inflammatory

Th2 polarization can contribute to the reduction of immune mediated damage in the context of Parkinson's disease pathology ultimately leading to delayed disease progression.

4.3 H63D *HFE* and Parkinson's disease therapy development

H63D *HFE* genotype may have a direct impact on the use of iron chelators as disease modifying therapies for Parkinson's disease. As it was shown in Chapter 3, deferiprone treatment was unable to rescue H63D *HFE* cells from pre-formed fibril mediated toxicity. This was attributed to the failure of iron chelator to induce autophagy in the H63D *HFE* expressing cells that already have a higher basal autophagic flux. Furthermore, mTOR inhibitor rapamycin treatment was also unable to induce autophagy in H63D *HFE* cells due to baseline inhibition of the mTORC1 pathway. With active investigations into the use of autophagy enhancers for Parkinson's disease[346], elevated autophagy and neuroprotection seen in H63D *HFE* provides further evidence for potential efficacy of these drugs. However, it also provides a unique challenge in treating Parkinson's disease patients with H63D *HFE* genotype. From the presented preclinical studies in cell culture, H63D *HFE* expression seems to "max out" the autophagy pathway and further induction cannot be achieved. This may lead to failure to respond to autophagy-related treatments.

Another novel therapeutic target for Parkinson's disease is neuroinflammation. Neuroinflammation is thought to play a significant role in exacerbation of the neurodegenerative process as dopaminergic neurons continue to die and release immunogenic α-synuclein into the extracellular space. Interestingly, pre-treatment with non-steroidal anti-inflammatory drugs (NSAIDs) before MTPT or 6-OHDA exposure has been shown to provide neuroprotection[347]. Moreover, chronic NSAID use has been shown to decrease risk for developing Parkinson's disease[348]. Again, because patients with *HFE* variants may already have a lower inflammatory profile, the use of anti-

inflammatory therapy in this subset of patients may be ineffective, further indicating the importance of patient stratification by *HFE* genotype in clinical trials.

With already elevated autophagy and reduced inflammation, the question becomes then how should we treat Parkinson's disease in H63D *HFE* carriers? Anti-α-synuclein antibody therapy has been under investigation by multiple pharmaceutical companies[349,350]. Anti-α-synuclein therapy directly targets the protein that is thought to be the toxic component of Parkinson's disease pathology and has the potential to stop disease progression. A potential pitfall in this approach is that merely removing α-synuclein may not provide neuroprotective effects as expected. This has been seen with failures in phase III trials of anti-Aβ therapy of Alzheimer's disease[351].

4.4 H63D *HFE* and autophagy: Beyond Parkinson's disease

The induction of autophagy by H63D *HFE* expression has implications beyond altered α-synuclein homeostasis in Parkinson's disease. Not only is α-synuclein aggregation found in other diseases such as dementia with Lewy bodies, multiple system atrophy, and certain subtypes of Neurodegeneration with Brain Iron Accumulation, protein aggregation and toxicity are key pathological features in other neurodegenerative diseases[352]. In amyotrophic lateral sclerosis, TDP-43 aggregation is seen in greater than 90% of all sporadic cases[194]. In Alzheimer's disease, aggregated Aβ and tau form plaques and neurofibrillary tangles[127]. Chronic traumatic encephalopathy caused by repeated traumatic brain injuries also show extensive depositions of hyperphosphorylated tau along with accumulation of TDP-43, Aβ, and α-synuclein[353]. Disruption in protein degradation pathways, both the ubiquitin-proteasome system and autophagy, is a fundamental pathological process in neurodegenerative diseases. Alterations in autophagy by

H63D *HFE,* therefore, has consequences far beyond Parkinson's diseases in the central nervous system.

Another important aspect of autophagy is its role as a pro-survival pathway. This plays a significant role in terminally differentiated cells like neurons and myocytes. Dysregulation of autophagy has been observed in various myopathies like Pompe disease and excessive activation of autophagy has been associated with muscle wasting[354,355]. Additionally, autophagy has been found to be essential maintenance of skeletal muscle homeostasis. Conditional knockout of the Atg7 gene, involved in initiation of autophagy, in the skeletal muscle was shown to increase abnormal mitochondria and disorganization of sarcomeres[356]. Autophagy inhibition was also shown to increase muscle loss during denervation and fasting[357]. This finding is of particular interest in the context of amyotrophic lateral sclerosis. ALS is a neurodegeneration of motor neurons resulting in the loss of muscle function and muscle mass. Because inhibition of autophagy was shown to exacerbate muscle loss with denervation, it can be logically hypothesized that slight increase in autophagy can lead to better maintenance of muscle even with nerve degeneration. One study has also reported that 80% of French athletes who have won international competition are heterozygous for a mutation in *HFE*, which much higher than the ~20% seen in the general population[358]. This finding may also support the idea that even outside the context of disease, H63D *HFE* genotype can lead to better maintenance of muscle and consequently better performance in sports.

Autophagy induction can also be a double-edged sword. In the context of muscle and nerve degeneration the autophagy can promote cell survival leading to better outcomes. However, with cancer which is characterized by uncontrolled growth, induction of autophagy can result in tumor promotion[359]. Often times, tumors are exposed to high stress due to increased metabolic demands as well as constant exposure to hypoxia and nutrient deprivation. Autophagy has been shown to be

activated at the center of solid tumors[360]. Furthermore, autophagy is also implicated in cancer metastasis. In the early stages, autophagy induction can be anti-metastatic due to inhibition of proliferation, migration and invasion[361]. However, in advanced stages autophagy induction can be pro-metastatic by promoting cancer cell survival at secondary sites[362]. Multiple studies have found that *HFE* variants can modulate cancer risk and progression. C282Y *HFE* was associated with increased risk for breast cancer, colorectal cancer, and hepatocellular carcinoma[363]. With H63D *HFE*, increased risk for adenocarcinomas of breast and prostate has been reported[364]. Additionally, high frequency of H63D *HFE* mutation is found in malignant gliomas, where it has been found to decrease patient survival[365]. In a cell culture model, loss of HFE expression was shown to accelerate tumor progression through decreased senescence, increased cell migration, and increased glucose uptake[366]. As mentioned above, H63D *HFE* can play a role in modulation of the immune system and therefore immune response to cancer. However, the direct effect of autophagy induction on tumor promotion should also be considered when interrogating cancer and *HFE* genotype.

4.5 Conclusion

In this dissertation, H63D *HFE* was shown to alter Parkinson's disease clinical profile and α-synuclein pathology through modulation of autophagy. However, H63D *HFE* expression has consequences beyond altered protein degradation that may also influence the disease process and subsequently affect the development of novel therapeutics for Parkinson's disease. Furthermore, dysregulation of autophagy can be linked various other diseases logically leading to speculations on the role of H63D *HFE* outside the Parkinson's disease pathology and the central nervous system. In conclusion, the impact of H63D *HFE* beyond its role in iron uptake regulation can lead to modulation of multiple diseases and cellular processes with significant clinical consequences. The

clear outcome of this dissertation work is that *HFE* genotype should not be disregarded in evaluation of therapies for neurodegenerative diseases.

References

1. Hallervorden, J. & Spatz, H. Eigenartige Erkrankung im extrapyramidalen System mit besonderer Beteiligung des Globus pallidus und der Substantia nigra (Peculiar disease of the extrapyramidal system with particular affection of the globus pallidus and the substantia nigra). *Zeitschrift für die gesamte Neurol. und Psychiatr.* **79**, 254–302 (1922).
2. L'hermitte, J., Kraus, W. M. & McAlpine, D. On the occurrence of abnormal deposits of iron in the brain in parkinsonism with special reference to its localisation. *J. Neurol. Neurosurg. Psychiatry* **S1-5**, 195–208 (1924).
3. Goodman, L. Alzheimer's disease: a clinicopathologic analysis of twenty-three cases with a theory on pathogenesis. *J. Nerv. Ment. Dis.* **118**, 97–130 (1953).
4. Beard, J. L. & Connor, J. R. Iron status and neural functioning. *Annu. Rev. Nutr.* **23**, 41–58 (2003).
5. Markova, V., Holm, C., Pinborg, A., Thomsen, L. & Moos, T. Impairment of the Developing Human Brain in Iron Deficiency: Correlations to Findings in Experimental Animals and Prospects for Early Intervention Therapy. *Pharmaceuticals* **12**, 120 (2019).
6. Ward, R. J., Zucca, F. A., Duyn, J. H., Crichton, R. R. & Zecca, L. The role of iron in brain ageing and neurodegenerative disorders. *Lancet. Neurol.* **13**, 1045–60 (2014).
7. Frey, P. A. & Reed, G. H. The ubiquity of iron. *ACS Chem. Biol.* **7**, 1477–1481 (2012).
8. Crichton, R. The importance of Iron for biological systems. in *Inorganic Biochemistry of Iron Metabolism: From Molecular Mechanisms to Clinical Consequences* 17–48 (John Wiley & Sons, Ltd, 2001). doi:10.1002/0470845791
9. Kruszewski, M. Labile iron pool: the main determinant of cellular response to oxidative stress. *Mutat. Res.* **531**, 81–92 (2003).
10. Dixon, S. J. & Stockwell, B. R. The role of iron and reactive oxygen species in cell death. *Nat. Chem. Biol.* **10**, 9–17 (2014).
11. Lane, D. J. R. *et al.* Cellular iron uptake, trafficking and metabolism: Key molecules and mechanisms and their roles in disease. *Biochim. Biophys. Acta - Mol. Cell Res.* **1853**, 1130–1144 (2015).
12. Gunshin, H. *et al.* Cloning and characterization of a mammalian proton-coupled metal-ion transporter. *Nature* **388**, 482–488 (1997).
13. Jenkitkasemwong, S., Wang, C. Y., MacKenzie, B. & Knutson, M. D. Physiologic implications of metal-ion transport by ZIP14 and ZIP8. *BioMetals* **25**, 643–655 (2012).
14. Hentze, M. W., Muckenthaler, M. U., Galy, B. & Camaschella, C. Two to Tango: Regulation of Mammalian Iron Metabolism. *Cell* **142**, 24–38 (2010).
15. Ohgami, R. S. *et al.* Identification of a ferrireductase required for efficient transferrin-dependent iron uptake in erythroid cells. *Nat. Genet.* **37**, 1264–1269 (2005).
16. Bradley, J. M., Le Brun, N. E. & Moore, G. R. Ferritins: Furnishing proteins with iron Topical Issue in Honor of R.J.P. Williams. *Journal of Biological Inorganic Chemistry* **21**, 13–28 (2016).
17. Mancias, J. D., Wang, X., Gygi, S. P., Harper, J. W. & Kimmelman, A. C. Quantitative proteomics identifies NCOA4 as the cargo receptor mediating ferritinophagy. *Nature* **508**, 105–109 (2014).
18. Cassavaugh, J. & Lounsbury, K. M. Hypoxia-mediated biological control. *Journal of Cellular Biochemistry* **112**, 735–744 (2011).

19. Mole, D. R. Iron Homeostasis and Its Interaction with Prolyl Hydroxylases. *Antioxidants and Redox Signaling* **12**, 445–458 (2010).
20. Muckenthaler, M. U., Galy, B. & Hentze, M. W. Systemic Iron Homeostasis and the Iron-Responsive Element/Iron-Regulatory Protein (IRE/IRP) Regulatory Network. *Annu. Rev. Nutr.* **28**, 197–213 (2008).
21. Hentze, M. W. & Kühn, L. C. Molecular control of vertebrate iron metabolism: mRNA-based regulatory circuits operated by iron, nitric oxide, and oxidative stress. *Proceedings of the National Academy of Sciences of the United States of America* **93**, 8175–8182 (1996).
22. Muckenthaler, M., Gray, N. K. & Hentze, M. W. IRP-1 binding to ferritin mRNA prevents the recruitment of the small ribosomal subunit by the cap-binding complex elF4F. *Mol. Cell* **2**, 383–388 (1998).
23. Müllner, E. W., Neupert, B. & Kühn, L. C. A specific mRNA binding factor regulates the iron-dependent stability of cytoplasmic transferrin receptor mRNA. *Cell* **58**, 373–382 (1989).
24. Koeller, D. M. *et al.* A cytosolic protein binds to structural elements within the iron regulatory region of the transferrin receptor mRNA. *Proc. Natl. Acad. Sci. U. S. A.* **86**, 3574–3578 (1989).
25. Guo, B., Phillips, J. D., Yu, Y. & Leibold, E. A. Iron regulates the intracellular degradation of iron regulatory protein 2 by the proteasome. *J. Biol. Chem.* **270**, 21645–21651 (1995).
26. Giannetti, A. M. & Björkman, P. J. HFE and transferrin directly compete for transferrin receptor in solution and at the cell surface. *J. Biol. Chem.* **279**, 25866–25875 (2004).
27. Han, O., Fleet, J. C. & Wood, R. J. Reciprocal Regulation of HFE and Nramp2 Gene Expression by Iron in Human Intestinal Cells. *J. Nutr.* **129**, 98–104 (1999).
28. Feder, J. N. *et al.* A novel MHC class I-like gene is mutated in patients with hereditary haemochromatosis. *Nat. Genet.* **13**, 399–408 (1996).
29. Bhatt, L., Horgan, C. P., Walsh, M. & McCaffrey, M. W. The Hereditary Hemochromatosis protein HFE and its chaperone β2-microglobulin localise predominantly to the endosomal-recycling compartment. *Biochem. Biophys. Res. Commun.* **359**, 277–284 (2007).
30. Simon, M., Bourel, M., Fauchet, R. & Genetet, B. Association of HLA A3 and HLA B14 antigens with idiopathic haemochromatosis. *Gut* **17**, 332–334 (1976).
31. Feder, J. N. *et al.* The hemochromatosis gene product complexes with the transferrin receptor and lowers its affinity for ligand binding. *Proc. Natl. Acad. Sci. U. S. A.* **95**, 1472–7 (1998).
32. Acton, R. T. *et al.* Geographic and racial/ethnic differences in HFE mutation frequencies in the hemochromatosis and iron overload screening (HEIRS) study. *Ethn. Dis.* **16**, 815–821 (2006).
33. Hollerer, I., Bachmann, A. & Muckenthaler, M. U. Pathophysiological consequences and benefits of HFE mutations: 20 years of research. *Haematologica* **102**, (2017).
34. Puig, S., Ramos-Alonso, L., Romero, A. M. & Martínez-Pastor, M. T. The elemental role of iron in DNA synthesis and repair. *Metallomics* **9**, 1483–1500 (2017).
35. Reinert, A., Morawski, M., Seeger, J., Arendt, T. & Reinert, T. Iron concentrations in neurons and glial cells with estimates on ferritin concentrations. *BMC Neurosci.* **20**, (2019).
36. Connor, J. R., Pavlick, G., Karli, D., Menzies, S. L. & Palmer, C. A histochemical study of iron-positive cells in the developing rat brain. *J. Comp. Neurol.* **355**, 111–123 (1995).
37. Benkovic, S. A. & Connor, J. R. Ferritin, transferrin, and iron in selected regions of the

adult and aged rat brain. *J. Comp. Neurol.* **338**, 97–113 (1993).
38. Todorich, B., Pasquini, J. M., Garcia, C. I., Paez, P. M. & Connor, J. R. Oligodendrocytes and myelination: The role of iron. *Glia* **57**, 467–478 (2009).
39. Connor, J. R. & Menzies, S. L. Relationship of iron to oligodendrocytes and myelination. *Glia* **17**, 83–93 (1996).
40. Wu, L. ling *et al.* Effect of perinatal iron deficiency on myelination and associated behaviors in rat pups. *Behav. Brain Res.* **188**, 263–270 (2008).
41. Rosato-Siri, M. V. *et al.* Iron Availability Compromises Not Only Oligodendrocytes But Also Astrocytes and Microglial Cells. *Mol. Neurobiol.* **55**, 1068–1081 (2018).
42. Mason, J. L., Suzuki, K., Chaplin, D. D. & Matsushima, G. K. Interleukin-1β promotes repair of the CNS. *J. Neurosci.* **21**, 7046–7052 (2001).
43. Youdim, M. B. H. *et al.* The effects of iron deficiency on brain biogenic monoamine biochemistry and function in rats. *Neuropharmacology* **19**, 259–267 (1980).
44. Rudisill, S. S., Martin, B. R., Mankowski, K. M. & Tessier, C. R. Iron Deficiency Reduces Synapse Formation in the Drosophila Clock Circuit. *Biol. Trace Elem. Res.* **189**, 241–250 (2019).
45. Bastian, T. W., Von Hohenberg, W. C., Mickelson, D. J., Lanier, L. M. & Georgieff, M. K. Iron Deficiency Impairs Developing Hippocampal Neuron Gene Expression, Energy Metabolism, and Dendrite Complexity. *Dev. Neurosci.* **38**, 264–276 (2016).
46. Matak, P. *et al.* Disrupted iron homeostasis causes dopaminergic neurodegeneration in mice. *Proc. Natl. Acad. Sci. U. S. A.* **113**, 3428–3435 (2016).
47. Hayflick, S. J. *et al.* Beta-propeller protein-associated neurodegeneration: a new X-linked dominant disorder with brain iron accumulation. *Brain* **136**, 1708–1717 (2013).
48. Zecca, L. *et al.* The role of iron and molecules in the neuronal vulnerability of locus coeruleus and substantia nigra during aging. *Proc. Natl. Acad. Sci. U. S. A.* **101**, 9843–9848 (2004).
49. Bartzokis, G. *et al.* MR evaluation of age-related increase of brain iron in young adult and older normal males. *Magn. Reson. Imaging* **15**, 29–35 (1997).
50. Martin, W. R. W., Ye, F. Q. & Allen, P. S. Increasing striatal iron content associated with normal aging. *Mov. Disord.* **13**, 281–286 (1998).
51. Ashraf, A., Clark, M. & So, P. W. The aging of iron man. *Frontiers in Aging Neuroscience* **10**, (2018).
52. Hydén, H. & Lange, P. W. The Steady State and Endogenous Respiration in Neuron and Glia. *Acta Physiol. Scand.* **64**, 6–14 (1965).
53. Hänninen, M. M. *et al.* Expression of iron-related genes in human brain and brain tumors. *BMC Neurosci.* **10**, 36 (2009).
54. Nandar, W. & Connor, J. R. HFE Gene Variants Affect Iron in the Brain. *J. Nutr.* **141**, 729S-739S (2011).
55. Nandar, W., Neely, E. B., Unger, E. & Connor, J. R. A mutation in the HFE gene is associated with altered brain iron profiles and increased oxidative stress in mice. *Biochim. Biophys. Acta - Mol. Basis Dis.* **1832**, 729–741 (2013).
56. Liu, Y. *et al.* Mutant HFE H63D Protein Is Associated with Prolonged Endoplasmic Reticulum Stress and Increased Neuronal Vulnerability. *J. Biol. Chem.* **286**, 13161–13170 (2011).
57. Meadowcroft, M. D. *et al.* Reduced white matter MRI transverse relaxation rate in cognitively normal H63D-HFE human carriers and H67D-HFE mice. *Brain Imaging Behav.* **10**, 1231–1242 (2016).
58. Meadowcroft, M. D. *et al.* Reduced Cerebral White Matter Integrity Assessed by DTI in Cognitively Normal H63D-HFE Polymorphism Carriers. *J. Neuroimaging* **28**, 126–133

(2018).
59. Ali-Rahmani, F. *et al.* H63D mutation in hemochromatosis alters cholesterol metabolism and induces memory impairment. *Neurobiol. Aging* **35**, 1511.e1-1511.e12 (2014).
60. Dorsey, E. R., Sherer, T., Okun, M. S. & Bloemd, B. R. The emerging evidence of the Parkinson pandemic. *Journal of Parkinson's Disease* **8**, S3–S8 (2018).
61. Kalia, L. V. & Lang, A. E. Parkinson's disease. *The Lancet* **386**, 896–912 (2015).
62. Spillantini, M. G. *et al.* Alpha-synuclein in Lewy bodies. *Nature* **388**, 839–840 (1997).
63. Shahmoradian, S. H. *et al.* Lewy pathology in Parkinson's disease consists of crowded organelles and lipid membranes. *Nat. Neurosci.* **22**, 1099–1109 (2019).
64. Wang, J.-Y. *et al.* Meta-analysis of brain iron levels of Parkinson's disease patients determined by postmortem and MRI measurements. *Sci. Rep.* **6**, 36669 (2016).
65. An, H. *et al.* Quantifying iron deposition within the substantia nigra of Parkinson's disease by quantitative susceptibility mapping. *J. Neurol. Sci.* **386**, 46–52 (2018).
66. Chen, Q. *et al.* Iron deposition in Parkinson's disease by quantitative susceptibility mapping. *BMC Neurosci.* **20**, 23 (2019).
67. Sun, H. *et al.* Validation of quantitative susceptibility mapping with Perls' iron staining for subcortical gray matter. *Neuroimage* **105**, 486–492 (2015).
68. Langkammer, C. *et al.* Quantitative susceptibility mapping (QSM) as a means to measure brain iron? A post mortem validation study. *Neuroimage* **62**, 1593–1599 (2012).
69. Devos, D. *et al.* Targeting chelatable iron as a therapeutic modality in Parkinson's disease. *Antioxid. Redox Signal.* **21**, 195–210 (2014).
70. Sian-Hülsmann, J., Mandel, S., Youdim, M. B. H. & Riederer, P. The relevance of iron in the pathogenesis of Parkinson's disease. *J. Neurochem.* **118**, 939–957 (2011).
71. Dexter, D. T. *et al.* Increased Nigral Iron Content In Postmortem Parkinsonian Brain. *Lancet* **330**, 1219–1220 (1987).
72. Jellinger, K. *et al.* Iron-Melanin Complex in Substantia Nigra of Parkinsonian Brains: An X-Ray Microanalysis. *J. Neurochem.* **59**, 1168–1171 (1992).
73. Mirza, B., Hadberg, H., Thomsen, P. & Moos, T. The absence of reactive astrocytosis is indicative of a unique inflammatory process in Parkinson's disease. *Neuroscience* **95**, 425–432 (1999).
74. Castillo, X. *et al.* Re-thinking the etiological framework of neurodegeneration. *Frontiers in Neuroscience* **13**, (2019).
75. Salazar, J. *et al.* Divalent metal transporter 1 (DMT1) contributes to neurodegeneration in animal models of Parkinson's disease. *Proc. Natl. Acad. Sci. U. S. A.* **105**, 18578–18583 (2008).
76. Howitt, J. *et al.* Increased Ndfip1 in the Substantia Nigra of Parkinsonian Brains Is Associated with Elevated Iron Levels. *PLoS One* **9**, e87119 (2014).
77. Li, X. *et al.* A Mechanistic Study of Proteasome Inhibition-Induced Iron Misregulation in Dopamine Neuron Degeneration. *Neurosignals* **20**, 223–236 (2012).
78. Jakes, R., Spillantini, M. G. & Goedert, M. Identification of two distinct synucleins from human brain. *FEBS Lett.* **345**, 27–32 (1994).
79. Villar-Piqué, A., Lopes da Fonseca, T. & Outeiro, T. F. Structure, function and toxicity of alpha-synuclein: the Bermuda triangle in synucleinopathies. *Journal of Neurochemistry* **139**, 240–255 (2016).
80. Burré, J. *et al.* α-Synuclein promotes SNARE-complex assembly in vivo and in vitro. *Science (80-.).* **329**, 1663–1667 (2010).
81. Febbraro, F., Giorgi, M., Caldarola, S., Loreni, F. & Romero-Ramos, M. α-Synuclein expression is modulated at the translational level by iron. *Neuroreport* **23**, 576–580 (2012).

82. Friedlich, A. L., Tanzi, R. E. & Rogers, J. T. The 5′-untranslated region of Parkinson's disease α-synuclein messengerRNA contains a predicted iron responsive element. *Mol. Psychiatry* **12**, 222–223 (2007).
83. Pantopoulos, K. Iron metabolism and the IRE/IRP regulatory system: An update. *Annals of the New York Academy of Sciences* **1012**, 1–13 (2004).
84. Koukouraki, P. & Doxakis, E. Constitutive translation of human α-synuclein is mediated by the 5'-untranslated region. *Open Biol.* (2016). doi:10.1098/rsob.160022
85. Chen, S.-C. & Olsthoorn, R. C. L. Relevance of the iron-responsive element (IRE) pseudotriloop structure for IRP1/2 binding and validation of IRE-like structures using the yeast three-hybrid system. *Gene* **710**, 399–405 (2019).
86. Sanchez, M. *et al.* Iron regulatory protein-1 and -2: Transcriptome-wide definition of binding mRNAs and shaping of the cellular proteome by iron regulatory proteins. *Blood* **118**, 168–180 (2011).
87. Meade, R. M., Fairlie, D. P. & Mason, J. M. Alpha-synuclein structure and Parkinson's disease - Lessons and emerging principles. *Molecular Neurodegeneration* **14**, (2019).
88. Theillet, F. X. *et al.* Structural disorder of monomeric α-synuclein persists in mammalian cells. *Nature* **530**, 45–50 (2016).
89. Binolfi, A. *et al.* Interaction of α-synuclein with divalent metal ions reveals key differences: A link between structure, binding specificity and fibrillation enhancement. *J. Am. Chem. Soc.* **128**, 9893–9901 (2006).
90. Uversky, V. N., Li, J. & Fink, A. L. Metal-triggered structural transformations, aggregation, and fibrillation of human α-synuclein: A possible molecular link between parkinson's disease and heavy metal exposure. *J. Biol. Chem.* **276**, 44284–44296 (2001).
91. Xiao, Y. *et al.* Iron promotes α-synuclein aggregation and transmission by inhibiting TFEB-mediated autophagosome-lysosome fusion. *J. Neurochem.* **145**, 34–50 (2018).
92. Bartels, M. *et al.* Iron-mediated aggregation and toxicity in a novel neuronal cell culture model with inducible alpha-synuclein expression. *Sci. Rep.* **9**, (2019).
93. Ranjan, P. *et al.* Differential copper binding to alpha-synuclein and its disease-associated mutants affect the aggregation and amyloid formation. *Biochim. Biophys. Acta - Gen. Subj.* **1861**, 365–374 (2017).
94. Davies, P., Moualla, D., Brown, D. R., Moore, E. & Hainsworth, L. Alpha-Synuclein Is a Cellular Ferrireductase. *PLoS One* **6**, e15814 (2011).
95. Daubner, S. C., Le, T. & Wang, S. Tyrosine hydroxylase and regulation of dopamine synthesis. *Archives of Biochemistry and Biophysics* **508**, 1–12 (2011).
96. Levin, J. *et al.* Generation of ferric iron links oxidative stress to α-synuclein oligomer formation. *J. Parkinsons. Dis.* **1**, 205–216 (2011).
97. Bose, A. & Beal, M. F. Mitochondrial dysfunction in Parkinson's disease. *Journal of Neurochemistry* 216–231 (2016). doi:10.1111/jnc.13731
98. Vakifahmetoglu-Norberg, H., Ouchida, A. T. & Norberg, E. The role of mitochondria in metabolism and cell death. *Biochemical and Biophysical Research Communications* **482**, 426–431 (2017).
99. Sian, J. *et al.* Glutathione-related enzymes in brain in Parkinson's disease. *Ann. Neurol.* **36**, 356–361 (1994).
100. Keeney, P. M., Xie, J., Capaldi, R. A. & Bennett, J. P. Parkinson's disease brain mitochondrial complex I has oxidatively damaged subunits and is functionally impaired and misassembled. *J. Neurosci.* **26**, 5256–5264 (2006).
101. Ludtmann, M. H. R. *et al.* α-synuclein oligomers interact with ATP synthase and open the permeability transition pore in Parkinson's disease. *Nat. Commun.* **9**, (2018).
102. Paillusson, S. *et al.* α-Synuclein binds to the ER–mitochondria tethering protein VAPB to

disrupt Ca2+ homeostasis and mitochondrial ATP production. *Acta Neuropathol.* **134**, 129–149 (2017).
103. Levi, S. & Rovida, E. The role of iron in mitochondrial function. *Biochimica et Biophysica Acta - General Subjects* **1790**, 629–636 (2009).
104. Park, J. *et al.* Iron overload triggers mitochondrial fragmentation via calcineurin-sensitive signals in HT-22 hippocampal neuron cells. *Toxicology* **337**, 39–46 (2015).
105. Fonseca, T. B., Sánchez-Guerrero, Á., Milosevic, I. & Raimundo, N. Mitochondrial fission requires DRP1 but not dynamins. *Nature* **570**, E34–E42 (2019).
106. Urrutia, P. J. *et al.* Cell death induced by mitochondrial complex I inhibition is mediated by Iron Regulatory Protein 1. *Biochim. Biophys. Acta - Mol. Basis Dis.* **1863**, 2202–2209 (2017).
107. Nixon, A. M. *et al.* HFE Genotype Restricts the Response to Paraquat in a Mouse Model of Neurotoxicity. *J. Neurochem.* **145**, 299–311 (2018).
108. Ye, Q. & Kim, J. Mutation in HFE gene decreases manganese accumulation and oxidative stress in the brain after olfactory manganese exposure. *Metallomics* **8**, 618–627 (2016).
109. Borie, C. *et al.* Association study between iron-related genes polymorphisms and Parkinson's disease. *J. Neurol.* **249**, 801–804 (2002).
110. Buchanan, D. ., Silburn, P. ., Chalk, J. ., Le Couteur, D. . & Mellick, G. . The Cys282Tyr polymorphism in the HFE gene in Australian Parkinson's disease patients. *Neurosci. Lett.* **327**, 91–94 (2002).
111. Dekker, M. C. J. *et al.* Mutations in the hemochromatosis gene (HFE), Parkinson's disease and parkinsonism. *Neurosci. Lett.* **348**, 117–119 (2003).
112. Guerreiro, R. J. *et al.* Association of HFE common mutations with Parkinson's disease, Alzheimer's disease and mild cognitive impairment in a Portuguese cohort. *BMC Neurol.* **6**, 24 (2006).
113. Akbas, N. *et al.* Screening for mutations of the HFE gene in Parkinson's disease patients with hyperechogenicity of the substantia nigra. *Neurosci. Lett.* **407**, 16–19 (2006).
114. Aamodt, A. H. *et al.* Prevalence of haemochromatosis gene mutations in Parkinson's disease. *J. Neurol. Neurosurg. Psychiatry* **78**, 315–7 (2007).
115. Halling, J., Petersen, M. S., Grandjean, P., Weihe, P. & Brosen, K. Genetic predisposition to Parkinson's disease: CYP2D6 and HFE in the Faroe Islands. *Pharmacogenet. Genomics* **18**, 209–212 (2008).
116. Biasiotto, G. *et al.* HFE gene mutations in a population of Italian Parkinson's disease patients. *Park. Relat. Disord.* **14**, 426–430 (2008).
117. Greco, V. *et al.* Association study between four polymorphisms in the HFE, TF and TFR genes and Parkinson's disease in Southern Italy. *Neurol. Sci.* **32**, 525–527 (2011).
118. Mariani, S. *et al.* Effects of hemochromatosis and transferrin gene mutations on peripheral iron dyshomeostasis in mild cognitive impairment and Alzheimer's and Parkinson's diseases. *Front. Aging Neurosci.* **5**, (2013).
119. Pichler, I. *et al.* Serum Iron Levels and the Risk of Parkinson Disease: A Mendelian Randomization Study. *PLoS Med.* **10**, (2013).
120. Rhodes, S. L. *et al.* Pooled analysis of iron-related genes in Parkinson's disease: Association with transferrin. *Neurobiol. Dis.* **62**, 172–178 (2014).
121. Xia, J., Xu, H., Jiang, H. & Xie, J. The association between the C282Y and H63D polymorphisms of HFE gene and the risk of Parkinson's disease: A meta-analysis. *Neurosci. Lett.* **595**, 99–103 (2015).
122. Duan, C. *et al.* C282Y and H63D Polymorphisms in Hemochromatosis Gene and Risk of Parkinson's Disease: A Meta-Analysis. *American Journal of Alzheimer's Disease and other Dementias* **31**, 201–207 (2016).

123. Mariani, S. *et al.* Association between sex, systemic iron variation and probability of Parkinson's disease. *Int. J. Neurosci.* **126**, 354–360 (2016).
124. Greenland, J. C., Williams-Gray, C. H. & Barker, R. A. The clinical heterogeneity of Parkinson's disease and its therapeutic implications. *Eur. J. Neurosci.* **49**, 328–338 (2019).
125. 2020 Alzheimer's disease facts and figures. *Alzheimer's Dement.* **16**, 391–460 (2020).
126. Hebert, L. E., Weuve, J., Scherr, P. A. & Evans, D. A. Alzheimer disease in the United States (2010-2050) estimated using the 2010 census. *Neurology* **80**, 1778–1783 (2013).
127. Lane, C. A., Hardy, J. & Schott, J. M. Alzheimer's disease. *Eur. J. Neurol.* **25**, 59–70 (2018).
128. Hardy, J. A. & Higgins, G. A. Alzheimer's disease: The amyloid cascade hypothesis. *Science* **256**, 184–185 (1992).
129. Gómez-Isla, T. *et al.* Neuronal loss correlates with but exceeds neurofibrillary tangles in Alzheimer's disease. *Ann. Neurol.* **41**, 17–24 (1997).
130. Birks, J. Cholinesterase inhibitors for Alzheimer's disease. *Cochrane Database of Systematic Reviews* (2006). doi:10.1002/14651858.CD005593
131. Huang, L.-K., Chao, S.-P. & Hu, C.-J. Clinical trials of new drugs for Alzheimer disease. *J. Biomed. Sci.* **27**, 18 (2020).
132. Hane, F. T. *et al.* Recent Progress in Alzheimer's Disease Research, Part 3: Diagnosis and Treatment. *Journal of Alzheimer's Disease* **57**, 645–665 (2017).
133. Van Duijn, S. *et al.* Cortical Iron Reflects Severity of Alzheimer's Disease. *J. Alzheimer's Dis.* **60**, 1533–1545 (2017).
134. Van Bergen, J. M. G. *et al.* Colocalization of cerebral iron with Amyloid beta in Mild Cognitive Impairment. *Sci. Rep.* **6**, (2016).
135. Du, L. *et al.* Increased Iron Deposition on Brain Quantitative Susceptibility Mapping Correlates with Decreased Cognitive Function in Alzheimer's Disease. *ACS Chem. Neurosci.* **9**, 1849–1857 (2018).
136. Ayton, S. *et al.* Brain iron is associated with accelerated cognitive decline in people with Alzheimer pathology. *Mol. Psychiatry* (2019). doi:10.1038/s41380-019-0375-7
137. Rogers, J. T. *et al.* Iron and the translation of the amyloid precursor protein (APP) and ferritin mRNAs: Riboregulation against neural oxidative damage in Alzheimer's disease. *Biochem. Soc. Trans.* **36**, 1282–1287 (2008).
138. Belaidi, A. A. *et al.* Marked Age-Related Changes in Brain Iron Homeostasis in Amyloid Protein Precursor Knockout Mice. *Neurotherapeutics* **15**, 1055–1062 (2018).
139. Dlouhy, A. C., Bailey, D. K., Steimle, B. L., Parker, H. V. & Kosman, D. J. Fluorescence resonance energy transfer links membrane ferroportin, hephaestin but not ferroportin, amyloid precursor protein complex with iron efflux. *J. Biol. Chem.* **294**, 4202–4214 (2019).
140. Li, X. *et al.* Ferritin light chain interacts with PEN-2 and affects γ-secretase activity. *Neurosci. Lett.* **548**, 90–94 (2013).
141. Bodovitz, S., Falduto, M. T., Frail, D. E. & Klein, W. L. Iron Levels Modulate α-Secretase Cleavage of Amyloid Precursor Protein. *J. Neurochem.* **64**, 307–315 (1995).
142. Chen, Y. T., Chen, W. Y., Huang, X. T., Xu, Y. C. & Zhang, H. Y. Iron dysregulates APP processing accompanying with sAPPα cellular retention and β-secretase inhibition in rat cortical neurons. *Acta Pharmacol. Sin.* **39**, 177–183 (2018).
143. Boopathi, S. & Kolandaivel, P. Fe2+ binding on amyloid β-peptide promotes aggregation. *Proteins Struct. Funct. Bioinforma.* **84**, 1257–1274 (2016).
144. Amit, T., Avramovich-Tirosh, Y., Youdim, M. B. H. & Mandel, S. Targeting multiple Alzheimer's disease etiologies with multimodal neuroprotective and neurorestorative iron chelators. *FASEB Journal* **22**, 1296–1305 (2008).

145. Telling, N. D. *et al.* Iron Biochemistry is Correlated with Amyloid Plaque Morphology in an Established Mouse Model of Alzheimer's Disease. *Cell Chem. Biol.* **24**, 1205-1215.e3 (2017).
146. Dixon, S. J. *et al.* Ferroptosis: An iron-dependent form of nonapoptotic cell death. *Cell* **149**, 1060–1072 (2012).
147. Zhang, Y. H. *et al.* α-Lipoic acid improves abnormal behavior by mitigation of oxidative stress, inflammation, ferroptosis, and tauopathy in P301S Tau transgenic mice. *Redox Biol.* **14**, 535–548 (2018).
148. Fava, A. *et al.* The Effect of Lipoic Acid Therapy on Cognitive Functioning in Patients with Alzheimer's Disease. *J. Neurodegener. Dis.* **2013**, 1–7 (2013).
149. Tisato, V. *et al.* Gene-gene interactions among coding genes of iron-homeostasis proteins and APOE-alleles in cognitive impairment diseases. *PLoS One* **13**, (2018).
150. Wang, Z. X. *et al.* Genetic Association of HLA Gene Variants with MRI Brain Structure in Alzheimer's Disease. *Mol. Neurobiol.* **54**, 3195–3204 (2017).
151. Correia, A. P. *et al.* CAT53 and HFE alleles in Alzheimer's disease: A putative protective role of the C282Y HFE mutation. *Neurosci. Lett.* **457**, 129–132 (2009).
152. Percy, M. *et al.* Involvement of ApoE E4 and H63D in sporadic Alzheimer's disease in a folate-supplemented Ontario population. *J. Alzheimers. Dis.* **14**, 69–84 (2008).
153. Lin, M. *et al.* Association between HFE polymorphisms and susceptibility to Alzheimer's disease: A meta-analysis of 22 studies including 4,365 cases and 8,652 controls. *Mol. Biol. Rep.* **39**, 3089–3095 (2012).
154. Blázquez, L. *et al.* Genes related to iron metabolism and susceptibility to Alzheimer's disease in Basque population. *Neurobiol. Aging* **28**, 1941–1943 (2007).
155. Lehmann, D. J. *et al.* Transferrin and HFE genes interact in Alzheimer's disease risk: The Epistasis Project. *Neurobiol. Aging* **33**, 202.e1-202.e13 (2012).
156. Kauwe, J. S. K. *et al.* Suggestive synergy between genetic variants in TF and HFE as risk factors for Alzheimer's disease. *Am. J. Med. Genet. Part B Neuropsychiatr. Genet.* **153**, 955–959 (2010).
157. Robson, K. J. H. *et al.* Synergy between the C2 allele of transferrin and the C282Y allele of the haemochromatosis gene (HFE) as risk factors for developing Alzheimer's disease. *J. Med. Genet.* **41**, 261–265 (2004).
158. Alizadeh, B. Z. *et al.* HFE variants, APOE and Alzheimer's disease: Findings from the population-based Rotterdam Study. *Neurobiol. Aging* **30**, 330–332 (2009).
159. Avila-Gomez, I. C., Jiménez-Del-Rio, M., Lopera-Restrepo, F. & Velez-Pardo, C. Association between HFE 187 C>G (H63D) mutation and early-onset familial Alzheimer's disease PSEN-1 839A>C (E280A) mutation. *Ann. Hematol.* **87**, 671–673 (2008).
160. Combarros, O. *et al.* Interaction of the H63D mutation in the hemochromatosis gene with the apolipoprotein E epsilon 4 allele modulates age at onset of Alzheimer's disease. *Dement. Geriatr. Cogn. Disord.* **15**, 151–154 (2003).
161. Sampietro, M. *et al.* The hemochromatosis gene affects the age of onset of sporadic Alzheimer's disease. *Neurobiol. Aging* **22**, 563–568 (2001).
162. Mairuae, N., Hall, E. C., Cheepsunthorn, P., Lee, S. Y. & Connor, J. R. The H63D HFE gene variant promotes activation of the intrinsic apoptotic pathway via mitochondria dysfunction following β-amyloid peptide exposure. *J. Neurosci. Res.* **88**, 3079–3089 (2010).
163. Jahanshad, N. *et al.* Brain structure in healthy adults is related to serum transferrin and the H63D polymorphism in the HFE gene. *Proc. Natl. Acad. Sci. U. S. A.* **109**, (2012).
164. Gebril, O. H., Kirby, J., Savva, G., Brayne, C. & Ince, P. G. HFE H63D, C282Y and

AGTR1 A1166C polymorphisms and brain white matter lesions in the aging brain. *J. Neurogenet.* **25**, 7–14 (2011).
165. Johnstone, D. M. *et al.* Changes in brain transcripts related to alzheimer's disease in a model of hfe hemochromatosis are not consistent with increased alzheimer's disease risk. *J. Alzheimer's Dis.* **30**, 791–803 (2012).
166. Hogarth, P. Neurodegeneration with Brain Iron Accumulation: Diagnosis and Management. *J. Mov. Disord.* **8**, 1–13 (2015).
167. Di Meo, I. & Tiranti, V. Classification and molecular pathogenesis of NBIA syndromes. *European Journal of Paediatric Neurology* **22**, 272–284 (2018).
168. Klopstock, T. *et al.* Safety and efficacy of deferiprone for pantothenate kinase-associated neurodegeneration: a randomised, double-blind, controlled trial and an open-label extension study. *Lancet Neurol.* **18**, 631–642 (2019).
169. Löbel, U. *et al.* Brain iron quantification by MRI in mitochondrial membrane protein-associated neurodegeneration under iron-chelating therapy. *Ann. Clin. Transl. Neurol.* **1**, 1041–1046 (2014).
170. Fonderico, M. *et al.* Patient Affected by Beta-Propeller Protein-Associated Neurodegeneration: A Therapeutic Attempt with Iron Chelation Therapy. *Front. Neurol.* **8**, 385 (2017).
171. Lim, S.-Y. *et al.* A Patient with Beta-Propeller Protein-Associated Neurodegeneration: Treatment with Iron Chelation Therapy. *J. Mov. Disord.* **11**, 89–92 (2018).
172. Dusi, S. *et al.* Exome sequence reveals mutations in CoA synthase as a cause of neurodegeneration with brain iron accumulation. *Am. J. Hum. Genet.* **94**, 11–22 (2014).
173. Alfonso-Pecchio, A., Garcia, M., Leonardi, R. & Jackowski, S. Compartmentalization of Mammalian Pantothenate Kinases. *PLoS One* **7**, (2012).
174. Lopez Martinez, D., Tsuchiya, Y. & Gout, I. Coenzyme A biosynthetic machinery in mammalian cells. in *Biochemical Society Transactions* **42**, 1112–1117 (Portland Press Ltd, 2014).
175. Razmeh, S. *et al.* Pantothenate kinase-associated neurodegeneration: Clinical aspects, diangnosis and treatments. *Neurology International* **10**, 32–34 (2018).
176. Li, A. *et al.* Pantothenate kinase-associated neurodegeneration is not a synucleinopathy. *Neuropathol. Appl. Neurobiol.* **39**, 121–131 (2013).
177. Kruer, M. C. *et al.* Novel histopathologic findings in molecularly-confirmed pantothenate kinase-associated neurodegeneration. *Brain* **134**, 947–958 (2011).
178. Hogarth, P. *et al.* New NBIA subtype: Genetic, clinical, pathologic, and radiographic features of MPAN. *Neurology* **80**, 268–275 (2013).
179. Landouré, G. *et al.* Hereditary spastic paraplegia Type 43 (SPG43) is caused by mutation in C19orf12. *Hum. Mutat.* **34**, 1357–1360 (2013).
180. Kruer, M. C. *et al.* C19orf12 mutation leads to a pallido-pyramidal syndrome. *Gene* **537**, 352–356 (2014).
181. Deschauer, M. *et al.* C19orf12 mutations in neurodegeneration with brain iron accumulation mimicking juvenile amyotrophic lateral sclerosis. *J. Neurol.* **259**, 2434–2439 (2012).
182. Gregory, A. *et al.* Neurodegeneration associated with genetic defects in phospholipase A2. *Neurology* **71**, 1402–1409 (2008).
183. Hooks, S. B. & Cummings, B. S. Role of Ca2+-independent phospholipase A2 in cell growth and signaling. *Biochemical Pharmacology* **76**, 1059–1067 (2008).
184. Malik, I. *et al.* Disrupted membrane homeostasis and accumulation of ubiquitinated proteins in a mouse model of infantile neuroaxonal dystrophy caused by PLA2G6 mutations. *Am. J. Pathol.* **172**, 406–416 (2008).

185. Illingworth, M. A. *et al.* PLA2G6-associated neurodegeneration (PLAN): Further expansion of the clinical, radiological and mutation spectrum associated with infantile and atypical childhood-onset disease. *Mol. Genet. Metab.* **112**, 183–189 (2014).
186. Shen, T. *et al.* Early-onset parkinson's disease caused by pla2g6 compound heterozygous mutation, a case report and literature review. *Front. Neurol.* **10**, (2019).
187. Kapoor, S. *et al.* Genetic analysis of PLA2G6 in 22 Indian families with infantile neuroaxonal dystrophy, atypical late-onset neuroaxonal dystrophy and dystonia parkinsonism complex. *PLoS One* **11**, (2016).
188. Paisán-Ruiz, C. *et al.* Widespread Lewy body and tau accumulation in childhood and adult onset dystonia-parkinsonism cases with PLA2G6 mutations. *Neurobiol. Aging* **33**, 814–823 (2012).
189. Riku, Y. *et al.* Extensive aggregation of α-synuclein and tau in juvenile-onset neuroaxonal dystrophy: An autopsied individual with a novel mutation in the PLA2G6 gene-splicing site. *Acta Neuropathol. Commun.* **2**, (2014).
190. Saitsu, H. *et al.* De novo mutations in the autophagy gene WDR45 cause static encephalopathy of childhood with neurodegeneration in adulthood. *Nat. Genet.* **45**, 445–449 (2013).
191. Bakula, D. *et al.* WIPI3 and WIPI4 β-propellers are scaffolds for LKB1-AMPK-TSC signalling circuits in the control of autophagy. *Nat. Commun.* **8**, 15637 (2017).
192. Zhao, Y. G. *et al.* The autophagy gene Wdr45/Wipi4 regulates learning and memory function and axonal homeostasis. *Autophagy* **11**, 881–90 (2015).
193. Paudel, R. *et al.* Neuropathology of Beta-propeller protein associated neurodegeneration (BPAN): a new tauopathy. *Acta Neuropathol. Commun.* **3**, 39 (2015).
194. Hardiman, O. *et al.* Amyotrophic lateral sclerosis. *Nature Reviews Disease Primers* **3**, (2017).
195. Marin, B. *et al.* Clinical and demographic factors and outcome of amyotrophic lateral sclerosis in relation to population ancestral origin. *European Journal of Epidemiology* **31**, 229–245 (2016).
196. Miller, R., Mitchell, J., Lyon, M. & Moore, D. Riluzole for amyotrophic lateral sclerosis (ALS)/motor neuron disease (MND). in *Cochrane Database of Systematic Reviews* (John Wiley & Sons, Ltd, 2002). doi:10.1002/14651858.cd001447
197. Lacomblez, L., Bensimon, G., Leigh, P. N., Guillet, P. & Meininger, V. Dose-ranging study of riluzole in amyotrophic lateral sclerosis. *Lancet* **347**, 1425–1431 (1996).
198. Abe, K. *et al.* Safety and efficacy of edaravone in well defined patients with amyotrophic lateral sclerosis: a randomised, double-blind, placebo-controlled trial. *Lancet Neurol.* **16**, 505–512 (2017).
199. van Es, M. A. *et al.* Amyotrophic lateral sclerosis. *The Lancet* **390**, 2084–2098 (2017).
200. Neumann, M. *et al.* Ubiquitinated TDP-43 in frontotemporal lobar degeneration and amyotrophic lateral sclerosis. *Science (80-.).* **314**, 130–133 (2006).
201. McAlary, L., Plotkin, S. S., Yerbury, J. J. & Cashman, N. Prion-like Propagation of Protein Misfolding and Aggregation in Amyotrophic Lateral Sclerosis. *Front. Mol. Neurosci.* **12**, 262 (2019).
202. Iacoangeli, A. *et al.* C9orf72 intermediate expansions of 24–30 repeats are associated with ALS. *Acta Neuropathol. Commun.* **7**, 115 (2019).
203. A. Lu, M. *et al.* The 5'-Untranslated Region of the C9orf72 mRNA Exhibits a Phylogenetic Alignment to the Cis-Aconitase Iron-Responsive Element; Novel Therapies for Amytrophic Lateral Sclerosis. *Neurosci. Med.* **07**, 15–26 (2016).
204. Oba, H. *et al.* Amyotrophic lateral sclerosis: T2 shortening in motor cortex at MR imaging. *Radiology* **189**, 843–846 (1993).

205. Acosta-Cabronero, J. *et al.* Quantitative susceptibility MRI to detect brain iron in amyotrophic lateral sclerosis. *Radiology* **289**, 195–203 (2018).
206. Nadjar, Y. *et al.* Elevated Serum Ferritin Is Associated with Reduced Survival in Amyotrophic Lateral Sclerosis. *PLoS One* **7**, (2012).
207. Hu, X., Yang, Y., Su, J. & Yao, C. Meta-analysis of the relationship between amyotrophic lateral sclerosis and susceptibility to serum ferritin level elevation. *Neurosciences* **21**, 120–125 (2016).
208. Chaves-Filho, A. B. *et al.* Alterations in lipid metabolism of spinal cord linked to amyotrophic lateral sclerosis. *Sci. Rep.* **9**, (2019).
209. Simpson, E. P., Henry, Y. K., Henkel, J. S., Smith, R. G. & Appel, S. H. Increased lipid peroxidation in sera of ALS patients: A potential biomarker of disease burden. *Neurology* **62**, 1758–1765 (2004).
210. Devos, D. *et al.* A ferroptosis–based panel of prognostic biomarkers for Amyotrophic Lateral Sclerosis. *Sci. Rep.* **9**, (2019).
211. Chiò, A. *et al.* HFE p.H63D polymorphism does not influence ALS phenotype and survival. *Neurobiol. Aging* **36**, 2906.e7-2906.e11 (2015).
212. Su, X. W. *et al.* H63D HFE polymorphisms are associated with increased disease duration and decreased muscle superoxide dismutase-1 expression in amyotrophic lateral sclerosis patients. *Muscle Nerve* **48**, 242–246 (2013).
213. Sutedja, N. A. *et al.* The association between H63D mutations in HFE and amyotrophic lateral sclerosis in a Dutch population. *Arch. Neurol.* **64**, 63–67 (2007).
214. Wang, X.-S. *et al.* Increased incidence of the Hfe mutation in amyotrophic lateral sclerosis and related cellular consequences. *J. Neurol. Sci.* **227**, 27–33 (2004).
215. Goodall, E. F. *et al.* Association of the H63D polymorphism in the hemochromatosis gene with sporadic ALS. *Neurology* **65**, 934–937 (2005).
216. He, X. *et al.* H63D polymorphism in the hemochromatosis gene is associated with sporadic amyotrophic lateral sclerosis in China. *Eur. J. Neurol.* **18**, 359–361 (2011).
217. Nandar, W., Neely, E. B., Simmons, Z. & Connor, J. R. H63D HFE genotype accelerates disease progression in animal models of amyotrophic lateral sclerosis. *Biochim. Biophys. Acta - Mol. Basis Dis.* **1842**, 2413–2426 (2014).
218. Yen, A. A., Simpson, E. P., Henkel, J. S., Beers, D. R. & Appel, S. H. HFE mutations are not strongly associated with sporadic ALS. *Neurology* **62**, 1611–2 (2004).
219. Praline, J. *et al.* Study of the HFE gene common polymorphisms in French patients with sporadic amyotrophic lateral sclerosis. *J. Neurol. Sci.* **317**, 58–61 (2012).
220. van Rheenen, W. *et al.* H63D polymorphism in HFE is not associated with amyotrophic lateral sclerosis. *Neurobiol. Aging* **34**, 1517.e5-1517.e7 (2013).
221. Li, M., Wang, L., Wang, W., Qi, X. L. & Tang, Z. Y. Mutations in the HFE gene and sporadic amyotrophic lateral sclerosis risk: A meta-analysis of observational studies. *Brazilian J. Med. Biol. Res.* **47**, 215–222 (2014).
222. Campuzano, V. *et al.* Friedreich's ataxia: Autosomal recessive disease caused by an intronic GAA triplet repeat expansion. *Science (80-.).* **271**, 1423–1427 (1996).
223. Schmucker, S. *et al.* Mammalian frataxin: An essential function for cellular viability through an interaction with a preformed ISCU/ NFS1/ISD11 iron-sulfur assembly complex. *PLoS One* **6**, (2011).
224. Branda, S. S., Yang, Z. Y., Chew, A. & Isaya, G. Mitochondrial intermediate peptidase and the yeast frataxin homolog together maintain mitochondrial iron homeostasis in Saccharomyces cerevisiae. *Hum. Mol. Genet.* **8**, 1099–1110 (1999).
225. Martelli, A. & Puccio, H. Dysregulation of cellular iron metabolism in Friedreich ataxia: From primary iron-sulfur cluster deficit to mitochondrial iron accumulation. *Frontiers in*

Pharmacology **5 JUN**, (2014).
226. Koeppen, A. H. *et al.* Friedreich's ataxia causes redistribution of iron, copper, and zinc in the dentate nucleus. *Cerebellum* **11**, 845–860 (2012).
227. Solbach, K. *et al.* Cerebellar pathology in Friedreich's ataxia: Atrophied dentate nuclei with normal iron content. *NeuroImage Clin.* **6**, 93–99 (2014).
228. Koeppen, A. H. & Mazurkiewicz, J. E. Friedreich ataxia: Neuropathology revised. *Journal of Neuropathology and Experimental Neurology* **72**, 78–90 (2013).
229. Delatycki, M. B. *et al.* HFE p.C282Y heterozygosity is associated with earlier disease onset in Friedreich ataxia. *Mov. Disord.* **29**, 940–943 (2014).
230. Reich, D. S., Lucchinetti, C. F. & Calabresi, P. A. Multiple Sclerosis. *N. Engl. J. Med.* **378**, 169–180 (2018).
231. Haacke, E. M. *et al.* Characterizing iron deposition in multiple sclerosis lesions using susceptibility weighted imaging. *J. Magn. Reson. Imaging* **29**, 537–544 (2009).
232. Bakshi, R. *et al.* T2 hypointensity in the deep gray matter of patients with multiple sclerosis: A quantitative magnetic resonance imaging study. *Arch. Neurol.* **59**, 62–68 (2002).
233. Bermel, R. A. *et al.* Prediction of longitudinal brain atrophy in multiple sclerosis by gray matter magnetic resonance imaging T2 hypointensity. *Arch. Neurol.* **62**, 1371–1376 (2005).
234. Brass, S. D., Benedict, R. H. B., Weinstock-Guttman, B., Munschauer, F. & Bakshi, R. Cognitive impairment is associated with subcortical magnetic resonance imaging grey matter T2 hypointensity in multiple sclerosis. *Mult. Scler.* **12**, 437–444 (2006).
235. Bettencourt, A., Martins da Silva, A., Pinho E Costa, P. & Martins Silva, B. Molecular genetic studies of multiple sclerosis in the portuguese population. *Acta Med. Port.* **25**, 224–30 (2012).
236. Gemmati, D. *et al.* Polymorphisms in the genes coding for iron binding and transporting proteins are associated with disability, severity, and early progression in multiple sclerosis. *BMC Med. Genet.* **13**, (2012).
237. Ristić, S. *et al.* Mutations in the hemochromatosis gene (HFE) and multiple sclerosis. *Neurosci. Lett.* **383**, 301–304 (2005).
238. Bettencourt, A. *et al.* HFE gene polymorphisms and severity in Portuguese patients with multiple sclerosis. *Eur. J. Neurol.* **18**, 663–666 (2011).
239. Hider, R. C. & Hoffbrand, A. V. The Role of Deferiprone in Iron Chelation. *N. Engl. J. Med.* **379**, 2140–2150 (2018).
240. Pandolfo, M. & Hausmann, L. Deferiprone for the treatment of Friedreich's ataxia. *J. Neurochem.* **126**, 142–146 (2013).
241. Aguirre, P. *et al.* Iron chelators and antioxidants regenerate neuritic tree and nigrostriatal fibers of MPP+/MPTP-Lesioned dopaminergic neurons. *PLoS One* **10**, (2015).
242. Molina-Holgado, F., Gaeta, A., Francis, P. T., Williams, R. J. & Hider, R. C. Neuroprotective actions of deferiprone in cultured cortical neurones and SHSY-5Y cells. *J. Neurochem.* **105**, 2466–2476 (2008).
243. Dexter, D. T. *et al.* Clinically available iron chelators induce neuroprotection in the 6-OHDA model of Parkinson's disease after peripheral administration. *J. Neural Transm.* **118**, 223–31 (2011).
244. Carboni, E. *et al.* Deferiprone Rescues Behavioral Deficits Induced by Mild Iron Exposure in a Mouse Model of Alpha-Synuclein Aggregation. *NeuroMolecular Med.* **19**, 309–321 (2017).
245. Crapper McLachlan, D. R. *et al.* Intramuscular desferrioxamine in patients with Alzheimer's disease. *Lancet (London, England)* **337**, 1304–8 (1991).

246. Ritchie, C. W. *et al.* Metal-Protein Attenuation with Iodochlorhydroxyquin (Clioquinol) Targeting Aβ Amyloid Deposition and Toxicity in Alzheimer Disease: A Pilot Phase 2 Clinical Trial. *Arch. Neurol.* **60**, 1685–1691 (2003).
247. Adlard, P. A. *et al.* Rapid Restoration of Cognition in Alzheimer's Transgenic Mice with 8-Hydroxy Quinoline Analogs Is Associated with Decreased Interstitial Aβ. *Neuron* **59**, 43–55 (2008).
248. Crouch, P. J. *et al.* The Alzheimer's therapeutic PBT2 promotes amyloid-β degradation and GSK3 phosphorylation via a metal chaperone activity. *J. Neurochem.* **119**, 220–230 (2011).
249. Fine, J. M. *et al.* Intranasal deferoxamine improves performance in radial arm water maze, stabilizes HIF-1α, and phosphorylates GSK3β in P301L tau transgenic mice. *Exp. Brain Res.* **219**, 381–390 (2012).
250. Guo, C. *et al.* Intranasal deferoxamine reverses iron-induced memory deficits and inhibits amyloidogenic APP processing in a transgenic mouse model of Alzheimer's disease. *Neurobiol. Aging* **34**, 562–575 (2013).
251. Zorzi, G. *et al.* Iron-related MRI images in patients with pantothenate kinase-associated neurodegeneration (PKAN) treated with deferiprone: Results of a phase II pilot trial. *Mov. Disord.* **26**, 1755–1759 (2011).
252. Abbruzzese, G. *et al.* A pilot trial of deferiprone for neurodegeneration with brain iron accumulation. *Haematologica* **96**, 1708–1711 (2011).
253. Cossu, G. *et al.* Efficacy and safety of deferiprone for the treatment of pantothenate kinase-associated neurodegeneration (PKAN) and neurodegeneration with brain iron accumulation (NBIA): Results from a four years follow-up. *Park. Relat. Disord.* **20**, 651–654 (2014).
254. Rohani, M., Razmeh, S., Shahidi, G. A. & Orooji, M. A pilot trial of deferiprone in pantothenate kinase-associated neurodegeneration patients. *Neurol. Int.* **9**, (2018).
255. Golko-Perez, S., Amit, T., Bar-Am, O., Youdim, M. B. H. & Weinreb, O. A Novel Iron Chelator-Radical Scavenger Ameliorates Motor Dysfunction and Improves Life Span and Mitochondrial Biogenesis in SOD1G93A ALS Mice. *Neurotox. Res.* **31**, 230–244 (2017).
256. Kupershmidt, L. *et al.* Neuroprotective and neuritogenic activities of novel multimodal iron-chelating drugs in motor-neuron-like NSC-34 cells and transgenic mouse model of amyotrophic lateral sclerosis. *FASEB J.* **23**, 3766–3779 (2009).
257. Wang, Q. *et al.* Prevention of Motor Neuron Degeneration by Novel Iron Chelators in SOD1(G93A) Transgenic Mice of Amyotrophic Lateral Sclerosis. *Neurodegener. Dis.* **8**, 310–321 (2011).
258. Moreau, C. *et al.* Could Conservative Iron Chelation Lead to Neuroprotection in Amyotrophic Lateral Sclerosis? *Antioxidants Redox Signal.* **29**, 742–748 (2018).
259. Ray Dorsey, E. *et al.* Global, regional, and national burden of Parkinson's disease, 1990–2016: a systematic analysis for the Global Burden of Disease Study 2016. *Lancet Neurol.* **17**, 939–953 (2018).
260. Rizek, P., Kumar, N. & Jog, M. S. An update on the diagnosis and treatment of Parkinson disease. *CMAJ* **188**, 1157–1165 (2016).
261. Marek, K. *et al.* The Parkinson's progression markers initiative (PPMI) – establishing a PD biomarker cohort. *Ann. Clin. Transl. Neurol.* **5**, 1460–1477 (2018).
262. Ramaker, C., Marinus, J., Stiggelbout, A. M. & van Hilten, B. J. Systematic evaluation of rating scales for impairment and disability in Parkinson's disease. *Movement Disorders* **17**, 867–876 (2002).
263. Holden, S. K., Finseth, T., Sillau, S. H. & Berman, B. D. Progression of MDS-UPDRS Scores Over Five Years in De Novo Parkinson Disease from the Parkinson's Progression

Markers Initiative Cohort. *Mov. Disord. Clin. Pract.* **5**, 47–53 (2018).
264. Jankovic, J. & Kapadia, A. S. Functional decline in Parkinson disease. *Arch. Neurol.* **58**, 1611–1615 (2001).
265. Alves, G., Wentzel-Larsen, T., Aarsland, D. & Larsen, J. P. Progression of motor impairment and disability in Parkinson disease: A population-based study. *Neurology* **65**, 1436–1441 (2005).
266. Benamer, H. T. *et al.* Correlation of Parkinson's disease severity and duration with 123I-FP-CIT SPECT striatal uptake. *Mov. Disord.* **15**, 692–8 (2000).
267. Ravina, B. *et al.* Dopamine transporter imaging is associated with long-term outcomes in Parkinson's disease. *Mov. Disord.* **27**, 1392–1397 (2012).
268. Goedert, M. Alpha-synuclein and neurodegenerative diseases. *Nat. Rev. Neurosci.* **2**, 492–501 (2001).
269. Zange, L., Noack, C., Hahn, K., Stenzel, W. & Lipp, A. Phosphorylated α-synuclein in skin nerve fibres differentiates Parkinson's disease from multiple system atrophy. *Brain* **138**, 2310–2321 (2015).
270. Yan, F. *et al.* Gastrointestinal nervous system a-synuclein as a potential biomarker of Parkinson disease. *Med. (United States)* **97**, (2018).
271. Tian, C. *et al.* Erythrocytic α-Synuclein as a potential biomarker for Parkinson's disease. *Transl. Neurodegener.* **8**, 15 (2019).
272. Wang, L. *et al.* Cerebrospinal fluid alpha-synuclein as a biomarker for Parkinson's disease diagnosis: A systematic review and meta-analysis. *Int. J. Neurosci.* **125**, 645–654 (2015).
273. Locascio, J. J. *et al.* Association between α-synuclein blood transcripts and early, neuroimaging-supported Parkinson's disease. *Brain* **138**, 2659–71 (2015).
274. Wang, X., Yu, S., Li, F. & Feng, T. Detection of α-synuclein oligomers in red blood cells as a potential biomarker of Parkinson's disease. *Neurosci. Lett.* **599**, 115–119 (2015).
275. Foulds, P. G. *et al.* A longitudinal study on a-synuclein in blood plasma as a biomarker for Parkinson's disease. *Sci. Rep.* **3**, (2013).
276. Barton, J. C., Edwards, C. Q. & Acton, R. T. HFE gene: Structure, function, mutations, and associated iron abnormalities. *Gene* **574**, 179–192 (2015).
277. Su, X. W. *et al.* H63D HFE polymorphisms are associated with increased disease duration and decreased muscle superoxide dismutase-1 expression in amyotrophic lateral sclerosis patients. *Muscle and Nerve* **48**, 242–246 (2013).
278. Ali-Rahmani, F., Schengrund, C.-L. & Connor, J. R. HFE gene variants, iron, and lipids: a novel connection in Alzheimer's disease. *Front. Pharmacol.* **5**, 165 (2014).
279. Steinberg, K. K. *et al.* Prevalence of C282Y and H63D mutations in the hemochromatosis (HFE) gene in the United States. *JAMA* **285**, 2216–22 (2001).
280. Borie, C. *et al.* Association study between iron-related genes polymorphisms and Parkinson's disease. *J. Neurol.* **249**, 801–804 (2002).
281. Mollenhauer, B. *et al.* Longitudinal analyses of cerebrospinal fluid α-Synuclein in prodromal and early Parkinson's disease. *Mov. Disord.* **34**, 1354–1364 (2019).
282. Mollenhauer, B. *et al.* A user's guide for α-synuclein biomarker studies in biological fluids: Perianalytical considerations. *Movement Disorders* **32**, 1117–1130 (2017).
283. Saunders-Pullman, R. *et al.* Progression in the LRRK2 -Associated Parkinson Disease Population. *JAMA Neurol.* **75**, 312 (2018).
284. Burciu, R. G. *et al.* Progression marker of Parkinson's disease: a 4-year multi-site imaging study. *Brain* **140**, 2183–2192 (2017).
285. Mollenhauer, B. *et al.* Longitudinal CSF biomarkers in patients with early Parkinson disease and healthy controls. *Neurology* **89**, 1959–1969 (2017).
286. Rhinn, H. *et al.* Alternative α-synuclein transcript usage as a convergent mechanism in

Parkinson's disease pathology. *Nat. Commun.* **3**, (2012).
287. Murray, I. V. J. *et al.* Role of α-synuclein carboxy-terminus on fibril formation in vitro. *Biochemistry* **42**, 8530–8540 (2003).
288. Kalivendi, S. V., Yedlapudi, D., Hillard, C. J. & Kalyanaraman, B. Oxidants induce alternative splicing of α-synuclein: Implications for Parkinson's disease. *Free Radic. Biol. Med.* **48**, 377–383 (2010).
289. Dolatshahi, M. *et al.* Longitudinal Alterations of Alpha-Synuclein, Amyloid Beta, Total, and Phosphorylated Tau in Cerebrospinal Fluid and Correlations Between Their Changes in Parkinson's Disease. *Front. Neurol.* **9**, 560 (2018).
290. Dexter, D. T. *et al.* Increased nigral iron content in postmortem Parkinsonian brain. *Lancet* **ii**, 1099–102 (1983).
291. Dexter, D. T. *et al.* Alterations in the levels of iron, ferritin and other trace metals in Parkinson's disease and other neurodegenerative diseases affecting the basal ganglia. *Brain* **114**, 1953–1975 (1991).
292. Chen, J. C. *et al.* MR of human postmortem brain tissue: correlative study between T2 and assays of iron and ferritin in Parkinson and Huntington disease. *AJNR. Am. J. Neuroradiol.* **14**, 275–81 (1993).
293. Winterbourn, C. C. Toxicity of iron and hydrogen peroxide: the Fenton reaction. *Toxicol. Lett.* **82**–**83**, 969–974 (1995).
294. Beard, J. L., Dawson, H. & Piñero, D. J. Iron metabolism: a comprehensive review. *Nutr. Rev.* **54**, 295–317 (1996).
295. Xiao, Y. *et al.* Iron promotes α-synuclein aggregation and transmission by inhibiting TFEB-mediated autophagosome-lysosome fusion. *J. Neurochem.* **145**, 34–50 (2018).
296. Abeyawardhane, D. L. *et al.* Iron Redox Chemistry Promotes Antiparallel Oligomerization of α-Synuclein. *J. Am. Chem. Soc.* **140**, 5028–5032 (2018).
297. Wang, R. *et al.* Iron-induced oxidative stress contributes to α-synuclein phosphorylation and up-regulation via polo-like kinase 2 and casein kinase 2. *Neurochem. Int.* **125**, 127–135 (2019).
298. Martin-Bastida, A. *et al.* Brain iron chelation by deferiprone in a phase 2 randomised double-blinded placebo controlled clinical trial in Parkinson's disease. *Sci. Rep.* **7**, 1398 (2017).
299. Winner, B. *et al.* In vivo demonstration that α-synuclein oligomers are toxic. *Proc. Natl. Acad. Sci. U. S. A.* **108**, 4194–4199 (2011).
300. Rockenstein, E. *et al.* Accumulation of oligomer-prone α-synuclein exacerbates synaptic and neuronal degeneration in vivo. *Brain* **137**, 1496–1513 (2014).
301. Wong, Y. C. & Krainc, D. α-Synuclein toxicity in neurodegeneration: mechanism and therapeutic strategies. *Nat. Med.* **23**, 1–13 (2017).
302. Manning-Bog, A. B. *et al.* The herbicide paraquat causes up-regulation and aggregation of α-synuclein in mice: Paraquat and α-synuclein. *J. Biol. Chem.* **277**, 1641–1644 (2002).
303. Naudet, N. *et al.* Oral exposure to paraquat triggers earlier expression of phosphorylated α-synuclein in the enteric nervous system of A53T mutant human α-synuclein transgenic mice. *J. Neuropathol. Exp. Neurol.* **76**, 1046–1057 (2017).
304. Volpicelli-Daley, L. A. *et al.* Exogenous Alpha-Synuclein Fibrils Induce Lewy Body Pathology Leading to Synaptic Dysfunction and Neuron Death. *Neuron* **72**, 57–71 (2011).
305. Luk, K. C. *et al.* Exogenous α-synuclein fibrils seed the formation of Lewy body-like intracellular inclusions in cultured cells. *Proc. Natl. Acad. Sci. U. S. A.* **106**, 20051–20056 (2009).
306. Volpicelli-Daley, L. A., Luk, K. C. & Lee, V. M.-Y. Addition of exogenous α-synuclein preformed fibrils to primary neuronal cultures to seed recruitment of endogenous α-

synuclein to Lewy body and Lewy neurite–like aggregates. *Nat. Protoc.* **9**, 2135–2146 (2014).
307. Vogiatzi, T., Xilouri, M., Vekrellis, K. & Stefanis, L. Wild type α-synuclein is degraded by chaperone-mediated autophagy and macroautophagy in neuronal cells. *J. Biol. Chem.* **283**, 23542–23556 (2008).
308. Hara, T. *et al.* Suppression of basal autophagy in neural cells causes neurodegenerative disease in mice. *Nature* **441**, 885–889 (2006).
309. Komatsu, M. *et al.* Loss of autophagy in the central nervous system causes neurodegeneration in mice. *Nature* **441**, 880–884 (2006).
310. Jung, C. H. *et al.* ULK-Atg13-FIP200 complexes mediate mTOR signaling to the autophagy machinery. *Mol. Biol. Cell* **20**, 1992–2003 (2009).
311. Heras-Sandoval, D., Pérez-Rojas, J. M., Hernández-Damián, J. & Pedraza-Chaverri, J. The role of PI3K/AKT/mTOR pathway in the modulation of autophagy and the clearance of protein aggregates in neurodegeneration. *Cellular Signalling* **26**, 2694–2701 (2014).
312. Ohyashiki, J. H. *et al.* The oral iron chelator deferasirox represses signaling through the mTOR in myeloid leukemia cells by enhancing expression of REDD1. *Cancer Sci.* **100**, 970–977 (2009).
313. Dennis, M. D., McGhee, N. K., Jefferson, L. S. & Kimball, S. R. Regulated in DNA damage and development 1 (REDD1) promotes cell survival during serum deprivation by sustaining repression of signaling through the mechanistic target of rapamycin in complex 1 (mTORC1). *Cell. Signal.* **25**, 2709–2716 (2013).
314. Whitney, M. L., Jefferson, L. S. & Kimball, S. R. ATF4 is necessary and sufficient for ER stress-induced upregulation of REDD1 expression. *Biochem. Biophys. Res. Commun.* **379**, 451–455 (2009).
315. Gan-Or, Z., Dion, P. A. & Rouleau, G. A. Genetic perspective on the role of the autophagy-lysosome pathway in Parkinson disease. *Autophagy* **11**, 1443–1457 (2015).
316. O'Regan, G., Desouza, R. M., Balestrino, R. & Schapira, A. H. Glucocerebrosidase Mutations in Parkinson Disease. *Journal of Parkinson's Disease* **7**, 411–422 (2017).
317. Du, T. T. *et al.* GBA deficiency promotes SNCA/α-synuclein accumulation through autophagic inhibition by inactivated PPP2A. *Autophagy* **11**, 1803–1820 (2015).
318. Friedlich, A. L., Tanzi, R. E. & Rogers, J. T. The 5'-untranslated region of Parkinson's disease alpha-synuclein messengerRNA contains a predicted iron responsive element. *Mol. Psychiatry* **12**, 222–223 (2007).
319. Steinberg, K. K. *et al.* Prevalence of C282Y and H63D Mutations in the Hemochromatosis (HFE) Gene in the United States. *JAMA* **285**, 2216 (2001).
320. Lee, S. Y., Patton, S. M., Henderson, R. J. & Connor, J. R. Consequences of expressing mutants of the hemochromatosis gene (HFE) into a human neuronal cell line lacking endogenous HFE. *FASEB J.* **21**, 564–576 (2007).
321. Lee, B. R. & Kamitani, T. Improved immunodetection of endogenous α-synuclein. *PLoS One* **6**, e23939 (2011).
322. Kimura, S., Fujita, N., Noda, T. & Yoshimori, T. Monitoring autophagy in mammalian cultured cells through the dynamics of LC3. in *Methods in Enzymology* **452**, 1–26 (Academic Press, 2009).
323. Mahul-Mellier, A. L. *et al.* Fibril growth and seeding capacity play key roles in α-synuclein-mediated apoptotic cell death. *Cell Death Differ.* **22**, 2107–2122 (2015).
324. Meyer, E., Kurian, M. A. & Hayflick, S. J. Neurodegeneration with Brain Iron Accumulation: Genetic Diversity and Pathophysiological Mechanisms. *Annu. Rev. Genomics Hum. Genet* **16**, 257–79 (2015).
325. Ali-Rahmani, F. *et al.* H63D mutation in hemochromatosis alters cholesterol metabolism

and induces memory impairment. *Neurobiol. Aging* **35**, 1511.e1–12 (2014).
326. Kim, J., Kundu, M., Viollet, B. & Guan, K. L. AMPK and mTOR regulate autophagy through direct phosphorylation of Ulk1. *Nat. Cell Biol.* **13**, 132–141 (2011).
327. Tonelli, C., Chio, I. I. C. & Tuveson, D. A. Transcriptional Regulation by Nrf2. *Antioxidants and Redox Signaling* **29**, 1727–1745 (2018).
328. Pearce, R. K. B., Owen, A., Daniel, S., Jenner, P. & Marsden, C. D. Alterations in the distribution of glutathione in the substantia nigra in Parkinson's disease. *J. Neural Transm.* **104**, 661–677 (1997).
329. Hastings, T. G. The role of dopamine oxidation in mitochondrial dysfunction: Implications for Parkinson's disease. *Journal of Bioenergetics and Biomembranes* **41**, 469–472 (2009).
330. Navarro, E. *et al.* Heme-Oxygenase i and PCG-1α Regulate Mitochondrial Biogenesis via Microglial Activation of Alpha7 Nicotinic Acetylcholine Receptors Using PNU282987. *Antioxidants Redox Signal.* **27**, 93–105 (2017).
331. East, D. A. *et al.* PMI: A ΔΨm independent pharmacological regulator of mitophagy. *Chem. Biol.* **21**, 1585–1596 (2014).
332. Reuben, A., Chung, J. W., Lapointe, R. & Santos, M. M. The hemochromatosis protein HFE 20 years later: An emerging role in antigen presentation and in the immune system. *Immunity Inflammation and Disease* **5**, 218–232 (2017).
333. Hansen, T. H., Huang, S., Arnold, P. L. & Fremont, D. H. Patterns of nonclassical MHC antigen presentation. *Nat. Immunol.* **8**, 563–568 (2007).
334. Reuben, A., Phénix, M., Santos, M. M. & Lapointe, R. The WT hemochromatosis protein HFE inhibits CD8+ T-lymphocyte activation. *Eur. J. Immunol.* **44**, 1604–1614 (2014).
335. De Almeida, S. F. *et al.* HFE cross-talks with the MHC class I antigen presentation pathway. *Blood* **106**, 971–977 (2005).
336. Porto, G. *et al.* Relative impact of HLA phenotype and CD4-CD8 ratios on the clinical expression of hemochromatosis. *Hepatology* **25**, 397–402 (1997).
337. Maia, M. L. *et al.* Invariant Natural Killer T Cells are Reduced in Hereditary Hemochromatosis Patients. *J. Clin. Immunol.* **35**, 68–74 (2015).
338. Costa, M. *et al.* Lymphocyte gene expression signatures from patients and mouse models of hereditary hemochromatosis reveal a function of hfe as a negative regulator of cd8+ t-Lymphocyte activation and differentiation in vivo. *PLoS One* **10**, (2015).
339. Fabio, G. *et al.* Peripheral lymphocytes and intracellular cytokines in C282Y homozygous hemochromatosis patients. *J. Hepatol.* **37**, 753–61 (2002).
340. Louveau, A. *et al.* Structural and functional features of central nervous system lymphatic vessels. *Nature* **523**, 337–341 (2015).
341. Gray, M. T. & Woulfe, J. M. Striatal blood-brain barrier permeability in Parkinson's disease. *J. Cereb. Blood Flow Metab.* **35**, 747–750 (2015).
342. Halle, S., Halle, O. & Förster, R. Mechanisms and Dynamics of T Cell-Mediated Cytotoxicity In Vivo. *Trends in Immunology* **38**, 432–443 (2017).
343. Brochard, V. *et al.* Infiltration of CD4+ lymphocytes into the brain contributes to neurodegeneration in a mouse model of Parkinson disease. *J. Clin. Invest.* **119**, 182–192 (2009).
344. Chandra, G., Roy, A., Rangasamy, S. B. & Pahan, K. Induction of Adaptive Immunity Leads to Nigrostriatal Disease Progression in MPTP Mouse Model of Parkinson's Disease. *J. Immunol.* **198**, 4312–4326 (2017).
345. Kustrimovic, N. *et al.* Dopaminergic Receptors on CD4+ T Naive and Memory Lymphocytes Correlate with Motor Impairment in Patients with Parkinson's Disease. *Sci. Rep.* **6**, (2016).

346. Moors, T. E. *et al.* Therapeutic potential of autophagy-enhancing agents in Parkinson's disease. *Molecular Neurodegeneration* **12**, (2017).
347. Carrasco, E. & Werner, P. Selective destruction of dopaminergic neurons by low concentrations of 6-OHDA and MPP+: protection by acetylsalicylic acid aspirin. *Parkinsonism Relat. Disord.* **8**, 407–11 (2002).
348. Gagne, J. J. & Power, M. C. Anti-inflammatory drugs and risk of Parkinson disease: A meta-analysis. *Neurology* **74**, 995–1002 (2010).
349. Jankovic, J. *et al.* Safety and Tolerability of Multiple Ascending Doses of PRX002/RG7935, an Anti--Synuclein Monoclonal Antibody, in Patients with Parkinson Disease: A Randomized Clinical Trial. *JAMA Neurol.* **75**, 1206–1214 (2018).
350. Wang, Z., Gao, G., Duan, C. & Yang, H. Progress of immunotherapy of anti-α-synuclein in Parkinson's disease. *Biomedicine and Pharmacotherapy* **115**, (2019).
351. Cummings, J., Ritter, A. & Zhong, K. Clinical Trials for Disease-Modifying Therapies in Alzheimer's Disease: A Primer, Lessons Learned, and a Blueprint for the Future. *Journal of Alzheimer's Disease* **64**, S3–S22 (2018).
352. Bourdenx, M. *et al.* Protein aggregation and neurodegeneration in prototypical neurodegenerative diseases: Examples of amyloidopathies, tauopathies and synucleinopathies. *Progress in Neurobiology* **155**, 171–193 (2017).
353. McKee, A. C. *et al.* The spectrum of disease in chronic traumatic encephalopathy. *Brain* **136**, 43–64 (2013).
354. Malicdan, M. C. V. & Nishino, I. Autophagy in lysosomal myopathies. in *Brain Pathology* **22**, 82–88 (2012).
355. Neel, B. A., Lin, Y. & Pessin, J. E. Skeletal muscle autophagy: A new metabolic regulator. *Trends in Endocrinology and Metabolism* **24**, 635–643 (2013).
356. Masiero, E. & Sandri, M. Autophagy inhibition induces atrophy and myopathy in adult skeletal muscles. *Autophagy* **6**, 307–309 (2010).
357. Masiero, E. *et al.* Autophagy Is Required to Maintain Muscle Mass. *Cell Metab.* **10**, 507–515 (2009).
358. Hermine, O. *et al.* Eighty percent of French sport winners in Olympic, World and Europeans competitions have mutations in the hemochromatosis HFE gene. *Biochimie* **119**, 1–5 (2015).
359. Yun, C. W. & Lee, S. H. The Roles of Autophagy in Cancer. *International journal of molecular sciences* **19**, (2018).
360. Degenhardt, K. *et al.* Autophagy promotes tumor cell survival and restricts necrosis, inflammation, and tumorigenesis. *Cancer Cell* **10**, 51–64 (2006).
361. Hashimoto, I. *et al.* Blocking on the CXCR4/mTOR signalling pathway induces the anti-metastatic properties and autophagic cell death in peritoneal disseminated gastric cancer cells. *Eur. J. Cancer* **44**, 1022–1029 (2008).
362. Peng, Y. F. *et al.* Autophagy inhibition suppresses pulmonary metastasis of HCC in mice via impairing anoikis resistance and colonization of HCC cells. *Autophagy* **9**, 2056–2068 (2013).
363. Osborne, N. J. *et al.* HFE c282y homozygotes are at increased risk of breast and colorectal cancer. *Hepatology* **51**, 1311–1318 (2010).
364. Lv, Y. F. *et al.* The risk of new-onset cancer associated with HFE C282Y and H63D mutations: evidence from 87,028 participants. *J. Cell. Mol. Med.* **20**, 1219–1233 (2016).
365. Lee, S. Y. *et al.* HFE polymorphisms affect survival of brain tumor patients. *J. Neurooncol.* **122**, 97–104 (2015).
366. Gnana-Prakasam, J. P. *et al.* Loss of Hfe leads to progression of tumor phenotype in primary retinal pigment epithelial cells. *Investig. Ophthalmol. Vis. Sci.* **54**, 63–71 (2013).

VITA

Yunsung Kim

Education

2014 – Present	M.D., Ph.D. Candidate Penn State College of Medicine, Hershey, Pennsylvania
2014	B.S. Biology Purdue University, West Lafayette, Indiana

Awards

2019	Association of American Physicians (AAP)/ American Society for Clinical Investigation (ASCI)/ American Physician Scientist Association (APSA) Joint Meeting Best Poster Award
2019	Association of American Physicians (AAP)/ American Society for Clinical Investigation (ASCI) Travel Award
2018-2019	Daniel A. Notterman Physician-Scientist Award for Outstanding Clinical Research Conference Presentation
2010-2014	Purdue University Trustee's Scholarship

Publications

Kim Y, Stahl M, Huang X, Connor J. H63D variant of hemostatic iron regulator (*HFE*) is a genetic modifier of Parkinson's disease. *Submitted.*

Kim Y, Stahl M, Huang X, Connor J. H63D *HFE* alters α-synuclein expression, aggregation, and cytotoxicity. *Submitted*.

Kim Y, Connor J. Iron and HFE in neurological diseases. *Molecular Aspects of Medicine*. In preparation.

Selected Presentations

Kim Y, Connor J, Stahl M. H63D *HFE* protects cells from α-synuclein mediated toxicity in pre-formed fibril model of Parkinson's Disease. Society for Neuroscience Meeting Oct 19-23, 2019 Chicago, IL.

Kim Y. Investigating the effects of H63D *HFE* variant on α-synuclein pre-formed fibril (PFF) model of Parkinson's disease. Translational Brain Research Center Inaugural Parkinson's Disease Symposium June 7, 2019 Hershey, PA.

Kim Y, Connor J, Stahl M. H63D HFE protects cells from α-synuclein mediated toxicity. APSA/AAP/ASCI Joint Meeting April 4-5, 2019 Chicago, IL.

Kim Y, and Stahl M. Alpha-Synuclein Protein Homeostasis and Oligomerization in Iron Overloaded Cells Expressing Mutant HFE. 21st International Congress of Parkinson's Disease and Movement Disorders June 4-8, 2017 Vancouver, BC, Canada